Improving the Efficiency of Ruthenium-Catalyzed Olefin Metathesis with Solid-Supported Catalysts, Microfluidic Reactors, and Novel X-Type Ligands

by

Matthew Martin Van Wingerden

In Partial Fulfillment of the Requirements

for the Degree of

Doctor of Philosophy

California Institute of Technology

Pasadena, California

2013

(Defended September 21, 2012)

Acknowledgments

First of all, I would like to thank my advisor, Robert Grubbs. Working for Bob means being given inspired ideas, world class resources, and lots of space to explore. It is impossible not to grow as a scientist under these conditions. Of course, in addition to the inspiring mentor, there are the top notch colleagues. Among the many friends and mentors I had in the group, Chris Daeffler, Keith Keitz, Jean Li, and Renee Thomas were there nearly my entire time in the group and were a tremendous source of support, fun, great ideas for chemistry research and terrible ideas for business ventures. Keith really showed me the ropes when I first joined the lab, and unless he figures out how to access that account in the Cayman Islands, I'll never be able to repay him.

In addition to friendship, camaraderie, and general mentorship, some group members were important mentors for specific projects. Daryl Allen started my first project, trained me during my first few months, and introduced me to the joy that is being friends with a Maritimer. Alexey Fedorov started my last project, helped me through my last few months of grad school, and was always willing to discuss chemistry, politics, history, and how much he loves sandwiches.

With all the great mentors around me it eventually became my privilege to turn around and mentor a younger chemistry student. Jomya Lei, a Caltech undergrad, worked with me for two summers. She was a lot of fun and synthesized ligands the same way she did all her work; patiently, carefully, and precisely.

I also would like to thank my committee, Professors John Bercaw, David Tirrell, and Sarah Reisman. Not only did they work hard to make meetings and exams pleasant, nurturing experiences, they have also been very helpful outside of meetings when I have come to them individually for help with chemistry, proposals, or pretty much anything else.

The science at Caltech would also not be possible without the amazing staff. On the scientific side I would like to thank Dr. David Vander Velde in the NMR facility, Dr. Mona Shahgoli in the Mass Spectrometry facility, and the ever cheerful and enthusiastic Lawrence Henley in the x-ray facility. On the technical side Thomas Dunn, Richard Gerhart, and Michael Roy are true experts in their own right and make possible the design, fabrication, and maintenance of all devices chemical, mechanical, and electrical, plus they are just some of the nicest guys you could ever hang out with.

I have had the privilege of working on some interesting collaborations. In particular, the group of Prof. Dong-pyo Kim in Korea has been great to me. They are now at Pohang University of Science and Technology, but I was able to work with them for two months back when they were at Chungnam National University in Daejeon. Dr. Chan-pil Park and Dr. Ram Awatar Maurya helped me with all my scientific needs, while Tae-ho Lee showed me the best restaurants and noraebang joints that Daejeon had to offer.

I would also like to thank my family, especially my mom and dad, for their patient support throughout grad school. Grad school is such a unique experience that it can be difficult for those outside of it to support someone in it. My parents did it from a thousand miles away, even though they had to rely on my sporadic and feeble attempts to explain what, exactly, I was doing.

Finally, thanks Catrina. You are a best friend, an ally, a sounding board, somebody who pushes me to succeed, and somebody who encourages me to goof off. I love you for all of it.

Abstract

Olefin metathesis has become an important tool in modern organic chemistry. Key to the development of olefin metathesis as a methodology has been the discovery of the highly active, selective, and tolerant ruthenium-based Grubbs catalysts. The overall efficiency and utility of these catalysts are determined by a complex set of parameters including catalyst design, reaction conditions, reactor design, and purification strategy. These parameters can be varied to achieve higher catalyst turnovers, better product selectivity and reduced product contamination. This research seeks to improve the efficiency and utility of olefin metathesis using three strategies; the covalent attachment of catalysts to silica supports, the development of biphasic microfluidic reactors, and the synthesis of novel catalyst architectures.

Solid-supported catalysts present an effective strategy to eliminate metal contamination in metathesis products. These catalysts, however, are generally ill defined and their active species and decomposition pathways are poorly understood. In order to further study both the activity and decomposition of silica-supported catalysts, both a brominated alkylidene ligand and a cleavable linker were prepared. The brominated ligand was designed to bind only active catalyst, but was found to indiscriminately bind all ruthenium species. The cleavable linker was synthesized with an ortho-benzyl nitro ether moiety, rendering it cleavable by UV light. Future studies will use this UV-triggered lability to study the solid-supported catalysts with solution phase techniques.

Biphasic microfluidic reactors were developed to address the generation or consumption of ethylene gas in metathesis. By using either alternating flow or parallel flow gas-liquid reactors, the mass transfer of ethylene was facilitated. The enhanced mass transfer gave higher yields and catalyst turnovers in ethenolysis and ring-closing metathesis reactions.

Novel catalyst architectures were designed and synthesized to increase catalyst activity. While chloride-based catalysts have generally been used because of their higher activity, the activity of fluoride and hydroxide catalysts remains under explored, due mainly to practical challenges associated with their synthesis. A set of fluoride catalysts based on the Piers-type catalyst and a hydroxide catalyst based on the recently developed Z-selective catalysts were synthesized and characterized. The hydroxide catalyst showed promising activity while the fluoride catalyst was found to be inactive under all but the most forcing of conditions.

In general, the utility of ruthenium-based catalysts has caused rapid growth in the field of olefin metathesis. The work presented herein covers a variety of strategies to improve the overall utility and efficiency of these catalysts, including insights into decomposition pathways, controlling phase interactions, and synthesizing novel catalysts. Further pursuits of these strategies will prove valuable to the advancement of olefin metathesis.

Contents

List of Figures

List of Tables

Chapter 1

Introduction to Olefin Metathesis

1.1 Early Mechanistic Studies

Since its discovery in the late 1950s,[1] the olefin metathesis reaction has experienced a remarkable development to become an important part of the industrial and academic synthetic repertoire.[2,3] Along with the cross-coupling reactions developed by Stille, Suzuki, Heck, Negishi and others, it is quite possibly the most significant, versatile, and widely used C-C bond forming reaction of the last 40 years.

Although olefin metathesis was originally discovered in and continues to be used by the bulk chemical industry, it has been adopted by the fine chemical industry, as well as by academic chemists and biochemists. Key to the shift in applications has been the shift in available methodologies. Where once were only poorly understood multicomponent heterogeneous catalysts are now well-defined single component homogeneous catalysts. Without the development of these well understood, user-friendly catalysts olefin metathesis would undoubtedly have remained in the relative obscurity in which it initially found itself.

The development of better catalysts would not have been possible, however, without the meticulous mechanistic studies that preceded their discovery. In 1971, sixteen years after the initial report of olefin metathesis, Chauvin proposed a mechanism involving the exchange between metal alkylidenes and metallacyclobutanes (Figure 1.1).[4] Chauvin's mechanistic proposal was not the first[5] and other, contradictory proposals would still follow[6,7] but by the end of the decade it would gain

widespread acceptance.[8–11]

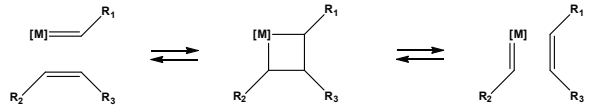

Figure 1.1: General mechanism of olefin metathesis

1.2 Catalyst Development

While initial mechanistic studies relied largely on isotopic labeling and product distributions, further studies sought out plausible mechanistic intermediates as the basis for new catalysts. Key to the development of early transition metal catalysts were the isolation of a tantalum complex with a purely alkyl carbene ligand by Schrock[12] and the isolation of a titanium metallacyclobutane complex derived from the Tebbe reagent by Grubbs.[13] These and other developments led to the first well-defined early transition metal catalysts based on niobium, tantalum, and tungsten.[14] The Schrock lab continued to develop these catalysts and eventually developed the popular and commercially available molybdenum catalyst 1.1.[15]

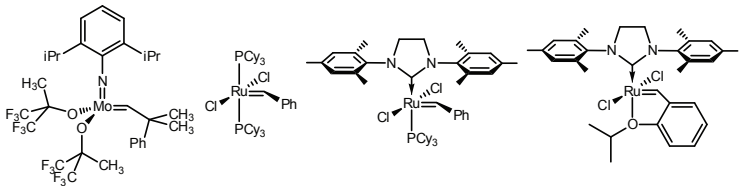

1.1 1.2 1.3 1.4

Figure 1.2: Important olefin metathesis catalysts

The Schrock-type catalysts, while highly active, were sensitive to air, water, and oxygen-containing functional groups. The Grubbs lab pursued catalysts from the later transition metals, particularly ruthenium, since they were known to be less oxophilic.[16] This line of research led to active ruthenium catalysts with phosphine ligands[17] such as 1.2,[18,19] now known as the first generation Grubbs catalyst. Further developments gave the more active second generation catalyst 1.3,[20] in which a phosphine ligand is replaced by an N-Heterocyclic Carbene (NHC) ligand and the more stable second generation Grubbs-Hoveyda catalyst 1.4,[21] in which the second phosphine ligand is replaced

by a chelating isopropyl ether. These ruthenium-based catalysts have gained popularity due to their increased tolerance to benchtop conditions and to a wide range of functional groups (Table 1.1).[22]

Table 1.1: Relative reactivity of olefin metathesis catalysts based on different transition metals

Titanium	**Tungsten**	**Molybdenum**	**Ruthenium**
Acids	Acids	Acids	**Olefins**
Alcohols, Water	Alcohols, Water	Alcohols, Water	Acids
Aldehydes	Aldehydes	Aldehydes	Alcohols, Water
Ketones	Ketones	**Olefins**	Aldehydes
Esters, Amides	**Olefins**	Ketones	Ketones
Olefins	Esters, Amides	Esters, Amides	Esters, Amides

↑ Increasing Reactivity

1.3 Reaction Types and Applications

Olefin metathesis, while simply a thermodynamic rearrangement of C-C double bonds, can be used for a variety of transformations. Depending on the substrates and conditions, metathesis can often be used with equal effectiveness for opposite reactions. Such is the case of ring-closing metathesis (RCM) and ring-opening metathesis (ROM), which form and break rings, respectively. Likewise, cross metathesis (CM) and ethenolysis can be used to either couple or break internal olefins in acyclic molecules. In the case of polymerization, namely ring-opening metathesis polymerization (ROMP) and acyclic diene metathesis polymerization (ADMET), it is theoretically possible to degrade polymers back to the monomers, but in practice the reaction is usually run to form polymers, not monomers (Figure 1.3).

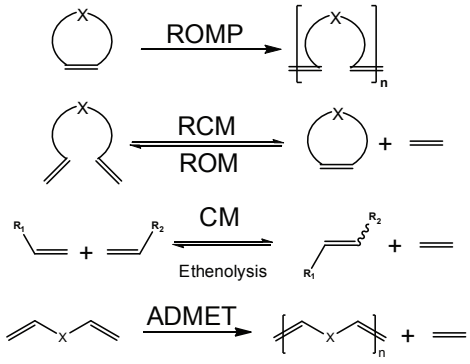

Figure 1.3: Olefin metathesis reaction types

In most cases of olefin metathesis, the forward and reverse reactions are possible and can be

catalyzed by the same complex. To favor RCM, the ring strain and the steric environment of the ring can be adjusted, often times taking advantage of the Thorpe-Ingold effect.[23] In controlling the formation of polymers the monomer concentration is a key variable.[24] In the case of ethenolysis, the ethylene concentration controls the overall reaction direction.[25] In the case of CM control can be difficult, as CM is a bimolecular reaction in which the product mixture is not controlled by the direct covalent tethering of olefins. For control of the product mixture, the two olefins may be temporarily tethered together using cleavable silicon-oxygen bonds,[3] but in general careful selection of substrate architecture is required.[24] To that end, a broad classification system has been developed in which olefins are grouped into categories based on how rapidly they homodimerize.[26] Because cross coupling is affected by the choice of catalyst, the many permutations of catalyst and substrate choices give a wide variety of possible product selectivities (Table 1.2).

Olefin metathesis has applied to a variety of challenges in the production of bulk chemicals, high strength materials and fine chemicals. In bulk chemicals, the olefins conversion technology (OCT) process (originally called the Phillips triolefin process) and the Shell higher olefins process (SHOP) are used to produce propylene and long chain α-olefins, respectively.[2] In materials, the ROMP of cyclooctene, norbornene and dicyclopentadiene is used commercially to produce materials with low crystallinity, high elasticity and high impact strength, respectively.[2] For fine chemicals RCM has been used to synthesize carbo- and heterocycle-containing natural products, and cross metathesis has been used to synthesize linear natural products.[3] Metathesis has also been used to selectively degrade seed oil derived chemicals to yield value-added products for use in fragrances, pheromones and pharmaceutical products in an interesting and growing application.[2]

Table 1.2: Olefin categories for selective cross metathesis[26]

Olefin type	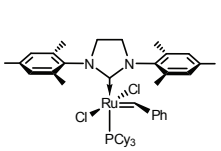 1.3	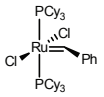 1.2	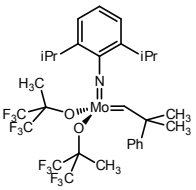 1.1
Type I (fast homodimerization)	terminal olefins,[27–36] 1° allylic alcohols, esters,[34,37] allyl boronate esters,[32] allyl halides,[32,35] styrenes (no large ortho sub.),[29,30,32,35] allyl phosphonates,[30] allyl silanes,[47] allyl phosphine oxides,[34] allyl sulfides,[34] protected allyl amines[34]	terminal olefins,[38] allyl silanes,[39–41] 1° allylic alcohols, ethers, esters,[38,41,45] allyl boronate esters,[46] allyl halides[48]	terminal olefins,[39,42–44] allyl silanes[43]
Type II (slow homodimerization)	styrenes (large ortho sub.),[30,32] acrylates,[28,35] acrylamides,[29] acrylic acid,[29] acrolein,[28,49] vinyl ketones,[28] unprotected 3° allylic alcohols,[32,34] vinyl epoxides,[28] 2° allylic alcohols, perfluorinated alkane olefins[28,53]	styrene,[50,51] 2° allylic alcohols, vinyl dioxolanes,[38] vinyl boronates[38]	styrene,[42,43] allyl stannanes[52]
Type III (no homodimerization)	1,1-disub. olefins,[27,33] non-bulky trisub. olefins,[27,33] vinyl phosphonates,[30] phenyl vinyl sulfone,[54] 4° allylic carbons (all alkyl substituents), 3° allylic alcohols (protected)	vinyl siloxanes[50,51]	3° allyl amines,[39] acrylonitrile[44]
Type IV (spectators to CM)	vinyl nitro olefins, trisubstituted allyl alcohols (protected)	1,1-disubstituted olefins,[38] disubstituted α,β-unsaturated carbonyls, 4° allylic carbon-containing olefins,[38] perfluorinated alkane olefins,[38] 3° allyl amines (protected)[39]	1,1-disubstituted olefins[42]

1.4 Current Challenges in Applications

Because of the expanding field of industrial applications of olefin metathesis, more practical constraints are being put on the reaction. To synthesize commodity chemicals or bulk materials the catalyst loadings must be much lower than what is typically used in the academic setting.[55] Additionally, the contamination caused by residual ruthenium is problematic in both pharmaceutical and advanced materials applications of olefin metathesis.[56] The use of low catalyst loadings is therefore not only cheaper when counting the cost of the catalyst but also when counting the cost of the purification. To achieve low catalyst loadings, studies have focused on proper catalyst choice and the optimal solvent and concentration.[55] To achieve low catalyst loadings in the context of the overall chemical process, solid-supported catalysts have also been studied due to the ease with which they can be recycled from reaction to reaction, or embedded in a fixed bed flow reactor.[57–59] In this thesis a study of solid supported catalysts is presented, with particular focus on characterizing the catalyst on the solid support. Additionally, an alternate strategy to low catalyst loadings based on microfluidic reactors is presented. In this case the use of ethylene permeable membranes allows for the rapid passage of ethylene, a typical reagent or product as previously described, into and out of solution, increasing the rate of reaction and the total catalyst turnovers.

1.5 Current Challenges in Catalyst Design

To achieve the maximum catalyst activity a wide variety of catalyst structures have been explored.[22] A key parameter that was optimized early was the halide ligand. Chloride was found to give higher activity than any other halide or pseudohalide.[60–64] An obvious exception is the case of fluoride, which has not yet been used in olefin metathesis catalysts.

The study of unique X-type ligands has been partially motivated by the recent interest in Z-selective olefin metathesis catalysts. The first effective Z-selective catalysts were based on molybdenum and reported by Schrock and Hoveyda in 2009.[65,66] The first report on Z-selective catalysts based on ruthenium followed shortly thereafter in 2011, primarily using of pivalate and nitrate

ligands.[67,68]

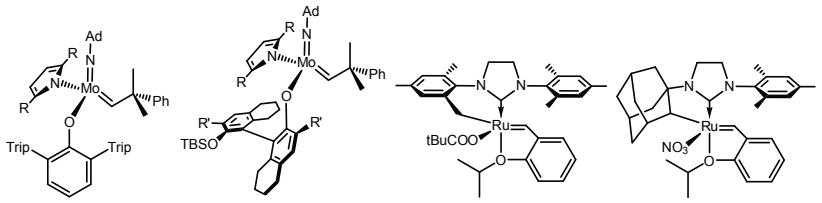

1.5 1.6 1.7 1.8

Table 1.3: Z-selective olefin metathesis catalysts

The advent of Z-selective olefin metathesis has opened up another dimension in product selectivity. Z-selective catalysts have been used to prepare highly stereoregular polymers via ROMP,[69] macrocycles with Z-olefins via RCM,[70] and acyclic Z-olefins via CM.[68] Challenges remain, however, as the activity of Z-selective catalysts is generally lower than of the standard catalysts.[67] Some of the activity in ruthenium catalysts has been restored by the use of anionic nitrate ligands,[68] but activity still lags behind for these catalysts.

An interesting and more general application of the Z-selective ruthenium catalysts is the presence of a more rigid ligand framework. The presence of a CH-activated NHC ligand restricts ligand flexibility and opens up new catalyst architectures. In this thesis a study of different halide ligands was made possible by the unique propensity for ligand exchange that these catalysts display. The formation of an unexpected hydroxide complex accompanies the facile exchange to form the iodide, bromide, and chloride versions of the Z-selective catalysts. The new catalyst structures and transformations that are possible starting with the CH-activated complex will provide important insights for the activity of both Z-selective catalysts and olefin metathesis catalysts in general.

References

[1] A.W. Anderson and N.G. Merckling. Polymeric bicyclo-(2,2,1)-2-heptene. *U.S. Patent 2,721,189*, 1955.

[2] J.C. Mol. Industrial applications of olefin metathesis. *Journal of Molecular Catalysis A — Chemical*, 213(1):39–45, 2004.

[3] J. Cossy, S. Arseniyadis, and C. Meyer, editors. *Metathesis in Natural Product Synthesis*. Wiley-VCH, 2010.

[4] J.L. Hérisson and Y. Chauvin. Catalyse de transformation des oléfines par les complexes du tungstène. II. Télomérisation des oléfines cycliques en présence d'oléfines acycliques. *Die Makromolekulare Chemie*, 141:161–176, 1971.

[5] N. Calderon, E.A. Ofstead, J.P. Ward, W.A. Judy, and K.W. Scott. Olefin Metathesis I. Acyclic Vinylenic Hydrocarbons. *Journal of the American Chemical Society*, 90(15):4133–4140, 1968.

[6] G.S. Lewandos and R. Pettit. Mechanism of Metal-Catalyzed Disproportionation of Olefins. *Journal of the American Chemical Society*, 93(25):7087–7088, 1971.

[7] R.H. Grubbs and T.K. Brunck. Possible Intermediate in Tungsten-Catalyzed Olefin Metathesis Reaction. *Journal of the American Chemical Society*, 94(7):2538–2540, 1972.

[8] T.J. Katz and J. McGinnis. The Mechanism of the Olefin Metathesis Reaction. *Journal of the American Chemical Society*, 97(6):1592–1594, 1975.

[9] R.H. Grubbs, P.L. Burk, and D.D. Carr. Consideration of the Mechanism of the Olefin Metathesis Reaction. *Journal of the American Chemical Society*, 97(11):3265–3267, 1975.

[10] R.H. Grubbs, D.D. Carr, C. Hoppin, and P.L. Burk. Consideration of the Mechanism of the Metal-Catalyzed Olefin Metathesis Reaction. *Journal of the American Chemical Society*, 98(12):3478–3483, 1976.

[11] Y Chauvin. Olefin metathesis: The early days (Nobel lecture). *Angewandte Chemie—International Edition*, 45(23):3740–3747, 2006.

[12] R.R. Schrock. Alkylcarbene Complex of Tantalum by Intramolecular α-Hydrogen Abstraction. *Journal of the American Chemical Society*, 96(21):6796–6797, 1974.

[13] T.R. Howard, J.B. Lee, and R.H. Grubbs. Titanium Metallacarbene-Metallacyclobutane Reactions—Stepwise Metathesis. *Journal of the American Chemical Society*, 102(22):6876–6878, 1980.

[14] R. Schrock, S. Rocklage, J. Wengrovius, G. Rupprech, and J. Fellmann. Preparation and Characterization of Active Niobium, Tantalum and Tungsten Metathesis Catalysts. *Journal of Molecular Catalysis*, 8(1–3):73–83, 1980.

[15] R.R. Schrock, J.S. Murdzek, G.C. Bazan, J. Robbins, M. DiMare, and M. O′Regan. Synthesis of Molybdenum Imido Alkylidene Complexes and Some Reactions Involving Acyclic Olefins. *Journal of the American Chemical Society*, 112(10):3875–3886, 1990.

[16] S.T. Nguyen, L.K. Johnson, R.H. Grubbs, and J.W. Ziller. Ring-Opening Metathesis Polymerization (ROMP) of Norbornene by a Group-VIII Carbene Complex in Protic Media. *Journal of the American Chemical Society*, 114(10):3974–3975, 1992.

[17] S.T. Nguyen, L.K. Johnson, R.H. Grubbs, and J.W. Ziller. Ring-Opening Metathesis Polymerization (ROMP) of Norbornene by a Group-VIII Carbene Complex in Protic Media. *Journal of the American Chemical Society*, 114(10):3974–3975, 1992.

[18] P. Schwab, M.B. France, J.W. Ziller, and R.H. Grubbs. A Series of Well-Defined Metathesis Catalysts—Synthesis of [$RuCl_2$(=CHR')($PR(_3)$)$(_2)$] and its Reactions. *Angewandte Chemie-International Edition in English*, 34(18):2039–2041, 1995.

[19] P. Schwab, R.H. Grubbs, and J.W. Ziller. Synthesis and applications of $RuCl_2$(=CHR')($PR(_3)$)$(_2)$: The influence of the alkylidene moiety on metathesis activity. *Journal of the American Chemical Society*, 118(1):100–110, 1996.

[20] M. Scholl, S. Ding, C.W. Lee, and R.H. Grubbs. Synthesis and activity of a new generation of ruthenium-based olefin metathesis catalysts coordinated with 1,3-dimesityl-4,5-dihydroimidazol-2-ylidene ligands. *Organic Letters*, 1(6):953–956, 1999.

[21] S.B. Garber, J.S. Kingsbury, B.L. Gray, and A.H. Hoveyda. Efficient and recyclable monomeric and dendritic Ru-based metathesis catalysts. *Journal of the American Chemical Society*, 122(34):8168–8179, 2000.

[22] T.M. Trnka and R.H. Grubbs. The development of $L_2X_2Ru = CHR$ olefin metathesis catalysts: An organometallic success story. *Accounts of Chemical Research*, 34(1):18–29, 2001.

[23] A. Fürstner and K. Langemann. A concise total synthesis of dactylol via ring closing metathesis. *The Journal of Organic Chemistry*, 61(25):8746–8749, 1996.

[24] R.H. Grubbs, editor. *Handbook of Metathesis*, volume 1–3. Wiley-VCH, Weinheim, 2003.

[25] Y. Schrodi, T. Ung, A. Vargas, G. Mkrtumyan, C.W. Lee, T.M. Champagne, R.L. Pederson, and S.H. Hong. Ruthenium olefin metathesis catalysts for the ethenolysis of renewable feedstocks. *Clean—Soil Air Water*, 36(8):669–673, 2008.

[26] A.K. Chatterjee, T.L. Choi, D.P. Sanders, and R.H. Grubbs. A general model for selectivity in olefin cross metathesis. *Journal of the American Chemical Society*, 125(37):11360–11370, 2003.

[27] R.H. Chatterjee, A.K.and Grubbs. Synthesis of trisubstituted alkenes via olefin cross-metathesis. *Organic Letters*, 1(11):1751–1753, 1999.

[28] A.K. Chatterjee, J.P. Morgan, M. Scholl, and R.H. Grubbs. Synthesis of functionalized olefins by cross and ring-closing metatheses. *Journal of the American Chemical Society*, 122(15):3783–3784, 2000.

[29] T.L. Choi, A.K. Chatterjee, and R.H. Grubbs. Synthesis of alpha,beta-unsaturated amides by olefin cross-metathesis. *Angewandte Chemie—International Edition*, 40(7):1277–1279, 2001.

[30] A.K. Chatterjee, T.L. Choi, and R.H. Grubbs. Synthesis of vinyl- and allylphosphonates by olefin cross-metathesis. *Synlett*, pages 1034–1037, 2001.

[31] T.L. Choi, C.W. Lee, A.K. Chatterjee, and R.H. Grubbs. Olefin metathesis involving ruthenium enoic carbene complexes. *Journal of the American Chemical Society*, 123(42):10417–10418, 2001.

[32] S.D. Goldberg and R.H. Grubbs. A one-pot cross-metathesis/allylboration reaction: A three-component coupling for the synthesis of functionalized homoallylic alcohols. *Angewandte Chemie—International Edition*, 41(5):807–810, 2002.

[33] A.K. Chatterjee, D.P. Sanders, and R.H. Grubbs. Synthesis of symmetrical trisubstituted olefins by cross metathesis. *Organic Letters*, 4(11):1939–1942, 2002.

[34] F.D. Toste, A.K. Chatterjee, and R.H. Grubbs. Functional group diversity by ruthenium-catalyzed olefin cross-metathesis. *Pure and Applied Chemistry*, 74(1):7–10, 2002.

[35] A.K. Chatterjee, F.D. Toste, T.L. Choi, and R.H. Grubbs. Ruthenium-catalyzed olefin cross metathesis of styrenes as an alternative to the Heck and cross-coupling reactions. *Advanced Synthesis & Catalysis*, 344(6–7):634–637, 2002.

[36] A.K. Chatterjee and R.H. Grubbs. Formal vinyl C-H activation and allylic oxidation by olefin metathesis. *Angewandte Chemie—International Edition*, 41(17):3171–3174, 2002.

[37] L. Zhang and J.W. Herndon. Cross metathesis reactions using gamma,delta-unsaturated chromium carbene complexes. *Tetrahedron Letters*, 43(25):4471–4473, 2002.

[38] H.E. Blackwell, D.J. O'Leary, A.K. Chatterjee, R.A. Washenfelder, D.A. Bussmann, and R.H. Grubbs. New approaches to olefin cross-metathesis. *Journal of the American Chemical Society*, 122(1):58–71, 2000.

[39] O. Brummer, A. Ruckert, and S. Blechert. Olefin cross-metathesis with monosubstituted olefins. *Chemistry-A European Journal*, 3(3):441–446, 1997.

[40] S. Faure, S. Piva-Le Blanc, and O. Piva. Synthesis of vinyl spirolactones and lactams by sequential cross-coupling metathesis, [2+2] photocycloaddition and cyclobutane ring-opening. *Tetrahedron Letters*, 40(33):6001–6004, 1999.

[41] P. Langer and E. Holtz. Olefin cross-metathesis of alkenyl epoxides with allyl- and vinyltrimethylsilane. *Synlett*, (1):110–112, 2002.

[42] W.E. Crowe and Z.J. Zhang. Highly Selective Cross-Metathesis of Terminal Olefins. *Journal of the American Chemical Society*, 115(23):10998–10999, 1993.

[43] W.E. Crowe, D.R. Goldberg, and Z.J. Zhang. Preparation of allylsilanes via cross-metathesis. *Tetrahedron Letters*, 37(13):2117–2120, 1996.

[44] W.E. Crowe and D.R. Goldberg. Acrylonitrile Cross-Metathesis—Coaxing Olefin Metathesis Reactivity from a Reluctant Substrate. *Journal of the American Chemical Society*, 117(18):5162–5163, 1995.

[45] T.K. Maishal, D.K. Sinha-Mahapatra, K. Paranjape, and A. Sarkar. Effect of a proximal oxygen substituent on the efficacy of ruthenium-catalyzed cross-metathesis and RCM. *Tetrahedron Letters*, 43(12):2263–2267, 2002.

[46] Y. Yamamoto, M. Takahashi, and N. Miyaura. Synthesis of pinacol allylic boronic esters via olefin cross-metathesis between pinacol allylboronate and terminal or internal alkenes. *Synlett*, (1):128–130, 2002.

[47] S. BouzBouz, E. De Lemos, and J. Cossy. Cross-metathesis reaction: Direct synthesis of functionalized allylsilanes. *Advanced Synthesis & Catalysis*, 344(6–7):627–630, 2002.

[48] O.M. Blanco and L. Castedo. New results on the functionalization of terminal alkenes by cross-metathesis reactions. *Synlett*, (5):557–558, 1999.

[49] S. BouzBouz and J. Cossy. Chemoselective cross-metathesis reaction. Application to the synthesis of the C1-C14 fragment of amphidinol 3. *Organic Letters*, 3(10):1451–1454, 2001.

[50] C. Pietraszuk, B. Marciniec, and H. Fischer. Cross-metathesis of vinylsilanes with styrene catalyzed by ruthenium-carbene complexes. *Organometallics*, 19(5):913–917, 2000.

[51] M. Kujawa-Welten, C. Pietraszuk, and B. Marciniec. Cross-metathesis of vinylsilanes with allyl alkyl ethers catalyzed by ruthenium-carbene complexes. *Organometallics*, 21(5):840–845, 2002.

[52] J. Feng, M. Schuster, and S. Blechert. A cross metathesis approach towards allyl stannanes. *Synlett*, (1):129–130, 1997.

[53] S. Imhof, S. Randl, and S. Blechert. Ruthenium catalysed cross metathesis with fluorinated olefins. *Chemical Communications*, (17):1692–1693, 2001.

[54] K. Grela and M. Bieniek. Highly selective cross-metathesis with phenyl vinyl sulphone using the 'second generation' Grubbs' catalyst. *Tetrahedron Letters*, 42(36):6425–6428, 2001.

[55] K.M. Kuhn, T.M. Champagne, S.H. Hong, W.-H. Wei, A. Nickel, C.W. Lee, S.C. Virgil, R.H. Grubbs, and R.L. Pederson. Low Catalyst Loadings in Olefin Metathesis: Synthesis of Nitrogen Heterocycles by Ring-Closing Metathesis. *Organic Letters*, 12(5):984–987, 2010.

[56] G.C. Vougioukalakis. Removing Ruthenium Residues from Olefin Metathesis Reaction Products. *Chemistry—A European Journal*, 18(29):8868–8880, 2012.

[57] B. De Clercq, F. Lefebvre, and F. Verpoort. Immobilization of multifunctional Schiff base containing ruthenium complexes on MCM-41. *Applied Catalysis A—General*, 247(2):345–364, 2003.

[58] D.P. Allen, M.M. Van Wingerden, and R.H. Grubbs. Well-Defined Silica-Supported Olefin Metathesis Catalysts. *Organic Letters*, 11(6):1261–1264, 2009.

[59] Details of a commercially available flow reactor are available at http://www.thalesnano.com/files/file/brochures/applications/X-CubeApplicationNote_Metathesis.pdf.

[60] E.L. Dias, S.T. Nguyen, and R.H. Grubbs. Well-defined ruthenium olefin metathesis catalysts: Mechanism and activity. *Journal of the American Chemical Society*, 119(17):3887–3897, 1997.

[61] M.S. Sanford, J.A. Love, and R.H. Grubbs. Mechanism and activity of ruthenium olefin metathesis catalysts. *Journal of the American Chemical Society*, 123(27):6543–6554, 2001.

[62] J. Wappel, C.A. Urbina-Blanco, M. Abbas, J.H. Albering, R. Saf, S.P. Nolan, and C. Slugovc. Halide exchanged Hoveyda-type complexes in olefin metathesis. *Beilstein Journal of Organic Chemistry*, 6:1091–1098, 2010.

[63] P. Teo and R.H. Grubbs. Facile Synthesis of Effcient and Selective Ruthenium Olefin Metathesis Catalysts with Sulfonate and Phosphate Ligands. *Organometallics*, 29(22):6045–6050, 2010.

[64] G.C. Vougioukalakis and R.H. Grubbs. Ruthenium-Based Heterocyclic Carbene-Coordinated Olefin Metathesis Catalysts. *Chemical Reviews*, 110(3):1746–1787, 2010.

[65] M.M. Flook, A.J. Jiang, R.R. Schrock, P. Mueller, and A.H. Hoveyda. Z-Selective Olefin Metathesis Processes Catalyzed by a Molybdenum Hexaisopropylterphenoxide Monopyrrolide Complex. *Journal of the American Chemical Society*, 131(23):7962–7963, 2009.

[66] A.J. Jiang, Y. Zhao, R.R. Schrock, and A.H. Hoveyda. Highly Z-Selective Metathesis Homocoupling of Terminal Olefins. *Journal of the American Chemical Society*, 131(46):16630–16631, 2009.

[67] K. Endo and R.H. Grubbs. Chelated Ruthenium Catalysts for Z-Selective Olefin Metathesis. *Journal of the American Chemical Society*, 133(22):8525–8527, 2011.

[68] B.K. Keitz, K. Endo, P.R. Patel, M.B. Herbert, and R.H. Grubbs. Improved Ruthenium Catalysts for Z-Selective Olefin Metathesis. *Journal of the American Chemical Society*, 134(1):693–699, 2012.

[69] B.K. Keitz, A. Fedorov, and R.H. Grubbs. Cis-Selective Ring-Opening Metathesis Polymerization with Ruthenium Catalysts. *Journal of the American Chemical Society*, 134(4):2040–2043, 2012.

[70] A.L. Gottumukkala, A.V.R. Madduri, and A.J. Minnaard. Z-Selectivity: A Novel Facet of Metathesis. *ChemCatChem*, 4(4):462–467, 2012.

Chapter 2

Solid-Supported Metathesis Catalysts

A method to accurately determine the loading of well-defined olefin metathesis catalysts immobilized on silica support was developed. Using a rhodium internal standard and hydrofluoric acid digestions, the amount of ruthenium embedded on the silica gel was measured. Using a bromine-containing ligand, it was determined that nonspecific binding of the ligand to supported catalyst prevented the quantification of active catalyst. A cleavable solid-supported ligand was developed for future use in catalyst release studies.

2.1 Introduction

Olefin metathesis was discovered in industry and first applied to produce bulk polymers and simple petrochemicals like butene and other α-olefins.[1] For these applications heterogeneous catalysts were not only the first catalysts to be discovered for the process but continue to be the catalysts of choice. While a range of homogeneous catalysts have since been developed, the inherent recyclability of the heterogeneous catalysts, as well as the lack of transition metal contamination of the products, continue to make heterogeneous catalysts the preferred option.

Outside of bulk chemical and polymer production, the olefin metathesis catalysts of choice have become homogeneous catalysts.[2] These catalysts, which have the advantage of being well defined and therefore precisely tunable, present new challenges for recycling and product purity.

The use of transition metal catalysts in the synthesis of pharmaceuticals in particular is complicated by the need for rigorous purity of the final product. The levels of ruthenium accepted by regulatory agencies are typically 5 ppm.[3,4] These low levels of catalyst require laborious purification,

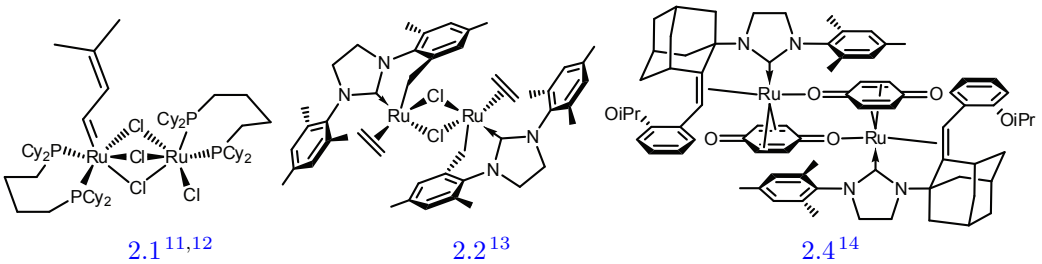

2.1[11,12] 2.2[13] 2.4[14]

Figure 2.1: Bimetallic decomposition products

often involving multiple consecutive silica gel columns.[5]

A strategy that has emerged to combine desirable characteristics of homogeneous and heterogeneous catalyst is the immobilization of heterogeneous catalysts on insoluble solid supports.[6] This strategy has been implemented with inorganic metal oxide supports such as silica[7] and alumina,[8] cross-linked polymeric supports,[9] and by the polymerization of the catalytic compound itself.[10]

In addition to combining the known benefits of heterogeneous and homogeneous catalysts, immobilizing homogeneous catalysts on solid supports can have additional benefits. A number of bimetallic decomposition products have been isolated from ruthenium olefin metathesis catalysts, including complex 2.1[11,12] from the first generation catalyst, 2.2[13] from the second generation catalyst, and 2.4[14] from the Z-selective catalyst (Figure 2.1). In cases where the solid support is rigid and does not swell in organic solvent, the isolation of one catalytic site from another (and therefore the prevention of bimolecular reactivity) has been demonstrated.[15–17]

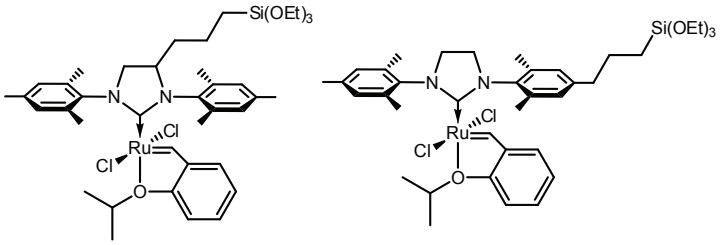

2.5 2.6

Figure 2.2: Silica-supported olefin metathesis catalysts

In order to prepare a catalyst that was both well defined and heterogeneous, the catalysts 2.5 and 2.6, both of which have pendant triethoxysilyl groups, have been prepared in our group.[18] Triethoxysilyl groups are a common motif for immobilizing well-defined catalysts on a solid support,

as they readily condense with silica gel under mild conditions, releasing ethanol and forming a covalent bond, thereby permanently immobilizing the catalyst.[6]

The silica-supported olefin metathesis catalysts 2.5 and 2.6 were shown to be active catalysts for ring-closing metathesis (RCM) and cross metathesis (CM).[18] The activity and selectivity of the supported catalyst reflected the activity and selectivity of the parent homogeneous catalyst. Catalyst 2.5 was successfully recycled over eight consecutive reactions by simple filtration.[18] The RCM product was demonstrated to be free of leached catalyst (concentration of ruthenium in the filtrate was less than the 5 ppb limit of detection).

2.2 ICP-MS Assay for Catalyst Loading

An important parameter to be measured for solid-supported catalysts is the loading of the catalyst on the support. While traditional well-defined catalysts have a defined molecular weight, there is no equivalent well-defined ratio for most solid-supported catalysts. Instead, the ratio of active catalyst to total mass of support must be experimentally determined for each catalyst preparation. In the case of catalysts with triethoxysilyl groups that condense with silica gel, the extent to which the catalyst binds to the surface depends on reaction conditions. A preliminary estimate of the catalyst loading can be calculated from the amount of catalyst that was added to the silica and the amount of catalyst that is recovered after the immobilization. However, this method only gives an estimate that is an upper limit to the catalyst loading.

A standard method of measuring the amount of transition metals embedded in silica gel is the use of inductively coupled plasma mass spectrometry (ICP-MS). This technique measures the concentration of the ion channels of interest after atomizing all compounds in a high energy plasma. All information relating to the chemical identity of each ion is lost in the atomization, but elemental concentrations can be accurately determined. Therefore the amount of immobilized ruthenium can be measured, although the amount of ruthenium that is in the form of active catalyst cannot be distinguished. The loading of ruthenium is again an upper bound to the loading of active catalyst, but a more precise limit than that calculated by measuring the recovered catalyst.

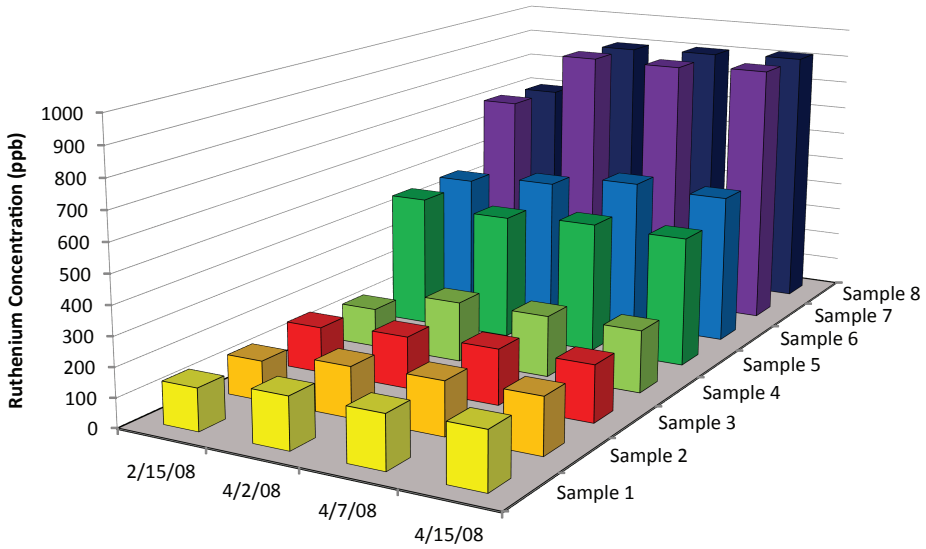

Figure 2.3: ICP-MS results (Details in the experimental section)

ICP-MS, which is performed from aqueous solution, requires the digestion of the solid-supported catalyst samples so the ruthenium is quantitatively released into solution. The method initially used in our studies was nitric acid digestion, in which the sample was boiled in a small amount of nitric acid for 48 hours, then diluted to a fixed volume using Milli-Q water.

After the nitric acid digestion the concentration of ruthenium was measured over several days using ICP-MS analysis. When the same sample was measured over the course of two months, it became apparent that the results were inconsistent from one measurement to the next (Figure 2.3). This led to a revision of the digestion and analysis methodology.

A simple test of the ICP-MS analysis was measuring the same sample multiple times on the same day. Each ICP-MS analysis run takes place over the course of several hours, and conditions such as the argon pressure, flow rate, plasma temperature and mass spectrometer response factor can vary widely across that time. To control for all the fluctuations, an internal standard was needed that has a similar atomic mass and ionization energy as the analyte but does not overlap with any of the mass channels used to measure the analyte. The elements with the most similar masses and ionization energies are molybdenum, rhodium and palladium. Molybdenum and palladium both have naturally occurring isotopes that overlap with ruthenium (^{96}Mo, ^{98}Mo, ^{100}Mo, ^{102}Pd and ^{104}Pd).

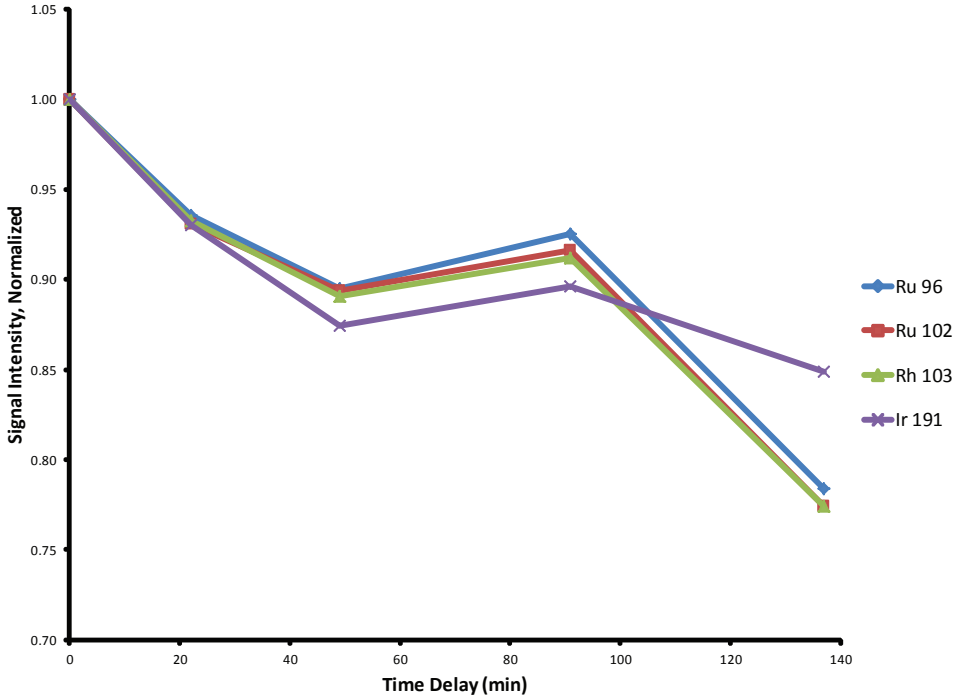

Figure 2.4: Drift of ICP-MS data

Rhodium, however, only has one naturally existing isotope (^{103}Rh), which does not overlap with any ruthenium isotopes. An internal standard with rhodium, and also iridium for comparison, was therefore prepared. A sample containing ruthenium (250 ppb), rhodium (200 ppb) and iridium (200 ppb) was analyzed by ICP-MS and the signals normalized to the highest data point and compared (Figure 2.4). The ruthenium signal (^{96}Ru and ^{102}Ru shown for simplicity) varies significantly from measurement to measurement, but the rhodium signal varies in exactly the same proportion as ruthenium, making it an ideal internal standard.

A closer inspection of the variability in the ICP-MS data reveals a more clear trend (Table 2.1). As more time passed from the digestion, the analysis gave higher and higher measured concentrations. A slow evaporation of the solvent could cause the growing concentration, but the samples were sealed and the water level did not change noticeably in the intervening two months. The silica gel that had been digested was still present in the digestion tubes, however, and a slow leaching of the ruthenium into solution could explain the growing concentration.

To test the leaching of ruthenium a new digestion method was devised. Instead of using nitric

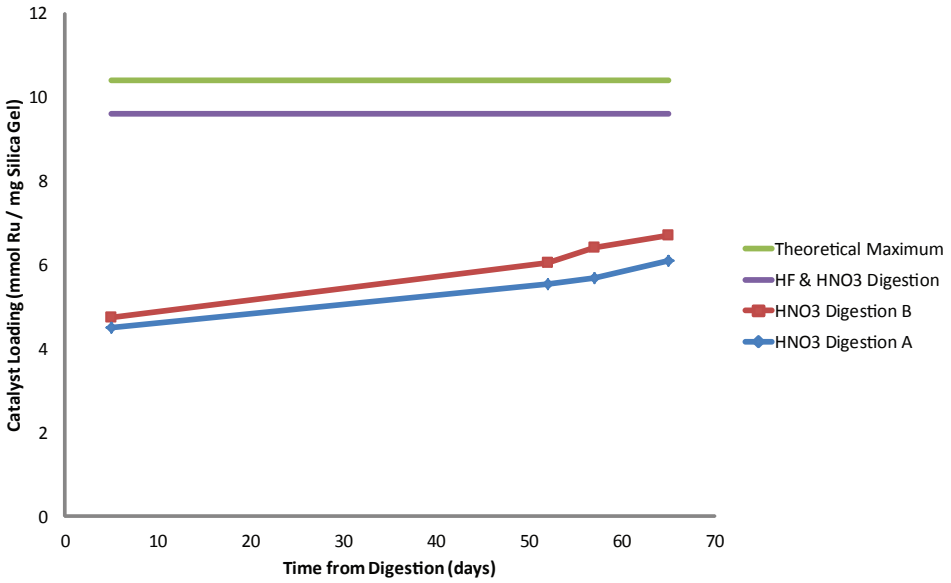

Figure 2.5: Digestion methods

acid only, a combination of nitric acid and hydrofluoric acid was used. Each acid (2.0 mL) was added to a small sample of solid-supported catalyst, and each sample was heated to the boiling point for 48 hours and then diluted to 50.0 mL. When these samples were analyzed by ICP-MS and corrected using the rhodium internal standard, the loading (9.59 mmol Ru / g silica gel) was found to be less than the limit calculated by measuring the recovered catalyst (10.4 mmol Ru / g silica gel) but more than the slowing growing level measured after nitric acid digestion, which ranged from 4 to 7 mmol Ru / g silica gel (Figure 2.5). Additionally, when hydrofluoric acid was used there was no remaining silica gel present at the bottom of the digestion tube, indicating the expected total degradation of the silica gel.

Using the rhodium internal standard and hydrofluoric acid digestion, accurate levels of the loading of ruthenium were determined. However, as previously mentioned, the ruthenium loading does not strictly equal the active catalyst loading. In order to determine the loading of active catalyst a second ICP-MS assay was devised.

2.3 Active Catalyst ICP-MS Assay

Since all chemical information is lost during ICP-MS analysis, any ICP-MS based assay of active catalyst has to rely on quantification of another element whose presence or absence can identify a specific structural motif. Bromine was selected due to the ease with which it can be introduced into organic compounds, its stability and its heavy mass, which is easier to measure by ICP-MS. A brominated tag was sought that could be introduced in situ and would selectively incorporate into active catalysts.

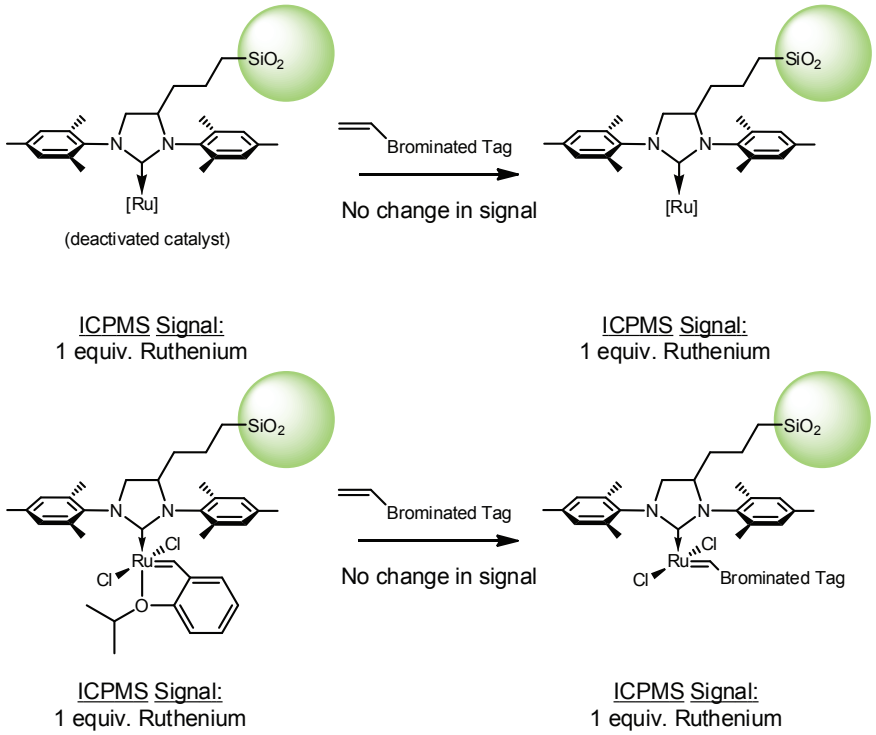

Figure 2.6: ICP-MS using ruthenium, no difference is observed between active and deactivated catalyst.

Since only active catalysts will incorporate an olefin from solution, a brominated olefin was selected as the probe molecule. Using only the ruthenium level measured by ICP-MS, active catalysts and deactivated catalysts that are still physically attached to the surface give the same signal (Figure 2.6). But when a bromine is attached to an olefin that can exchange with the alkylidene moiety of the catalyst, only the active catalyst will give both a ruthenium and bromine signal. A deactivated catalyst will still give a ruthenium signal for reference, but not a bromine (Figure 2.7).

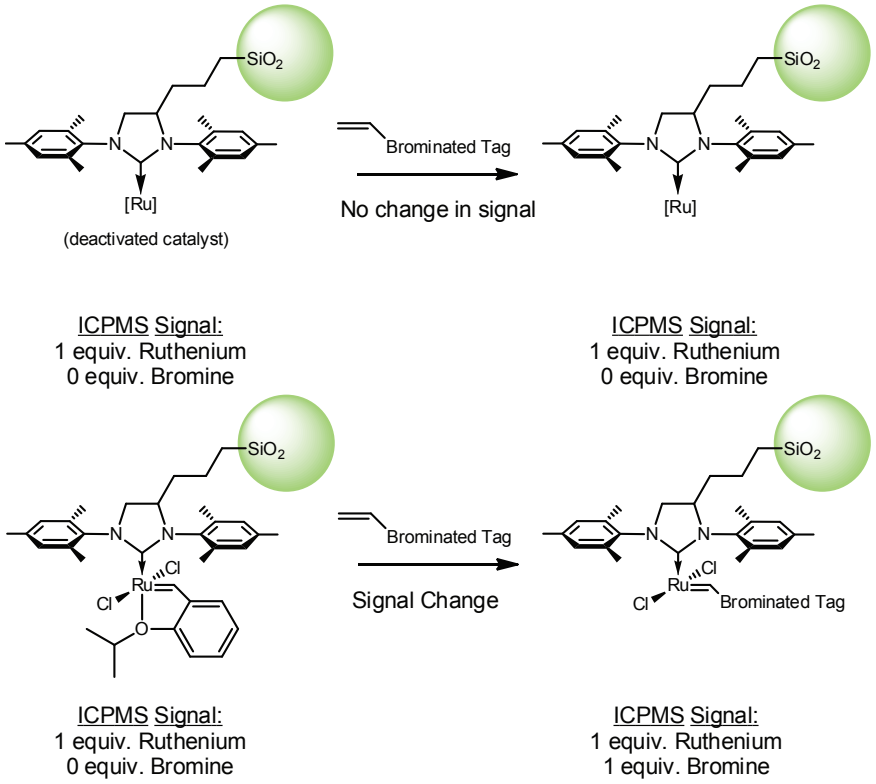

Figure 2.7: ICP-MS using ruthenium and bromine, active catalyst gives a different signal than deactivated catalyst.

A brominated tag was sought that would bind completely and selectively to active catalyst centers. Three possibilities were conceived. Using a simple chelating benzylidene ligand with bromine was considered (Figure 2.8 A), but the exchange would give a statistical mixture of labeled and unlabeled active catalyst. Brominated pyridine is known to quantitatively displace phosphine ligands (Figure 2.8 B), but this strategy requires the use of phosphine-based catalysts as pyridine does not displace the chelating isopropoxystyrene ligand in complex 2.5. A final strategy is the use of chelating thioether ligands (Figure 2.8 C). These ligands are known to quantitatively displace traditional chelating isopropoxystyrene ligands when used in excess.[19,20]

A synthesis for the brominated thioether chelate was devised, beginning with 2.7 (Figure 2.9). 2-propanethiol, deprotonated with sodium hydride, was used to displace the phenyl fluoride and form thioether 2.8. Ethylmagnesium bromide was then reacted with the aldehyde moiety to give benzyl alcohol 2.9. The alcohol was eliminated to form styrene 2.10 using a catalytic amount of *p*-toluenesulfonic acid. The synthesis can be performed on multi-gram scale and utilizes distillation

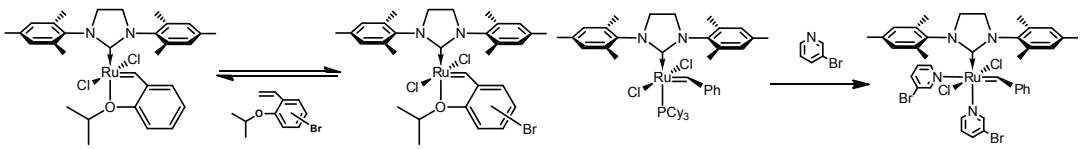

A) Brominated isopropoxyether chelate B) Brominated pyridine

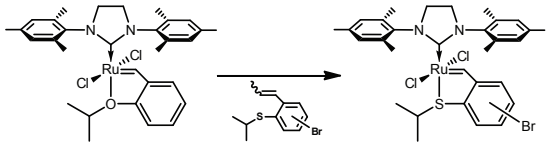

C) Brominated thioether chelate

Figure 2.8: Labeling strategies for an active catalyst assay

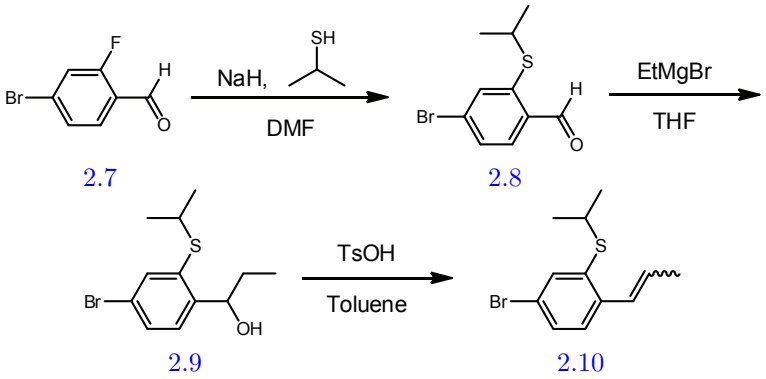

2.7 2.8 2.9 2.10

Figure 2.9: Synthesis of brominated chelate

for purification.

To test the active catalyst assay the brominated probe 2.10 was added to the catalyst under a variety of conditions (Figure 2.10). A positive control was prepared by immobilizing a well-defined complex with one ruthenium and one bromine atom. A negative control was prepared by immobilizing catalyst 2.5 on silica gel. To test the ability of the ligand to bind immobilized active catalyst, complex 2.5 on silica gel was subjected to the chelating ligand 2.10 before being rinsed and digested. A second negative control was prepared with completely deactivated catalyst. A sample of 2.5 on silica gel was subjected to olefin metathesis conditions with 1-hexene under air for 24 hours. By the end of the exposure the color of the silica gel had changed from light green to light brown. The deactivated catalyst sample was then subjected to the chelating ligand 2.10 before being rinsed with dichloromethane for two days in a Soxhlet extractor and then digested.

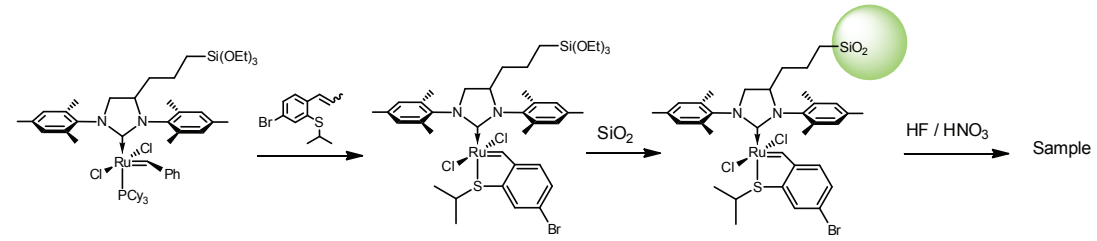

A) Positive control sample

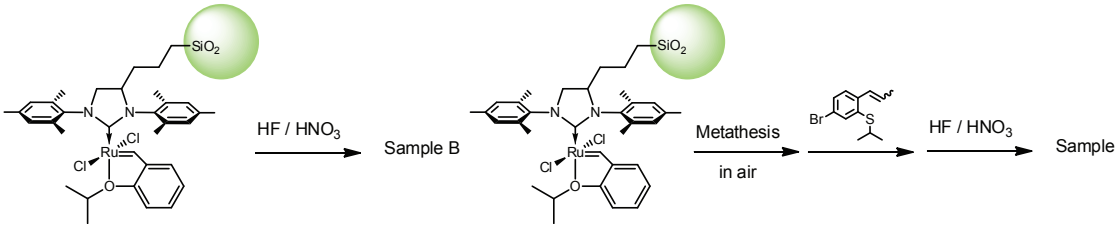

B) Negative control sample A

C) Negative control sample B

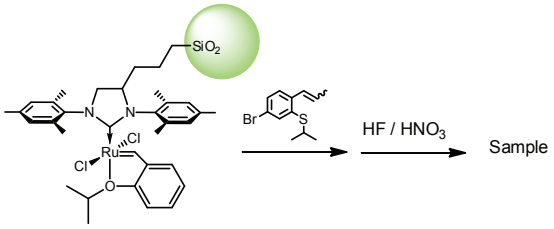

D) Assay of active catalyst

Figure 2.10: Preparation of control and test samples for the ICP-MS active catalyst assay

The ICP-MS analysis of the test samples revealed the measured concentrations of bromine to be less reliable than those of ruthenium (Table 2.11). In sample A, where equal amounts of bromine and ruthenium were present, the two concentrations differed by over 15%. In sample B, where no bromine was introduced at any point, the concentration of bromine was measured to be 28 ppb. In the case of ruthenium, the concentration of blank samples is measured to be less than 5 ppb in all cases, even without the use of an internal standard. The use of an internal standard is difficult in the case of bromine, because there are no elements with both a similar ionization energy and a similar atomic mass. The use of selenium and iodine was explored, but the normalized signal the isotopes of selenium varied over 10% from measurement to measurement, relative to the normalized signal for either ^{79}Br or ^{81}Br, and the normalized signal for ^{127}I varied over 25% from measurement

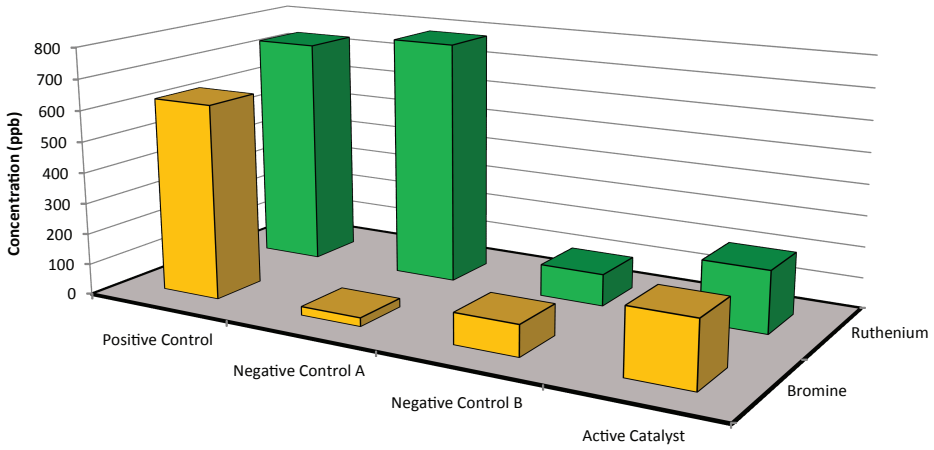

Figure 2.11: ICP-MS active catalyst assay results (Details in experimental section)

to measurement, relative to the normalized signal for either ^{79}Br or ^{81}Br. An effective alternative to using selenium or iodine is the use of isotopic dilution, in which a solution of one isotope of the element of interest is added in as an internal standard.[21] An accurate concentration can then be calculated from the resulting unnatural isotopic abundance. However, due to the high cost of acquiring isotopically pure bromide salts the studies continued with the bromine data as it was for preliminary studies.

The concentrations measured from the assay experiments indicate a difficulty in distinguishing between active and deactivated catalyst. In both sample C and sample D the concentrations of bromine and ruthenium were nearly equal. However, in the case of sample D the catalyst had been intentionally deactivated and in the case of sample C this was not the case. Ligand 2.10 was binding nonspecifically to both active and dead catalyst. The lack of specificity precludes its use for the assay, but the exact nature of the interaction between the ligand and the decomposed catalyst remains to be determined (Figure 2.12).

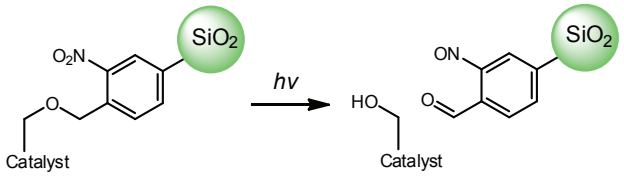

Figure 2.12: Schematic of catalyst release

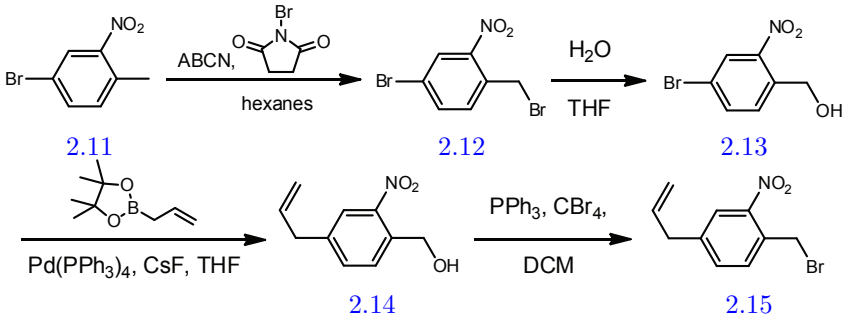

Figure 2.13: Synthesis of o-nitrobenzyl ether

2.4 Cleavable Solid-Supported Ligand

Because ICP-MS gives only limited information about the species bound to silica gel, a more in-depth characterization method was sought for the species on the silica gel. Since characterization on the solid support is difficult, a means to selectively cleave the catalyst from the solid support was designed so a full characterization could be done in the solution phase. The *o*-nitrobenzyl ether moiety was selected because of the facile cleavage under UV light. The *o*-nitrobenzyl ether was incorporated in between the NHC ligand and the triethoxysilane, so upon irradiation the bond between the catalyst and the solid support is severed.

The first step in synthesizing the cleavable NHC ligand is the preparation of the *o*-nitrobenzyl ether moiety itself (Figure 2.13). Beginning with commercially available 4-bromo-2-nitrotoluene (2.11) and brominating at the benzylic position gives 2.12. 2.12 was converted to the benzylic alcohol 2.13 in a water-THF mixture in a microwave reactor. The conversion to the alcohol was necessary for the subsequent cross-coupling step, in which the palladium catalyst is poisoned by the benzylic bromide. The palladium-catalyzed Suzuki coupling yields 2.14, which can be converted back to the bromide 2.15 using CBr_4 and PPh_3.

With the *o*-benzylnitro ether in hand the focus shifted to preparing the NHC with a pendant

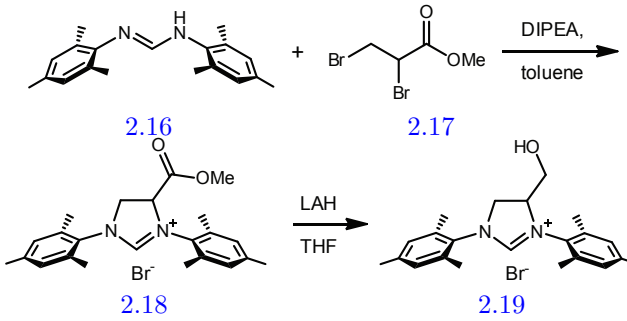

Figure 2.14: Synthesis of imidazolinium salt with pendant alcohol

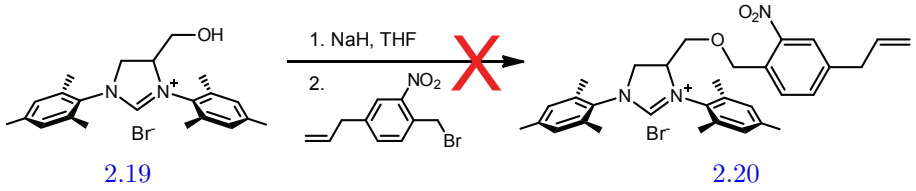

Figure 2.15: Attempted synthesis of o-nitrobenzyl ether-containing NHC ligand

alcohol. The synthesis of an NHC with a pendant alcohol has been reported,[22] but a more facile synthesis was developed using methodology developed in our group for the unmodified NHC ligands (Figure 2.14).[23] Combining formamidine 2.16 and 2.17 (derived in one step from methyl acrylate) in the presence of a base gives NHC ligand precursor 2.18 in one step. Reducing the methyl ester with LAH yields the NHC ligand salt 2.19 in a scalable, two-step synthesis.

With large amounts of the NHC ligand with a pendant alcohol, the synthesis of the ether was attempted (Figure 2.15). Unfortunately, our efforts to synthesize ether 2.20 from the NHC ligand salt and the benzyl bromide were unsuccessful.

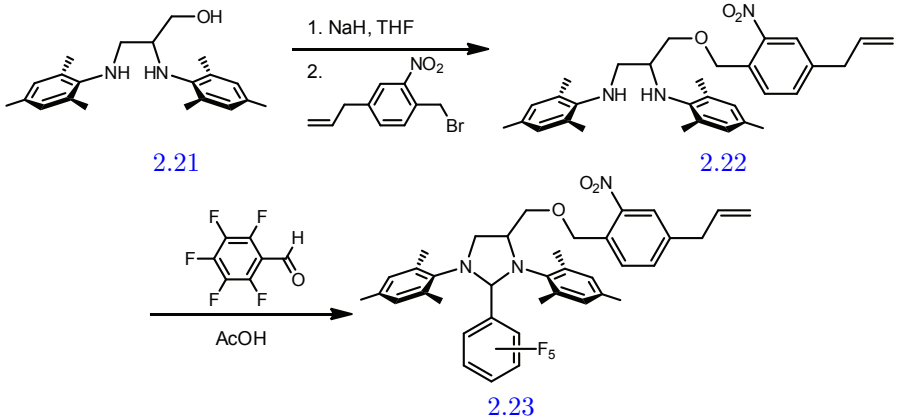

Figure 2.16: Synthesis of o-nitrobenzyl ether-containing pentafluorophenyl NHC adduct

An alternate route to an ether-containing ligand precursor was modeled after a literature report.[24] In the literature report an ether was formed prior to formation of a pentafluorophenyl adduct of an NHC ligand. In our case the same strategy was employed (Figure 2.16), and ether 2.22 was formed successfully from 2.21. Using pentafluorobenzaldehyde the NHC precursor 2.23 was formed.

This cleavable ligand has thus far not been used to characterize solid-supported catalysts. However, the scalable synthesis of ligand 2.19 replaces a more arduous synthesis that relies on a protection-deprotection strategy. The synthesis of ligand 2.23 can be used in the future to study the fate of immobilized olefin metathesis catalysts at a level of detail that has not yet been achieved.

2.5 Conclusion

An accurate assay for the level of ruthenium immobilized on silica gel was developed using rhodium as an internal standard and hydrofluoric acid in the digestion. Efforts to use a brominated alkylidene ligand as an assay for active catalyst were hampered by the nonspecific retention of the probe molecule on the silica gel. A facile, scalable route to an alcohol-bearing NHC ligand was developed by the reduction of a methyl ester-bearing NHC ligand. An *o*-nitrobenzyl ether-bearing NHC ligand was successfully synthesized for future studies of solid-supported catalysts.

2.6 Experimental Details

Materials: DigiTUBE digestion tubes, PlasmaPure brand acids, and 10,000 ppm standard solutions of ruthenium, rhodium and iridium were obtained from SCP Science (Baie-D'Urfe, Quebec) and diluted as needed to make stock solutions of internal standards and to make calibration standards. Potassium bromide (99.999% trace metals basis) and all organic precursors were purchased from Sigma-Alrich (St. Louis, MO). The potassium bromide was flame dried under vacuum before being weighed in a dry box to create a 10,000 ppm stock solution.

General procedure for ICP-MS analysis: 20-50 mg samples of solid-supported catalyst were added

to 50 mL DigiTUBE digestion tubes. 2.0 mL of PlasmaPure nitric acid and PlasmaPure hydrofluoric acid were added to each digestion tube. The digestion tubes, including a blank with only nitric and hydrofluoric acid, were then heated to 70 °C for 48 hours. After digestion a 1.0 mL aliquot of a 10 ppm rhodium solution was added to each sample, and then each sample was diluted using Milli-Q water to the 50 mL graduation.

Sample analysis was performed on an HP 4500 ICP-MS. Calibration was done using calibration standards of 10 ppb, 25 ppb, 75 ppb, 125 ppb, 250 ppb, 500 ppb, 750 ppb and 1.00 ppm of ruthenium. Each calibration standard had 200 ppb of rhodium as the internal standard. Each sample was then measured on mass channels 79, 81, 96 and 98–104 to quantify bromine, ruthenium, and rhodium. A concentration was calculated using each isotope of ruthenium separately, and the concentrations were averaged using a natural isotopic abundance-based weighted average. Whenever th signal overwhelmed the pulse mode of the detector and caused it to go into analog mode the analog signal was discarded to maintain maximum continuity, and the remaining isotopes were then used to calculate the concentration.

Preparation of 4-bromo-2-(isopropylthio)benzaldehyde (2.8). 1.52g sodium hydride (95%, 63.1 mmol) was added to a 100 mL round bottom flask in a dry box. The flask was capped with a septum, removed from the dry box, and put under argon. 40 mL of DMF was added from a SureSeal bottle via cannula. 6.3 mL of 2-propanethiol (67.8 mmol) were added via syringe at 0 °C. 5.00 g 4-bromo-2-fluorobenzaldehyde (24.6 mmol) were then added and the reaction was stirred for 24 hours. After 24 hours the reaction mixture was partitioned between hexane and water. The hexane layer was washed with water and a saturated aqueous solution of sodium chloride, and dried over magnesium sulfate. The product was pure enough to use without further purification. 4.33 g were collected for 67.9% yield. ^{1}H NMR ($CDCl_3$): δ 10.41 (s, 1H), 7.76 (d, 1H), 7.36 (d, 1H), 7.20 (d, 1H). ^{13}C NMR ($CDCl_3$): δ 191.18, 145.63, 141.06, 132.87, 130.80, 130.66, 126.11.

Preparation of 1-(4-bromo-2-(isopropylthio)phenyl)propan-1-ol (2.9). 4.33 g 2.8 (16.7 mmol) was added to a 500 mL flame-dried round bottom flask and put under argon. 250 mL of diethyl ether were added from a Strauss flask via cannula. The reaction flask was cooled to 0 °C, and 20 mL of

ethylmagnesium bromide solution (3.0 M in THF, 60 mmol) were added via syringe. The reaction was allowed to warm to room temperature. After 1 hour at room temperature a saturated aqueous solution of ammonium chloride was added slowly, dropwise at first. The organic layer was separated, and the aqueous layer was extracted twice with diethyl ether. The combined organic layers were washed with water and a saturated aqueous solution of sodium chloride, then dried over magnesium sulfate. The product was used without further purification. 4.54 g were collected for 94% yield. ^{1}H NMR ($CDCl_3$): δ 7.46-7.40 (m, 1H), 7.39 (s, 1H), 7.29 (d, 1H), 5.13-5.07 (m, 1H, OH), 3.47 (q, 1H), 3.44-3.31 (m, 1H), 1.80-1.70 (m, 2H), 1.29 (d, 6H), 0.97 (t, 3H). ^{13}C NMR ($CDCl_3$): δ 144.32, 135.09, 134.69, 133.95, 130.69, 126.80, 72.59, 39.02, 31.22, 23.32, 23.10, 10.47.

Preparation of 1-(4-(prop-1-en-1-yl)-2-(isopropylthio)phenyl)propan-1-ol (2.10). 4.54 g 2.9 (15.7 mmol) was added to a 1.0 L round bottom flask. 592 mg p-toluenesulfonic acid hydrate (3.1 mmol) was added, followed by 500 mL toluene. A Dean-Stark trap was attached and the reaction was heated at 140 °C for 6 hours. Upon cooling the reaction mixture was washed with water, a 1.0 M aqueous solution of sodium hydroxide, water again, and a concentrated aqueous solution of sodium chloride. The organic layer was dried over magnesium sulfate. The product was distilled under vacuum to give a colorless oil. ^{1}H NMR ($CDCl_3$): δ 7.44-7.16 (m, 3H), 6.98-6.90 (m, 1H), 6.22-6.10 (m, 1H), 3.41-3.23 (m, 1H), 1.91 (dd, 3H), 1.27 (d, 6H). ^{13}C NMR ($CDCl_3$): δ 138.71, 136.36, 133.90, 131.09, 129.87, 128.77, 127.78, 126.23, 38.60, 23.20, 18.93

Preparation of 4-bromo-1-(bromomethyl)-2-nitrobenzene (2.12). 10.0 g 4-bromo-2-nitrotoluene (46.3 mmol) and 20.02 g NBS (112.5 mmol) were added to a flame dried, 250 mL round bottom flask. 100 mL of benzene were added, and the resulting solution was stirred for 3 minutes. 2.58 g ABCN (10.6 mmol) were then added and the mixture was heated to reflux at 90 °C overnight. The solution is dark red with a yellow solid on the bottom. The reaction was allowed to cool in the morning and a concentrated aqueous solution of sodium thiosulfate was added. The organic layer was collected, washed with water and a concentratet aqueous solution of sodium chloride, dried over magnesium sulfate, and dried to a brown solid. The product was then purified on a silica gel column using 10% ethyl acetate in hexanes. Purified yield ranged from 80-90%. ^{1}H NMR ($CDCl_3$): δ 8.15

(d, 1H), 7.68 (dd, 1H), 7.46 (d, 1H), 4.77 (s, 2H). ^{13}C NMR ($CDCl_3$): δ 137.29, 134.35, 133.44, 132.03, 129.07, 128.80, 28.46

Preparation of (4-bromo-2-nitrophenyl)methanol (2.13). 3.0 g 2.12 (10.2 mmol) were added to a 20 mL microwave reactor vial. 5 mL THF and 15 mL water were added, the reaction vessel was sealed, and the reaction was heated to 150 °C for 1 hour with 1 minute pre-stirring. The reaction mixture was extracted three times with 50 mL diethyl ether. The combined organic layers were washed with water and a concentrated aqueous solution of sodium chloride before being dried to a yellow liquid. The product was then purified on a silica gel column using 10% ethyl acetate in hexanes. After the starting material eluded the solvent strength was increased to 50% or 100% ethyl acetate to flush out the product. Purified yield averaged around 75%. ^{1}H NMR ($CDCl_3$): δ 8.18 (d, 1H), 7.73 (dd, 1H), 7.45 (d, 1H), 5.06 (s, 1H, OH), 4.76 (s, 1H). ^{13}C NMR ($CDCl_3$): δ 137.19, 131.22, 129.17, 128.00, 125.42, 121.63, 62.11.

Preparation of (4-allyl-2-nitrophenyl)methanol (2.14). 970 mg 2.13, 850 mg allylboronic acid pinacol ester (5.1 mmol), 240 mg tetrakis(triphenylphosphine)palladium(0) (0.21 mmol) and 1.27 g cesium fluoride (8.36 mmol) were added to a Schlenk flask in the glove box. 25 mL THF were added, the vessel was sealed, and removed from the glove box. The reaction was heated to 77 °C overnight. Upon cooling the next morning water was added to the reaction and then extracted twice with diethyl ether. The combined organic layers were washed with water and a saturated aqueous solution of sodium chloride, dried over magnesium sulfate and dried to a yellow oil. The product was then purified on a silica gel column using 10% ethyl acetate in hexanes. The product was the first compound to elute. Purified yield averaged 70% ^{1}H NMR ($CDCl_3$): δ 7.93 (dd, 1H), 7.65 (d, 1H), 7.49 (d, 1H), 5.98-5.90 (m, 1H), 5.18-5.11 (m, 2H), 4.95 (s, 2H) 3.46 (d, 2H) ^{13}C NMR ($CDCl_3$): δ 141.7, 137.4, 136.0, 134.8, 131.5, 130.7, 125.4, 117.9, 62.9, 39.6

Preparation of 4-allyl-1-(bromomethyl)-2-nitrobenzene (2.15). 60 mg 2.14 (0.31 mmol) was added to a 100 mL round bottom flask. Minimal dichloromethane (about 3 mL) were added and the reaction was cooled to 0 °C. 280 mg carbon tetrabromide and 165 mg triphenylphosphine were added, and the reaction ran for 1 hour. The reaction was warmed to room temperature and diluted

with dichloromethane. It was then washed with sodium bicarbonate, water, and a saturated aqueous solution of sodium chloride. The product was dried over sodium sulfate and dried to a yellow oil. The product was purified by extraction into diethyl ether. Purified yield averaged 25%. ^{1}H NMR ($CDCl_3$): δ 7.65 (dd, 1H), 7.53 (t, 1H), 7.45 (d, 1H), 5.96-5.88 (m, 1H), 5.18-5.09 (m, 2H), 4.79 (s, 2H) 3.46 (d, 2H)

Preparation of 1,3-dimesityl-4-(methoxycarbonyl)-4,5-dihydro-1H-imidazol-3-ium bromide (2.18).[25] 5.0 g of 2.16[23] (17.85 mmol) was added to a solution of 6.15 g 2.17.[26] (30.0 mmol) and 3.43 mL DIPEA (19.65 mmol) in methanol (20 mL). The reaction was heated to reflux and stirred for 7 hours. The product was dried to a solid and triturated with hot toluene. The remaining solid was then dissolved in methylene chloride and washed with water and a concentrated aqueous solution of sodium chloride. The methylene chloride was then dried over magnesium sulfate and dried to a white powder. 2.4 g were collected for 37%. ^{1}H NMR ($CDCl_3$): δ 9.96 (s, 1H), 6.81-6.75 (m, 4H), 5.6 (dd, 1H), 4.93 (t, 1H), 4.3 (dd, 1H), 3.49 (s, 3H), 2.27-2.09 (m, 18H). ^{13}C NMR ($CDCl_3$): δ 167.55, 140.23, 129.96, 129.88, 129.75, 63.69, 53.27, 20.93 TOF-MS (ESI^+): calculated 365.2224, found 365.2293

Preparation of 4-(hydroxymethyl)-1,3-dimesityl-4,5-dihydro-1H-imidazol-3-ium bromide (2.19). 500 mg 2.18 (1.11 mmol) were added to a 25 mL flame-dried round bottom flask. 10 mL of THF were added, and the mixture was cooled to -78 °C. 70 mg LAH (1.89 mmol) were added, and the reaction was allowed to warm to room temp over 30 minutes. The reaction was worked up according to the Fieser method. 70 μL water, after 1 minute 70 μL of a 15% sodium hydroxide was added, followed by 210 μL water. The product was filtered through celite, washed with water and a saturated aqueous solution of sodium chloride, and dried over magnesium sulfate. 100 mg collected for 27% yield. ^{1}H NMR ($CDCl_3$): δ 9.82 (s, 1H), 6.93-6.90 (m, 4H), 4.62 (d, 1H), 4.45 (dd, 1H), 4.22 (d, 1H), 3.94 (t, 1H), 2.41 (s, 3H), 2.34 (s, 3H), 2.30-2.15 (s, 12H).

Preparation of diamine 2.22: A 250 mL flame-dried round bottom flask was charged with 4.56 g 2.21[22] (12.4 mmol) and 125 mL THF. 515 mg sodium hydride (60%, 12.9 mmol) was added at 0 °C. After one hour of stirring 3.26g 2.20 (12.9 mmol) was added and the reaction was heated to 80 °C

for 24 hours. After the reaction was cooled ethanol was added. The reaction was then partitioned between pentane and water, and the organic layer was washed with water and a concentrated aqueous solution of sodium bromide, and dried over magnesium sulfate. The product was purified by silica gel column using 10% ethyl acetate in hexanes. ^{1}H NMR ($CDCl_3$): 7.90 (s, 1H), 7.73 (d, 1H), 7.48 (dd, 1H), 6.83 (s, 2H), 6.82 (s, 2H), 6.00-5.92 (m, 1H), 5.21-5.13 (m, 1H), 5.0 (d, 1H), 4.96 (s, 1H), 3.66-3.62 (m, 1H), 3.48 (t, 1H), 3.43 (dd, 1H),3.38 (dd, 1H), 3.27 (q, 1H), 2.99 (quint, 1H), 2.29 (br s, 6H), 2.28 (s, 6H), 2.24 (s, 6H),

	Measured previously at UCLA	2/15/2008	4/2/2008	4/7/2008	4/15/2008
Sample 1	428.5 ppb		500.0 ppb	501.4 ppb	539.0 ppb
Sample 2	232.1 ppb		252.9 ppb	256.7 ppb	274.5 ppb
Sample 3	408.2 ppb		532.0 ppb	532.5 ppb	559.0 ppb
Sample 4	575.3 ppb		713.7 ppb	700.5 ppb	700.1 ppb
Sample 5	573.6 ppb		853.8 ppb	831.2 ppb	837.5 ppb
Sample 6	684.0 ppb		950.2 ppb	915.2 ppb	929.7 ppb
Sample 7		134.4 ppb	208.1 ppb	210.6 ppb	213.0 ppb
Sample 8		460.3 ppb	434.1 ppb	452.0 ppb	446.1 ppb
Sample 9		463.3 ppb	490.4 ppb	529.1 ppb	516.7 ppb
Sample 10		157.3 ppb	177.4 ppb	190.1 ppb	193.0 ppb
Sample 11		704.5 ppb	906.5 ppb	902.4 ppb	915.4 ppb
Sample 12		696.3 ppb	895.5 ppb	903.3 ppb	912.9 ppb
Sample 13		143.6 ppb	176.3 ppb	181.1 ppb	193.9 ppb
Sample 14		135.0 ppb	172.5 ppb	182.4 ppb	191.2 ppb

Table 2.1: ICP-MS results from Figure 2.3

	Sample A	Sample B	Sample C	Sample D
Ruthenium Concentration in Solution	737 ppb	783 ppb	200 ppb	103 ppb
Bromine Concentration in Solution	627 ppb	28 ppb	211 ppb	100 ppb

Table 2.2: ICP-MS active catalyst assay results

References

[1] J.C. Mol. Industrial applications of olefin metathesis. *Journal of Molecular Catalysis A—Chemical*, 213(1):39–45, 2004.

[2] J. Cossy, S. Arseniyadis, and C. Meyer, editors. *Metathesis in Natural Product Synthesis*. Wiley-VCH, 2010.

[3] K. Zaidi. General Chapter on Inorganic Impurities: Heavy Metals. *Pharmacopeial Forum*, 34(5):1345–1348, 2008.

[4] Information concerning EMEA regulations can be found at http://www.emea.europa.eu/pdfs/human/swp/444600en.pdf.

[5] G.C. Vougioukalakis. Removing Ruthenium Residues from Olefin Metathesis Reaction Products. *Chemistry—A European Journal*, 18(29):8868–8880, 2012.

[6] O.A. Ferretti and M.L. Casella. Transition Metal Single Site Catalysts-From Homogeneous to Immobilized Systems. In J.-M. Basset, R. Psaro, D. Roberto and R. Ugo, editor, *Modern Surface Organometallic Chemistry*, pages 167–238. Wiley-VCH, 2009.

[7] A. Corma, E. Gutierrez-Puebla, M. Iglesias, A. Monge, S. Perez-Ferreras, and F. Sanchez. New Heterogenized Gold(I)-heterocyclic Carbene Complexes as Reusable Catalysts in Hydrogenation and Cross-Coupling Reactions. *Advanced Synthesis & Catalysis*, 348(14):1899–1907, 2006.

[8] J.A.M. Brandts and P.H. Berben. Application of Immobilized Rhodium Catalyst Precursors in Enantio- and Chemoselective Hydrogenation Reactions. *Organic Process Research & Development*, 7(3):393–398, 2003.

[9] K. Smith and C.H. Liu. Asymmetric Epoxidation Using a Singly-bound Supported Katsuki-type (salen) Mn Complex. *Chemical Communications*, (8):886–887, 2002.

[10] M.A. Kwon and G.J. Kim. Synthesis of Polymeric Salen Complexes and Application in the

Enantioselective Hydrolytic Kinetic Resolution of Epoxides as Catalysts. *Catalysis Today*, 87(1–4):145–151, 2003.

[11] D. Amoroso, G.P.A. Yap, and D.E. Fogg. Deactivation of Ruthenium Metathesis Catalysts via Facile Formation of Face-bridged Dimers. *Organometallics*, 21(16):3335–3343, 2002.

[12] D. Amoroso, J.L. Snelgrove, J.C. Conrad, S.D. Drouin, G.P.A. Yap, and D.E. Fogg. An Attractive Route to Olefin Metathesis Catalysts: Facile Synthesis of a Ruthenium Alkylidene Complex Containing Labile Phosphane Donors. *Advanced Synthesis & Catalysis*, 344(6–7):757–763, 2002.

[13] S.H. Hong, M.W. Day, and R.H. Grubbs. Decomposition of a Key Intermediate in Ruthenium-Catalyzed Olefin Metathesis Reactions. *Journal of the American Chemical Society*, 126(24):7414–7415, 2004.

[14] M.B. Herbert, Y. Lan, B.K. Keitz, P. Liu, K. Endo, M.W. Day, K.N. Houk, and R.H. Grubbs. Decomposition Pathways of Z-Selective Ruthenium Metathesis Catalysts. *Journal of the American Chemical Society*, 134(18):7861–7866, 2012.

[15] J.P. Collman, J.A. Belmont, and J.I. Brauman. A Silica-Supported Rhodium Hydroformylation Catalyst—Evidence for Dinuclear Elimination. *Journal of the American Chemical Society*, 105(25):7288–7294, 1983.

[16] R.S. Drago and D.C. Pribich. A New Method for Enhancing Site Isolation on Silica-Gel and for Improving the Lifetime of Site-Isolated Catalysts. *Inorganic Chemistry*, 24(13):1983–1985, 1985.

[17] D.A. Annis and E.N. Jacobsen. Polymer-supported chiral Co(salen) complexes: Synthetic applications and mechanistic investigations in the hydrolytic kinetic resolution of terminal epoxides. *Journal of the American Chemical Society*, 121(17):4147–4154, 1999.

[18] D.P. Allen, M.M. Van Wingerden, and R.H. Grubbs. Well-Defined Silica-Supported Olefin Metathesis Catalysts. *Organic Letters*, 11(6):1261–1264, 2009.

[19] A. Hejl. *Controlling Olefin Metathesis Through Catalyst and Monomer Design*. PhD thesis, California Institute of Technology, 2007.

[20] A. Ben-Asuly, E. Tzur, C.E. Diesendruck, M. Sigalov, I. Goldberg, and N.G. Lemcoff. A thermally switchable latent ruthenium olefin metathesis catalyst. *Organometallics*, 27(5):811–813, 2008.

[21] Information from the EPA on isotopic dilution mass spectrometry can be found at http://www.epa.gov/wastes/hazard/testmethods/sw846/pdfs/6800.pdf.

[22] M. Mayr, M.R. Buchmeiser, and K. Wurst. Synthesis of a silica-based heterogeneous second generation Grubbs catalyst. *Advanced Synthesis & Catalysis*, 344(6–7):712–719, 2002.

[23] K.M. Kuhn and R.H. Grubbs. A facile preparation of imidazolinium chlorides. *Organic Letters*, 10(10):2075–2077, 2008.

[24] C. Lang, U. Gaertner, and O. Trapp. Catalysts by the meter: rapid screening approach of N-heterocyclic carbene ligand based catalysts. *Chemical Communications*, 47(1):391–393, 2011.

[25] This reaction protocol was developed by Myles Herbert.

[26] B. Moon, S. Han, and D. Kim. Efficient synthesis of highly functionalized cyclic aminimides. *Organic Letters*, 7(15):3359–3361, 2005.

Chapter 3

Ethenolysis and Ring-Closing Metathesis in Microfluidic Devices

In order to improve the efficiency of multi-phase olefin metathesis reactions, a series of novel microfluidic reactors were designed and built to increase phase contact areas. Two reactor designs were explored to achieve increased phase contact areas: segmented flow and parallel flow reactors. In the segmented flow reactor the gas and liquid phases flow in the same channel in alternating gas bubbles and liquid slugs. Using ethylene as the gas phase gave enhanced ethenolysis at lower pressures. In the parallel flow reactors the liquid phase flows through a gas permeable microfluidic channel which is in direct contact with the gas phase. Using an active vacuum as the gas phase in the parallel flow reactor gives enhanced ring-closing metathesis at low catalyst loadings. The use of ethylene as the gas phase in the parallel flow reactor was hampered by leakage found at the high pressures typically used for ethenolysis.

3.1 Introduction

The use of microfluidic devices in chemical processes has provided new strategies, opportunities and challenges.[1–4] The high surface area-to-volume ratios and rapid mixing result in highly precise control of reaction variables, as well as unparalleled rates of mass and thermal transfer.[4] These systems offer the benefits of reduced waste, higher yields, and reduced reaction times. Furthermore, the difficulties of scale-up so prevalent in batch reactions can largely be avoided by simple and seamless parallelization of small-scale microfluidic test reactors.

In addition to traditional, one-step microchemical reactions, several consecutive reactions, including separation, purification, and detection, have been successfully integrated as complete microchemical processes.[5–7] The repertoire of microfluidic reactors has rapidly increased to approach the goal of replicating the entire lab on a chip, but certain chemical transformations remain challenging

in these systems.

A particularly challenging type of microchemical system is the heterogeneous reaction involving any combination of the gas, liquid, and solid phases.[8–12] Solid-liquid and solid-gas biphasic systems have been reported and generally rely on the immobilization of the solid phase in the reaction channels. Liquid-liquid systems have also been reported using multiple liquid phases in laminar flow conditions.[13] However, in the case of liquid-gas systems no immobilization is possible and laminar flow is not feasible due to the high viscosity difference that leads to the formation of bubbles.

To overcome the challenges inherent to liquid-gas biphasic microfluidic systems two main strategies have been developed,[14–16] one with the two phases flowing in contact in parallel, the other with alternating bands of gas bubbles and liquid slugs. The use of gas bubbles and liquid slugs requires less technological development, due mainly to the simple, convenient setup and a broader choice of available capillary materials, allowing better chemical stability and mechanical strength even at high pressure. This segmented flow strategy is simple enough that it can often be applied to existing microfluidic devices. However, while increasing the interfacial contact area relative to that available in a traditional reaction flask, this approach does not achieve the exceptionally high contact area typical of other microfluidic devices. The use of gas permeable membranes does achieve the desired high contact area, but relies on new materials and cannot be applied to standard microfluidic devices. Systems have been reported using layers of polydimethylsiloxane (PDMS) that are thin enough to allow gas to permeate[17] and using material that is specifically designed to allow for the passage of gases.[18–22] However, these systems have mainly been tested for reactions involving simple inorganic gases, such as H_2, O_2 and NH_3, and their suitability for reactions involving ethylene has not been demonstrated.

Liquid-gas biphasic reactions are important in olefin metathesis, where many reactions either produce or consume volatile, low molecular weight olefins such as ethylene. In cross metathesis (CM) and ring-closing metathesis (RCM) one equivalent of ethylene is liberated.[23,24] In ethenolysis, a reaction long studied for its potential industrial applications, large volumes of ethylene are consumed (Figure 3.1).[25] The ability to facilitate the absorption and release of ethylene into and out of solution

is key for these reactions.

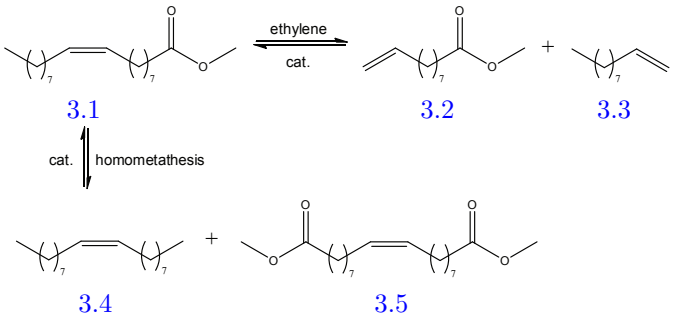

Figure 3.1: Ethenolysis of methyl oleate and the competitive homometathesis to form 3.4 and 3.5

A particular difficulty in ethenolysis reactions is the competing homometathesis reaction (Figure 3.1). This competing reaction is generally favored due to the poor solubility of ethylene in methyl oleate (mole fraction of ethylene/methyl oleate = 0.108, 60 psi)[26] and the slow diffusion of ethylene into solution. To overcome the bias for homometathesis two strategies can be pursued: developing catalysts with high kinetic selectivity for ethenolysis and developing processes to drive ethylene into the reaction. A number of catalyst development studies have found catalysts that show unusually high propensity to effect ethenolysis.[25,27,28] The focus of this research, however, is process development. The transfer of the ethylene into the methyl oleate phase was maximized with high diffusion efficiency by increasing the contact area between the methyl oleate and ethylene.[14–16]

3.2 Ethenolysis Using Segmented Gas/Liquid Flow

The work presented in this section was performed at Chungnam National University in collaboration with Dr. Chan-pil Park and Prof. Dong-pyo Kim. Reprinted with permission from Park, C.P.; Van Wingerden, M.M.; Han, S.-Y.; Kim, D.-P.; Grubbs, R.H. *Organic Letters* **2011**, *13* 2398. Copyright 2011 American Chemical Society.

A facile and efficient microchemical system for ethenolysis was developed and then tested under various reaction conditions. The development of the system proceeded in two phases. First the physical parameters of reactor setup, mixing, pressure and temperature were explored, and then ethenolysis was tested within the feasible physical parameters.

This system uses a continuous segmented flow of ethylene and methyl oleate in a capillary tube

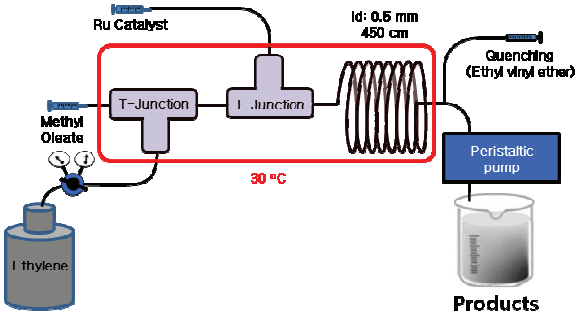

Figure 3.2: Initial strategy for the segmented flow ethenolysis reactor

with 0.5 mm inner diameter. The methyl oleate was pre-mixed with catalyst in nearly solvent-free conditions, except for a minimum amount of toluene to dissolve the catalyst (1.0 mg catalyst in 2.0 mL toluene), which avoids the use of excess organic solvent to facilitate the dissolution of ethylene gas as has been reported.[29,30]

Two modes of mixing were investigated in an attempt to minimize undesired homometathesis. In the initial setup homometathesis was limited by premixing the methyl oleate and ethylene gas at the first T-junction before any catalyst was introduced (Figure 3.2). The catalyst solution was then added to the ethylene-rich mixture at a second T-junction, forming larger slugs of the liquid phase. However, the distribution of catalyst was difficult to control due to the irregular flow rates between T-junctions and irregular sized liquid slugs. To overcome this challenge the methyl oleate and catalyst solution were mixed at the first T-junction and the ethylene was added at the second T-junction (Figure 3.3). To limit the homometathesis that would occur in the first mixing zone where no ethylene is present the first mixing zone was cooled in a 0 °C ice bath. Homometathesis of methyl oleate does not occur at 0 °C and the catalyst mixes evenly with the methyl oleate when the two are combined directly.

In both mixing strategies, injection of the liquid streams was done using syringe pumps and the ethylene was added by a direct connection to the pressure regulator of an ethylene tank. Overall flow control, necessary to prevent uncontrolled ethylene venting and sharp pressure gradients, was achieved using a peristaltic pump placed at the end of the channel, rather than the more traditional back pressure regulator. The only physical limitation that was found in this setup was that when

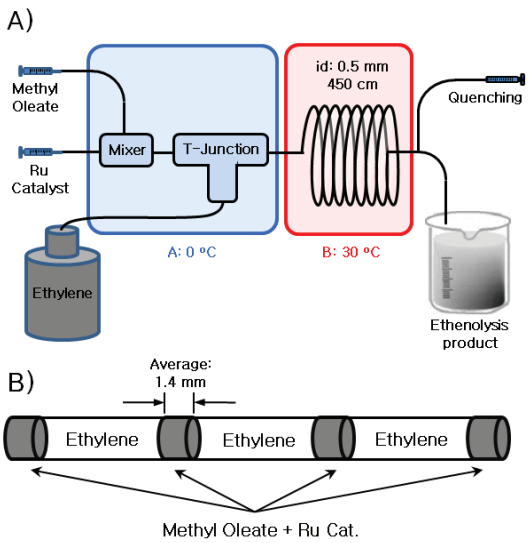

Figure 3.3: (A) Microchemical ethenolysis of methyl oleate 3.1 with Ru catalyst (1.0 mg/2 mL toluene). (B) Segmented flow of ethylene and methyl oleate in a capillary microreactor

the inlet pressure exceeded 60 psi the syringe pumps became overpowered and failed to inject any liquid. Pressure limitations are technical difficulties that can arise in all microfluidic reactors, and are generally overcome with the use of more robust and powerful pumps, such as those used in HPLC systems. However, in our case such pumps were not immediately available and the research progressed using 60 psi as the maximum pressure.

A potential concern unique to segmented flow reactors is the pressure drop across the length of the microfluidic channel. The constant wetting and drying of the channel walls by the bubbles and slugs causes an increase in friction for the moving liquid. However, in this case the pressure drop was found to be minimal, when the ethylene regulator was set to 60 psi the pressure at the peristaltic pump was measured at 56 psi. The difference in pressure and the resulting difference in ethylene solubility were therefore considered to be negligible.

The segmented flow reactor, once optimized for all physical parameters, was tested for ethenolysis. As the effects of pressure and temperature in the batch system have been well documented in reports of batch reactions,[25–27,31,32] the same variables were carefully studied in the microfluidic system. Initial optimization of reactor setup, ethylene pressure, temperature and dwell time was done using catalyst 3.6 (Figure 3.5).

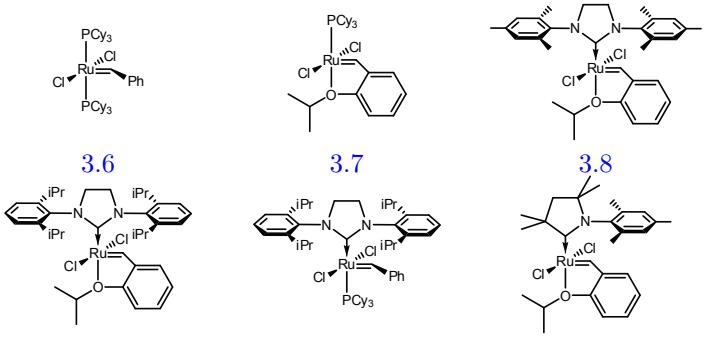

3.6 3.7 3.8

3.9 3.10 3.11

Figure 3.4: Important catalysts for ethenolysis

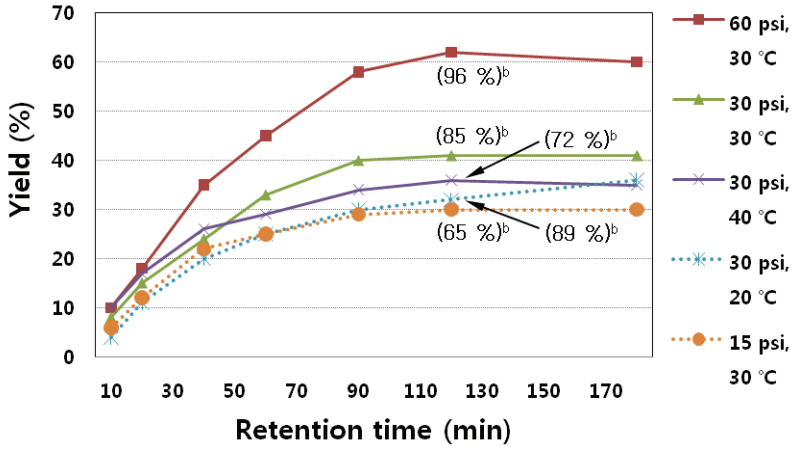

Figure 3.5: Ethenolysis under different temperature and pressure conditions. Catalyst 3.6 (300 ppm) was used. (a) Yield (%)=conversion × selectivity = (1 - final moles of 3.1/initial moles of 3.1) × {(3.2 + 3.3)/(3.2 + 3.3 + 3.4 + 3.5)} × 100. Conversion and selectivity were determined by GC analysis. (b) Selectivity after 120 min dwell time

With 300 ppm of 3.6 (Figure 3.4), the pressure was varied from 15 to 60 psi and the temperature was varied from 20 to 40 °C. The results illustrate that the pressure of ethylene has a direct impact on the yield (Figure 3.5). Elevating the temperature over 30 °C resulted in a 5% loss in the net yield after 120 min, due to the decreased selectivity (30 psi and 30 °C: 48% conversion, 85% selectivity, 30 psi and 40 °C: 50% conversion, 72% selectivity). These good results at low temperature and high pressure are well consistent with the batch studies, where the same factors increase the selectivity and yield of ethenolysis.[25–27,31,32]

To fully test the efficacy of the ethenolysis of methyl oleate 3.1 in the segmented flow reactor, a total of six ruthenium catalysts were used (Figure 3.4). In addition to standard catalysts 3.6, 3.7 and 3.8, catalysts known to be more effective for ethenolysis were tested. Second generation catalysts

Table 3.1: Ethenolysis of methyl oleate 3.1 in the segmented flow microfluidic reactor

	cat. (ppm)	t (°C)	time (min)	conv. (%)[c]	select. (%)[d]	yield (%)[e]
1	3.6(150)	0	180	3	99	3.0
2	3.6(300)	30	120	65	96	62.4
3	3.6[b](300)	30	120	66	91	60.1
4	3.7(100)	30	120	39	94.8	37.0
5	3.7(300)	30	120	69	93.7	64.7
6	3.8(50)	40	60	58	45	26.1
7	3.8(100)	30	120	59	43.5	25.7
8	3.8(100)	40	60	61	41	25.0
9	3.9(50)	40	60	54	52	28.1
10	3.9(100)	40	60	57	50	28.5
11	3.10(50)	40	40	61	58	35.4
12	3.10(100)	40	40	63	55	34.7
13	3.11(50)	40	60	80	87	69.6
14	3.11(100)	40	60	81	84	68.0
15	3.11(100)	40	30	72	88	63.4

[a]General reaction conditions: 60 psi ethylene, the microchemical system described in Figure 3.3A. Conversion and selectivity were determined by GC analysis. [b]No cooling of the mixing zone. [c]Conversion = (1 - final moles of 3.1/initial moles of 3.1) × 100. [d]Selectivity (%)=(3.2 + 3.3)/(3.2 + 3.3 + 3.4 + 3.5) × 100 [e]Yield (%) = conversion×selectivity/100.

3.9 and 3.10, as well as cyclic (alkyl)(amino)carbene (CAAC)-based catalyst 3.11[33] have been used extensively in ethenolysis testing and were therefore selected.[25] Each catalyst was screened at a variety of catalyst loadings, and the results were tabulated (Table 3.1). When catalyst 3.6 was used at 0 °C only a negligible amount of product was formed, confirming that no olefin metathesis occurs in the first cooled mixing zone as was expected in the redesigned system (entry 1). When the first mixing section was not cooled, an increase in homometathesis was observed as expected (entry 3). Hoveyda-type catalyst 3.7 was slightly more effective than catalyst 3.6 (entries 4 and 5), and the typical second generation catalyst 3.8 gave the poorest results in selectivity and yield, although the more active catalyst required less time than catalysts 3.6 and 3.7 to achieve a similar conversion (entries 6-8). The second generation catalysts 3.9 and 3.10, which contain a sterically hindered NHC ligand, also gave lower yields than PCy_3-based catalysts 3.6 and 3.7 (entries 9-12), even though it is known that catalysts with NHC ligands have better stability and activity toward olefin metathesis than catalysts with PCy_3 ligands. In this case the homocoupling reaction, while not significant for phosphine-based catalysts 3.6 and 3.7, accounted for about half the activity of the NHC-based catalysts 3.8, 3.9, and 3.10. The result from catalyst 3.11 is the most noteworthy

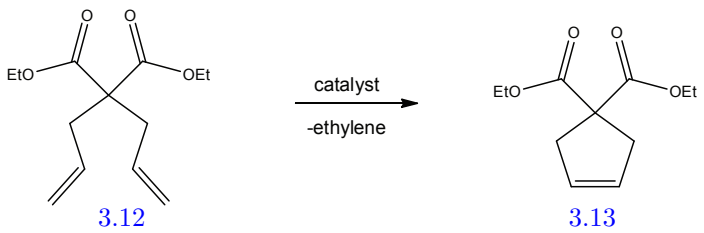

3.12 3.13

Figure 3.6: Ring-Closing Metathesis of 3.12 to form 3.13

as the catalyst is currently the most selective catalyst known for ethenolysis among the NHC-based catalysts. Catalyst 3.11 gives the highest yield in this study, even when compared with PCy_3-based catalysts 3.6 and 3.7. Catalyst 3.11 gave a 69.6% yield with only 50 ppm catalyst and a 60 min dwell time (entry 13). The selectivity is comparable to the result of the batch reaction tested at higher pressure (selectivities up to 83% were measured at 150 psi), but because of the higher conversion the yield was higher in the microchemical system.[25] Additionally, the selectivities of catalysts 3.6, 3.7, 3.8, 3.9, and 3.10 are superior in the microchemical system at 60 psi compared to the batch reaction at 150 psi.

Overall, the results at 60 psi of ethylene were comparable to the results of batch reactions at 150 psi of ethylene. This is expected to be due to the high surface area-to-volume ratio suitable for fast mass transfer of the gas into the solution phase. The sterically hindered CAAC-based ruthenium catalyst 3.11 gave 80% conversion and 87% selectivity for a yield of 69.5% with only 50 ppm catalyst.

Because of the success of the segmented flow reactor for ethenolysis the application of this system to ring-closing metathesis was explored. Using the same PTFE tubing and standard reactions conditions (0.1 M, 30 °C, 1 mol % 3.8),[34] RCM of diethyl diallyl malonate 3.12 was attempted. Conversion, which under batch conditions reaches completion in about 20 minutes, in this case tops out at 35-40 % (Figure 3.7A).

The poor reactivity in this case can be ascribed to product inhibition. At the relatively high concentrations of substrate used, a significant amount of ethylene is released and begins to favor the back reaction of ring-opening metathesis because of the confined reaction space. To overcome this product inhibition a means to allow the ethylene to escape was needed. A strategy of sonication-

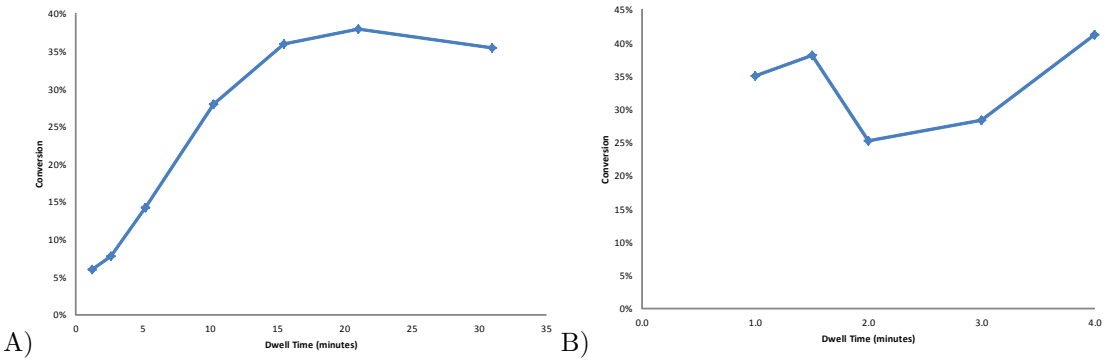

A) B)

Figure 3.7: RCM of 3.12 in PTFE Tubing without sonication (A) and with sonication (B)

induced bubble formation was used. The reaction only reached about 40 % conversion, but was unpredictable and erratic due mainly to unpredictable flow rates caused by the bubbles that were formed in the reaction (Figure 3.7B). In addition to irreproducible results, the microreactor began to be damaged after sustained exposure to sonication so further optimization was precluded.

3.3 Ring-Closing Metathesis Using a Permeable Membrane

As previously mentioned, the segmented flow reactor does not give as high of contact surface area as the parallel flow reactors. This, combined with the difficulty in using segmented flow reactors for RCM, led us to develop a parallel flow reactor.

A key requirement of parallel flow reactors with gas and liquid phases is the use of gas permeable, liquid impermeable membranes. Interesting materials for this are copolymers of perfluoro-2,2-dimethyl-1,3-dioxole-tetrafluoroethylene and tetrafluoroethylene, a formulation of which is commercially available under the name Teflon® AF 2400 (Figure 3.8). The bulky perfluoro-2,2-dimethyl-1,3-dioxole-tetrafluoroethylene comonomer disrupts the crystallinity of the perfluorinated polymer in much the same way that trimethylsilyl groups break up the crystallinity of poly(trimethylsilyl propyne) (PTMSP), giving high free volume and permeability in the resulting material.[35,36] An advantage of using the fluorinated bulky monomer over the bulky trimethylsilyl groups is that the desirable properties of perfluorinated polymers, chemical and mechanical stability, are largely maintained.[37,38] Teflon AF 2400, to a first approximation, can therefore be viewed as a gas permeable

Table 3.2: Permeability of Teflon AF 2400

Gas	P^b	Gas	P^b
He	2740	CH_4	435
H_2	2400	C_2H_2	480
O_2	1140	C_2H_4	325
N_2	554	C_2H_6	252
CO_2	2600	C_3H_8	97

[a]Measured at 22-30 °C.
[b]P (Barrer) = 10^{-10} (cm^3 gas (STP)) cm cm^{-2} s^{-1} $cmHg^{-1}$.

analog of PTFE polymers.

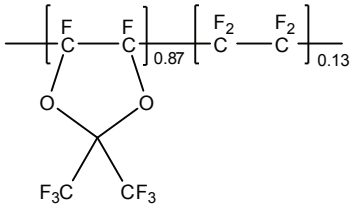

Figure 3.8: Microstructure of Teflon AF 2400

The gas permeability and physical properties in general of Teflon AF 2400 have been extensively studied (Table 3.2).[36,39–43] The experimental results show that the permeability of the material appears to be limited to small gases. Helium, hydrogen and carbon dioxide permeate particularly well, but the material does show permeability to C1 and C2 hydrocarbons in a trend inversely correlated with size (acetylene > ethylene > ethane). The permeability drops significantly for propane. As previously mentioned, existing literature reports on Teflon AF 2400 used in microfluidic reactors focus on the use of small, inorganic gases, particularly hydrogen. In the research described in this chapter we sought to apply this material to reactions involving ethylene gas.

The initial concept for the parallel flow reactor was similar to a reactor previously reported by our collaborators.[17] In the previous study a thin layer of PDMS was used as a gas permeable membrane in a PDMS microfluidic chip (Figure 3.9). In our study PDMS was not suitable as a membrane because of the swelling caused by nonpolar organic solvents and substrates, so a 350 μm thick sheet of Teflon AF 2400 was used. Unfortunately, due to the difficulty of bonding the Teflon AF 2400 to the PDMS reactor body a gas tight seal could not be achieved and reactions could not be carried out.

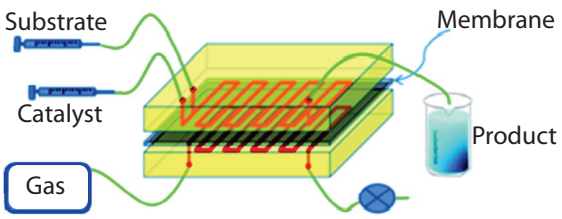

Figure 3.9: Initial parallel flow reactor design

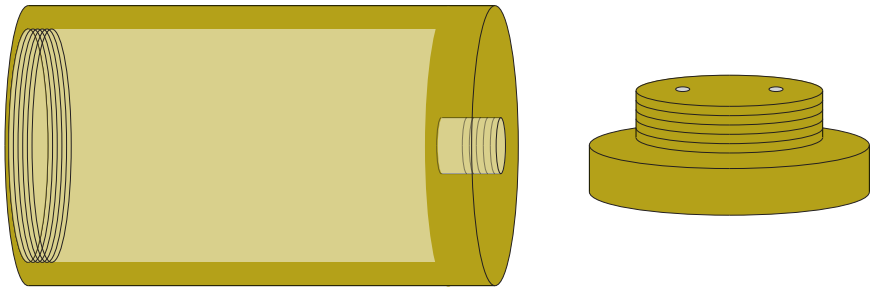

Figure 3.10: Diagram of the polysulfone reactor body and cap

Instead of using a flat membrane, Teflon AF 2400 tubing was used. This tubing is available in a variety of wall thicknesses and inner diameters, in order to balance the brittleness of the material against the gas permeability (thicker walls have increased strength but decreased permeability) 800 μm o.d. (600 μm i.d.) tubing was used. The 100 μm thick walls showed high permeability to ethylene and were only marginally susceptible to kinking and collapsing. This size also has the advantage of fitting into 1/32 inch HPLC fittings, giving a simple, airtight connection strategy.

To place the liquid flowing through the gas permeable tubing in contact with a parallel gas phase, a gas tight reactor body was prepared. The initial reactor body was prepared from a bored out section of polysulfone rod which was 2 inches wide and 1 foot long. On one end a 1/4 inch National Pipe Thread (NPT) female fitting was cut in and on the other end a full width fitted cap was prepared from a section of the 2 inch polysulfone rod (Figure 3.10). In the 1/4 NPT fitting a vacuum adapter was attached. In the cap two holes were drilled with 1/4-28 threads. These two holes fit HPLC fittings and allow for the passage of traditional polyether ether ketone (PEEK) based HPLC tubing while maintaining the gas tight seal on the reactor body. The reactor walls were 1/2 inch thick, which proved to be strong enough to be put under vacuum.

The substrate and catalyst, supplied by syringe pumps, were joined in a T-junction just outside

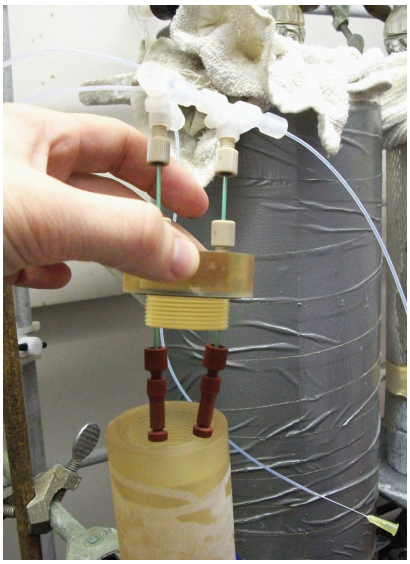

Figure 3.11: Photo of the initial polysulfone reactor

the reactor body. The mixture was then passed through one of the holes in the cap in a short section of 1/16 inch HPLC tubing (Figure 3.11). Once inside the reactor body the 1/16 inch tubing was coupled to the 3m long, 1/32 inch diameter Teflon AF 2400 tubing. On the other side the Teflon AF 2400 tubing was again coupled to standard HPLC tubing and passed through the cap. To prevent continued and uncontrolled reactivity beyond what is achieved in the microfluidic channel, a second T-junction was placed just outside the cap to introduce a quenching solution, also supplied by a syringe pump.

The polysulfone reactor body with Teflon AF 2400 tubing was first tested using the standard conditions of RCM. In the body of the reactor, however, instead of introducing a vacuum, an atmosphere of argon was introduced. In this case the maximum conversion again reached 35-40% before leveling out (Figure 3.12A), similar to the results in regular PTFE tubing. Additionally, gas bubbles could clearly be seen in the flow on the outlet side. Either ethylene gas was being formed and could not spontaneously escape fast enough, or argon was diffusing in through the tubing and escaping out the end of the reactor due to the slight overpressure of argon in the system (provided mainly by the bubbler on the argon manifold). The potential that argon was diffusing into the reaction was supported by later experiments with ethylene pressure, but regardless of the exact composition of the gas bubbles the RCM reaction was not effectively carried out.

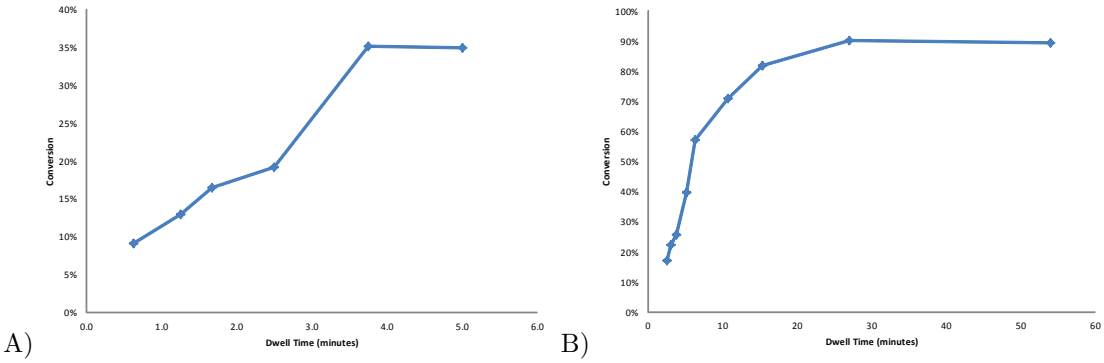

A) B)

Figure 3.12: RCM of 3.12 (0.1 M, 1 mol% catalyst loading) in Teflon AF 2400 tubing under argon (A) and vacuum (B)

The limited success of RCM of 3.12 in standard PTFE tubing or in Teflon AF 2400 tubing under an argon atmosphere were overcome by using the Teflon AF 2400 tubing under vacuum. In this case RCM quickly surpasses the limitation of the other setups and reaches 90% conversion (Figure 3.12B). Additionally, when vacuum was used no bubbles were present in the outflow of the reactor. Whether this was due to a lack of argon to diffuse in or the escaping of the ethylene out, it provided a simple visual test of the efficacy of the Teflon AF 2400 tubing. However, while these results were an improvement from the previous microfluidic results, they were lagged behind the results reported for the batch reaction, although by only a few percent at each time point.[34] Because of this apparent limitation, the reactor design was revisited.

A key item of control that is lacking from the simple polysulfone tube-style reactor is temperature control. Both heat transfer and mass transfer are very rapid in microfluidic reactors, and devices with either highly effective heating or highly effective transfer of gases are well known,[4] but the combination of temperature control and heat control remains challenging. In our situation, two methods to overcome this limitation in the context of the polysulfone tube reactor were attempted. Preheating the substrate and catalyst solution in a warm water bath was the first and simplest method, but was not found to give improved results. This was also found to be undesirable as potentially heat-sensitive catalysts would be heated for a significant period of time before reaching the reaction chamber. It was then unclear if the reaction solution maintained temperature for any amount of time, the rapid heat transfer of microfluidic reactors having potentially become a problem.

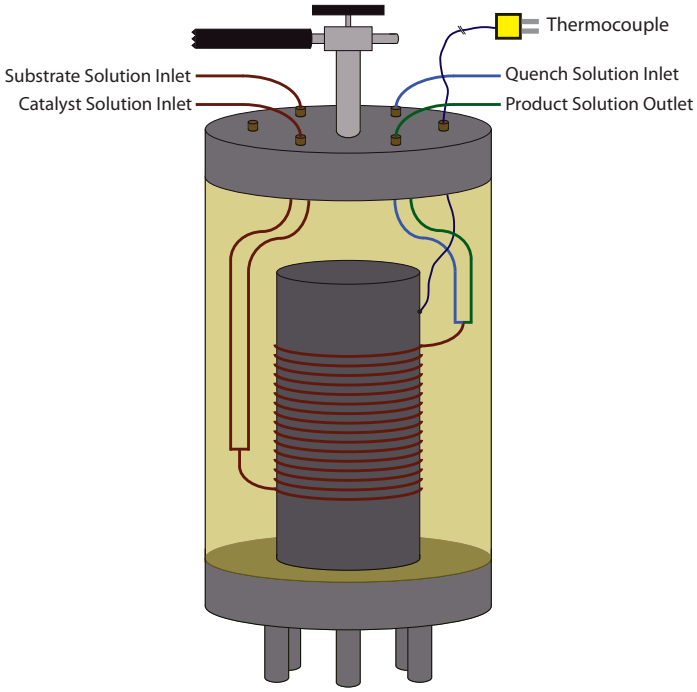

Figure 3.13: Heated microfluidic reactor

Heating the outside of the reactor body was the second method employed. A section of thermal tape was wrapped around the polysulfone tube and heated at various voltages from a Variac power supply. A long-stemmed thermocouple was then inserted into the reactor body through a hole drilled in the cap. The thermocouple was sealed into the cap using a quick-setting epoxy glue so that the reactor could again be put under vacuum. However, the thermocouple did not detect any heating in the interior of the reactor, even though the outside of the reactor was uncomfortably hot. A new heating method was sought that would more directly heat the reaction.

To simultaneously heat the reaction and place it under vacuum, a new reactor was designed and fabricated. The new reactor had a heated center spool, made of stainless steel, inside a gas tight chamber that was surrounded by a polysulfone sheath and closed with a stainless steel cap (Figure 3.13). The heated center core, which was 2 inches in diameter, was designed with interior divisions so that heated oil, when pumped into the center, would flow up through the center and out along the edges, heating the outside of the core (Figure 3.14). Since the heating spool acted as a cap for the bottom of the reactor, the polysulfone body, which was 4 inches in diameter with a wall thickness of 1/2 inch, was open and threaded at both ends. The vacuum adapter had to be shifted from the

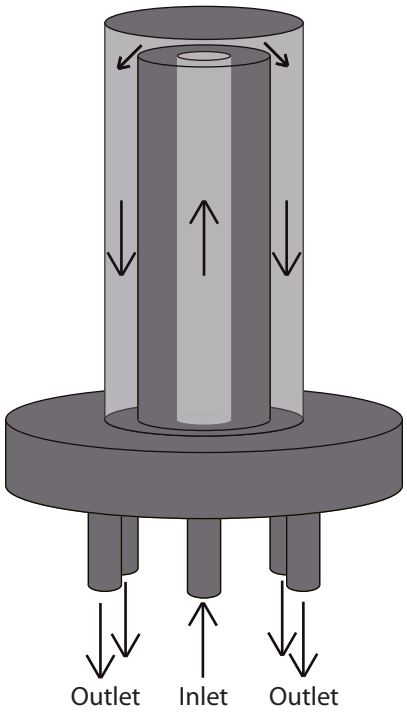

Figure 3.14: Heating element

bottom to the top of the reactor, so the reactor cap was fabricated with the vacuum adapter in the center and 6 HPLC fittings (1/4-28) arranged in a hexagon around it. The cap was made of stainless steel because the extra stress introduced by tightening the vacuum adapter into the center cracked the initial polysulfone cap. The extra HPLC fittings were used for temperature probes and so that the substrate, catalyst, and quenching solutions could all be mixed directly in the reactor body. By mixing and quenching in the reactor body the dead time, where the reaction had been mixed but was not heated or in the permeable tubing, could be limited to a minimum (the exact dead time depends on the flow rate, but is approximately 1% of the total dwell time of the reaction in all cases).

Once the heated microfluidic reactor was fabricated and successfully tested for leaks, the heating spool was tested. Oil, warmed in a controlled-temperature bath, was pumped by a peristaltic pump into the center of the heating element. The returned oil was channeled by plastic tubing back into the warm oil bath. The oil bath was set to a range of temperatures, and the temperature of the heating spool was monitored by thermocouples affixed to the top and bottom of the spool. The

A) 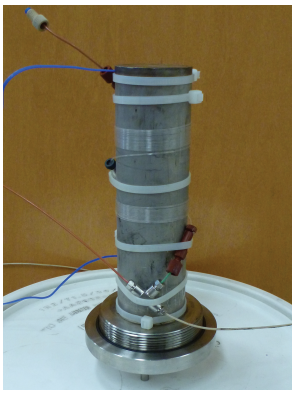 B) 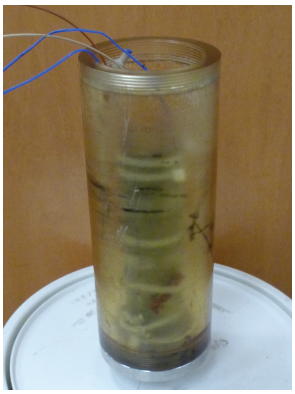 C) 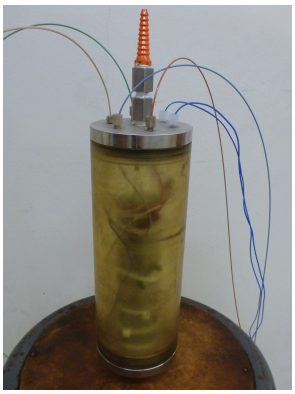

Figure 3.15: Photos of the heated microfluidic reactor. A) Heating spool wound with microfluidic tubing. B) Heating spool with polysulfone sheath. C) Assembled reactor

difference in temperature between the top and bottom of the spool was found to be negligible (less than 3 °C in all circumstances) but the difference in temperature between the oil bath and the heating spool surface ranged from 5 to 15 °C, and therefore at each temperature setting the system had to equilibrate and the temperature had to be measured. Reaction temperatures (measure at the heating spool) up to 50 °C were easily achieved, while temperatures above 50 °C required the oil to be heated to 70 °C which shortened the useful life of the tubing in the peristaltic pump to the point that it became difficult to complete a reaction before the tubing broke and had to be replaced.

The suitability of the heated microfluidic reactor was investigated for cross metathesis. A standard screening reaction was used, the cross between hexenyl acetate and methyl acrylate (Figure 3.16). Unfortunately, while the reaction proceeded smoothly it did not exhibit the enhanced performance over batch reactions (Figure 3.17), and was therefore not pursued any further.

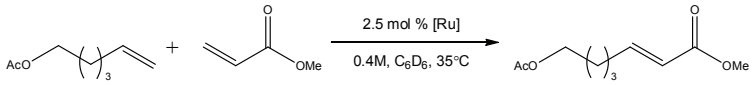

3.14 (1 equiv) 3.15 (1 equiv) 3.16

Figure 3.16: Cross metathesis to form 3.16

Because of consistently high yields and practical ease of RCM of 3.12 under general batch conditions, a more rigorous test of the new microfluidic reactor was devised. Following previous work in our group highlighting the potential of ruthenium-based olefin metathesis catalysts to be effective at low catalyst loadings,[24] RCM was tested using ppm levels of catalyst.

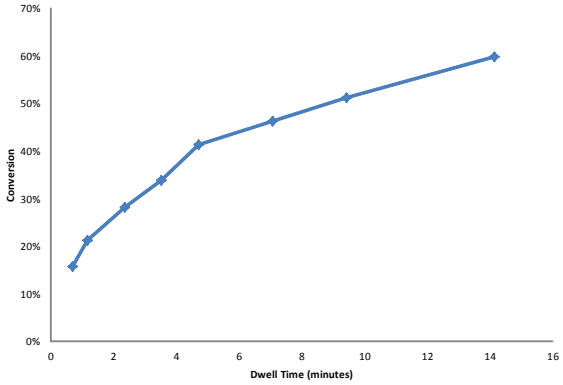

Figure 3.17: Cross metathesis of 3.14 and 3.15 (0.4 M, 2.5 mol% catalyst loading, 35 °C) in Teflon AF 2400 tubing under vacuum

For the low catalyst loading experiments, the oil bath temperature was set between 40 °C and 45 °C and adjusted as necessary to maintain the heated spool at 30 °C, the temperature used in standard RCM screens.[34] Using the heated microfluidic reactor at 30 °C and 500 ppm catalyst loading, 90% conversion, for a TON of 1,800, was reached within 20 minutes (Figure 3.18A). The conversion remained steady between 90% and 95% under longer reaction times, never reaching 100%. Due to the success at 500 ppm, the reactor was tested again using only 50 ppm catalyst loading (Figure 3.18B). In this case the reaction again reached 90%, for a TON of 18,000, but even after 12 hours of reaction time it never reached 100%. Incomplete conversion of RCM with low catalyst loadings is not unexpected, but conversion generally increases with increased catalyst loading,[24] and the RCM of diethyl diallylmalonate is known to proceed cleanly to 100%.[34] The difficulty in achieving complete conversion is consistent across all tests of RCM in Teflon AF 2400. The source of this limitation is unclear, but it does not depend on catalyst loading, temperature and reaction time. Neither does it limit the overall TON of the catalyst, which has reached higher levels than typically reported for RCM.[24] The turn-over frequency (TOF) was similar for the 50 ppm reaction (1.98 s^{-1} at 90.9% conversion) as for the 500 ppm reaction (2.00 s^{-1} at 90.7% conversion), indicating that the reaction is limited only by the catalyst, not by issues of mass transfer.

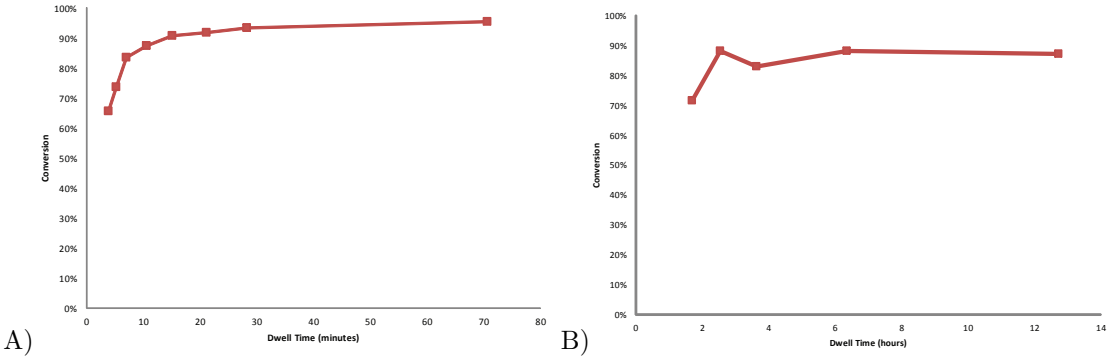

Figure 3.18: RCM of 3.12 (0.1 M, catalyst loading of 500 ppm (A) or 50 ppm (B), 30 °C) in Teflon AF 2400 tubing under vacuum

3.4 Progress Toward Ethenolysis Using a Permeable Membrane

In an effort to apply the parallel flow reactor to ethenolysis, a matching temperature-controlled reactor was built for high pressure applications. In this case all the walls were made of 1/2 inch thick stainless steel instead of polysulfone. The use of all stainless steel introduced new technical challenges, particularly the risk of galling of the stainless steel threaded joints. These challenges were overcome and a gas tight seal was eventually accomplished by cutting deeper threads into the cap and heating element, and by using a thick, molybdenum disulfide-based grease. Testing of the reactor body with ethylene pressures up to 150 psi, while always done behind safety shields, showed no leakage and never resulted in a structural failure of the stainless steel.

A new problem developed when the reactor was pressurized with ethylene and the microfluidic tubing was opened. The tubing proved to be so permeable to ethylene that ethylene entered the tubing and flowed out the end into the room at a rapid rate. This uncontrolled venting of ethylene prevented any controllable reaction, as any liquid reaction that was introduced would be immediately flushed out by ethylene, and the tank of compressed ethylene emptied at an unacceptably high rate. To remedy this problem a 250 psi back pressure regulator was added to the end of the tubing the reactor, before the junction with the quench solution. This back pressure regulator ensured that the pressure inside the gas permeable tubing would always be higher than the ethylene used to pressurize

the reactor, preventing any spontaneous outflow. However, the use of high pressure introduced a new challenge, as the simple syringe pumps were no longer capable of generating 250 psi of pressure.

To generate the necessary pressure, HPLC pumps were necessary. Retired Beckman-Coulter HPLC apparatuses were modified to pump catalyst and substrate solutions into the microfluidic reactor. In initial tests performed without the stainless steel jacket the microfluidic tubing did not leak under the increased pressure. However, when the stainless steel jacket, which was necessary to introduce ethylene gas, was added the tubing began to leak. The junctions between the HPLC tubing and the Teflon AF 2400 could be properly sealed by the use of stainless steel 1/32 inch fittings, but the Teflon AF 2400 leaked wherever anything was physically pressed against it. Contact with other tubing is unavoidable in the confined space of the reactor body, and no successful ethenolysis was performed due to the constant leaks under ethylene pressure. It is conjectured that leaks might be avoided by redesigning the reactor body so no other material rubs against the Teflon AF 2400, or by using a chip reactor design with Teflon AF 2400 fashioned into a membrane, as initially proposed. Both designs would require considerable development and so far neither has yet been pursued any further.

3.5 Conclusion

Microfluidic reactors were designed and developed for olefin metathesis. An alternating, segmented flow reactor was developed and used for ethenolysis, achieving high yield and selectivity at reduced pressures of ethylene. A temperature-controlled parallel flow reactor was developed and used for ring-closing metathesis, achieving high yield at low catalyst loading. A high pressure ethenolysis reactor was developed, but was not utilized due to technical difficulties inherent in the reactor design.

3.6 Experimental Details

Materials: Teflon AF 2400 tubing was used as purchased from Biogeneral, Inc. (San Diego, CA). Diethyl diallylmalonate 3.12 (98%) and methyl oleate 3.1 (97%) were purchased from Sigma-Aldrich

(St. Louis, MO). The methyl oleate was purified by passing through activated alumina prior to use. Ruthenium complexes 3.6–3.10 were used as provided by Materia, Inc. (Pasadena, CA). Ruthenium complex 3.11 was prepared according to literature procedure.[27,33] GC spectra were recorded on an Agilent 5975C GC/MSD System (Agilent Tech., USA/Germany), anhydrous toluene purchased from Sigma-Aldrich was used for dissolving the ruthenium catalysts and as an internal standard in the analysis. MiChS-(β) micromixer was obtained from MiChS Co., Ltd. (Japan). Polysulfone and type 304 stainless steel were obtained from McMaster-Carr (Elmhurst, Illinois). HPLC fittings, PEEK tubing, the inline microfilter assembly and the 250 psi back pressure regulator were obtained from IDEX Health & Science (Lake Forest, Illinois). Glass syringes were obtained from VWR International (Radnor, Pennsylvania). All the polysulfone and stainless steel reactor parts were fabricated in the machine shop of the Division of Chemistry and Chemical Engineering at Caltech.

General procedure for the ethenolysis of methyl oleate (in the optimized segmented flow microchemical system, as shown in Figure 3.3A): The appropriate ruthenium catalyst (1.0 mg) in toluene (2 mL) and methyl oleate (10 mL) were loaded into separate syringes. The ruthenium catalyst solution and methyl oleate were injected at flow rates in the range of 1–20 μL/min and mixed by MiChS-(β) micromixer in the first cooling zone. The pressure of injected ethylene was regulated from 15 to 60 psi. The total retention time in the capillary microreactor was controlled by the length of micro-tube and pumping speed of a peristaltic pump connected to the end of the tube. To terminate the reaction excess ethyl acetate solution of ethyl vinyl ether was added before the tubing reached the peristaltic pump. The results were monitored by GC analysis; peak areas were referenced to the toluene peak.

General procedure for the RCM of diethyl diallylmalonate in the heated microfluidic reactor: A 0.2 M solution of diethyl diallylmalonate in CH_2Cl_2 was loaded into a 20 mL glass syringe. The appropriate concentration of catalyst 3.8 was loaded into a second 20 mL glass syringe, taking into account the 2:1 dilution caused by mixing with the substrate (for 50 ppm catalyst loading a 10 μM solution was used). The two solutions were injected by syringe pump through the cap of the microfluidic reactor into the body, where they were mixed at a T-junction. After passing through a

short piece of HPLC tubing the reaction solution entered a 10 m section of Teflon AF 2400 tubing (800 μm o.d., 600 μm i.d., 283 μL total internal volume). The total internal volume was divided by the combined flow rate to determine the dwell time. At the outlet of the Teflon AF 2400 tubing a second T-junction combined the reaction mixture with a solution of ethyl vinyl ether to quench the catalyst, from which point the now quenched mixture flowed out through the HPLC fitting in the reactor cap to the collection vial. For each data point a new flow rate was set on the syringe pump and the reaction was allowed to equilibrate for over twice the dwell time. This was necessary to purge the reactor of samples of intermediate flow rates. Once the reaction had fully equilibrated, the liquid was collected from the outlet tubing, dried on a rotary evaporator, and measured by ^{1}NMR.

The following are detailed experimental results which are summed up in Figure 3.5

Table 3.3: Ethenolysis with catalyst 3.6 at 60 psi, 30 °C

Entry	**Time** (min)	**Conversion** (%)	**Selectivity** (%)	**Yield** (%)
1	10	10	99	9.9
2	20	18	98	17.6
3	40	36	98	35.3
4	60	46	97	44.6
5	90	60	97	58.2
6	120	65	96	62.4
7	180	65	92	60.5

Table 3.4: Ethenolysis with catalyst 3.6 at 30 psi, 30 °C

Entry	**Time** (min)	**Conversion** (%)	**Selectivity** (%)	**Yield** (%)
1	10	8	97	7.8
2	20	16	94	15.0
3	40	26	91	23.7
4	60	37	90	33.3
5	90	47	86	40.4
6	120	48	85	40.8
7	180	51	81	41.3

Table 3.5: Ethenolysis with catalyst 3.6 at 30 psi, 40 °C

Entry	**Time** (min)	**Conversion** (%)	**Selectivity** (%)	**Yield** (%)
1	10	10	95	9.5
2	20	18	93	16.7
3	40	30	86	25.8
4	60	36	80	28.8
5	90	44	78	34.3
6	120	50	72	36.0
7	180	53	66	35.0

Table 3.6: Ethenolysis with catalyst 3.6 at 30 psi, 20 °C

Entry	**Time** (min)	**Conversion** (%)	**Selectivity** (%)	**Yield** (%)
1	10	4	98	3.9
2	20	11	98	10.8
3	40	21	96	20.2
4	60	27	94	25.4
5	90	33	91	30.0
6	120	36	89	32.0
7	180	42	86	36.1

Table 3.7: Ethenolysis with catalyst 3.6 at 15 psi, 30 °C

Entry	**Time** (min)	**Conversion** (%)	**Selectivity** (%)	**Yield** (%)
1	10	7	85	6.0
2	20	14	85	11.9
3	40	27	80	21.6
4	60	33	76	25.1
5	90	41	70	28.7
6	120	46	65	29.9
7	180	49	61	29.9

References

[1] T. Fukuyama, T. Rahman, M. Sato, and I. Ryu. Adventures in inner space: Microflow systems for practical organic synthesis. *Synlett*, (2):151–163, 2008.

[2] B.P. Mason, K.E. Price, J.L. Steinbacher, A.R. Bogdan, and D.T. McQuade. Greener approaches to organic synthesis using microreactor technology. *Chemical Reviews*, 107(6):2300–2318, 2007.

[3] T. Wirth, editor. *Microreactors in Organic Syntheses*. Wiley-VCH, Weinheim, 2008.

[4] V. Hessel, J.C. Schouten, A. Renken, Y. Wang, and J.I. Yoshida, editors. *Handbook of Micro Reactors*. Wiley-VCH, Weinheim, 2009.

[5] D.R. Reyes, D. Iossifidis, P.A. Auroux, and A. Manz. Micro total analysis systems. 1. Introduction, theory, and technology. *Analytical Chemistry*, 74(12):2623–2636, 2002.

[6] P.A. Auroux, D. Iossifidis, D.R. Reyes, and A. Manz. Micro total analysis systems. 2. Analytical standard operations and applications. *Analytical Chemistry*, 74(12):2637–2652, 2002.

[7] G.M. Whitesides. The origins and the future of microfluidics. *Nature*, 442(7101):368–373, 2006.

[8] J. Kobayashi, Y. Mori, and S. Kobayashi. Triphase hydrogenation reactions utilizing palladium-immobilized capillary column reactors and a demonstration of suitability for large scale synthesis. *Advanced Synthesis & Catalysis*, 347(15):1889–1892, 2005.

[9] N. Wang, T. Matsumoto, M. Ueno, H. Miyamura, and S. Kobayashi. A Gold-Immobilized Microchannel Flow Reactor for Oxidation of Alcohols with Molecular Oxygen. *Angewandte Chemie—International Edition*, 48(26):4744–4746, 2009.

[10] G. Shore, S. Morin, and M.G. Organ. Catalysis in capillaries by Pd thin films using microwave-assisted continuous-flow organic synthesis (MACOS). *Angewandte Chemie—International Edition*, 45(17):2761–2766, 2006.

[11] G. Shore, S. Morin, D. Mallik, and M.G. Organ. Pd PEPPSI-IPr-mediated reactions in metal-coated capillaries under MACOS: The synthesis of indoles by sequential aryl amination/Heck coupling. *Chemistry—A European Journal*, 14(4):1351–1356, 2008.

[12] C.P. Park and D.-P. Kim. A Microchemical System with Continuous Recovery and Recirculation of Catalyst-Immobilized Magnetic Particles. *Angewandte Chemie—International Edition*, 49(38):6825–6829, 2010.

[13] R.A. Maurya, C.P. Park, J.H. Lee, and D.-P. Kim. Continuous in situ generation, separation, and reaction of diazomethane in a dual-channel microreactor. *Angewandte Chemie—International Edition*, 50(26):5952–5955, 2011.

[14] P.W. Miller, N.J. Long, A.J. de Mello, R. Vilar, H. Audrain, D. Bender, J. Passchier, and A. Gee. Rapid multiphase carbonylation reactions by using a microtube reactor: Applications in positron emission tomography C-11-radiolabeling. *Angewandte Chemie—International Edition*, 46(16):2875–2878, 2007.

[15] M.T. Rahman, T. Fukuyama, N. Kamata, M. Sato, and I. Ryu. Low pressure Pd-catalyzed carbonylation in an ionic liquid using a multiphase microflow system. *Chemical Communications*, (21):2236–2238, 2006.

[16] E.V. Rebrov, E.A. Klinger, A. Berenguer-Murcia, E.M. Sulman, and J.C. Schouten. Selective Hydrogenation of 2-Methyl-3-butyne-2-ol in a Wall-Coated Capillary Microreactor with a Pd25Zn75/TiO2 Catalyst. *Organic Process Research & Development*, 13(5):991–998, 2009.

[17] C.P. Park and D.-P. Kim. Dual-Channel Microreactor for Gas-Liquid Syntheses. *Journal of the American Chemical Society*, 132(29):10102–10106, 2010.

[18] M. O'Brien, I.R. Baxendale, and S.V. Ley. Flow ozonolysis using a semipermeable Teflon AF-2400 membrane to effect gas-liquid contact. *Organic Letters*, 12(7):1596–1598, 2010.

[19] D.L. Browne, M. O'Brien, P. Koos, P.B. Cranwell, A. Polyzos, and S.V. Ley. Continuous-

flow processing of gaseous ammonia using a Teflon AF-2400 tube-in-tube reactor: synthesis of thioureas and in-line titrations. *Synlett*, 23(9):1402–1406, 2012.

[20] S. Newton, S.V. Ley, E.C. Arcé, and D.M. Grainger. Asymmetric homogeneous hydrogenation in flow using a tube-in-tube reactor. *Advanced Synthesis & Catalysis*, 354(9):1805–1812, 2012.

[21] P.B. Cranwell, M. O'Brien, D.L. Browne, P. Koos, A. Polyzos, M. Peña Lopez, and S.V. Ley. Flow synthesis using gaseous ammonia in a Teflon AF-2400 tube-in-tube reactor: Paal-knorr pyrrole formation and gas concentration measurement by inline flow titration. *Organic & Biomolecular Chemistry*, 10:5774–5779, 2012.

[22] T.P. Petersen, A. Polyzos, M. O'Brien, T. Ulven, I.R. Baxendale, and S.V. Ley. The oxygen-mediated synthesis of 1,3-butadiynes in continuous flow: Using Teflon AF-2400 to effect gas/liquid contact. *ChemSusChem*, 5(2):274–277, 2012.

[23] A.K. Chatterjee, T.L. Choi, D.P. Sanders, and R.H. Grubbs. A general model for selectivity in olefin cross metathesis. *Journal of the American Chemical Society*, 125(37):11360–11370, 2003.

[24] K.M. Kuhn, T.M. Champagne, S.H. Hong, W.-H. Wei, A. Nickel, C.W. Lee, S.C. Virgil, R.H. Grubbs, and R.L. Pederson. Low Catalyst Loadings in Olefin Metathesis: Synthesis of Nitrogen Heterocycles by Ring-Closing Metathesis. *Organic Letters*, 12(5):984–987, 2010.

[25] Y. Schrodi, T. Ung, A. Vargas, G. Mkrtumyan, C.W. Lee, T.M. Champagne, R.L. Pederson, and S.H. Hong. Ruthenium olefin metathesis catalysts for the ethenolysis of renewable feedstocks. *Clean—Soil Air Water*, 36(8):669–673, 2008.

[26] K.A. Burdett, L.D. Harris, P. Margl, B.R. Maughon, T. Mokhtar-Zadeh, P.C. Saucier, and E.P. Wasserman. Renewable monomer feedstocks via olefin metathesis: Fundamental mechanistic studies of methyl oleate ethenolysis with the first-generation Grubbs catalyst. *Organometallics*, 23(9):2027–2047, 2004.

[27] D.R. Anderson, T. Ung, G. Mkrtumyan, G. Bertrand, R.H. Grubbs, and Y. Schrodi. Kinetic

selectivity of olefin metathesis catalysts bearing cyclic (alkyl)(amino)carbenes. *Organometallics*, 27(4):563–566, 2008.

[28] R.M. Thomas, B.K. Keitz, T.M. Champagne, and R.H. Grubbs. Highly Selective Ruthenium Metathesis Catalysts for Ethenolysis. *Journal of the American Chemical Society*, 133(19):7490–7496, 2011.

[29] S.C. Marinescu, R.R. Schrock, P. Müller, and A.H. Hoveyda. Ethenolysis Reactions Catalyzed by Imido Alkylidene Monoaryloxide Monopyrrolide (MAP) Complexes of Molybdenum. *Journal of the American Chemical Society*, 131(31):10840–10841, 2009.

[30] C. Thurier, C. Fischmeister, C. Bruneau, H. Olivier-Bourbigou, and P.H. Dixneuf. Ethenolysis of methyl oleate in room-temperature ionic liquids. *ChemSusChem*, 1(1–2):118–122, 2008.

[31] G.S. Forman, A.E. McConnell, M.J. Hanton, A.M.Z. Slawin, R.P. Tooze, W.J. van Rensburg, W.H. Meyer, C. Dwyer, M.M. Kirk, and D.W. Serfontein. A stable ruthenium catalyst for productive olefin metathesis. *Organometallics*, 23(21):4824–4827, 2004.

[32] G.S. Forman, R.M. Bellabarba, R.P. Tooze, A.M.Z. Slawin, R. Karch, and R. Winde. Metathesis of renewable unsaturated fatty acid esters catalysed by a phoban-indenylidene ruthenium catalyst. *Journal of Organometallic Chemistry*, 691(24–25):5513–5516, 2006.

[33] D.R. Anderson, V. Lavallo, D.J. O'Leary, G. Bertrand, and R.H. Grubbs. Synthesis and reactivity of olefin metathesis catalysts bearing cyclic (alkyl) (amino) carbenes. *Angewandte Chemie—International Edition*, 46(38):7262–7265, 2007.

[34] T. Ritter, A. Hejl, A.G. Wenzel, T.W. Funk, and R.H. Grubbs. A standard system of characterization for olefin metathesis catalysts. *Organometallics*, 25(24):5740–5745, 2006.

[35] T. Masuda, E. Isobe, T. Higashimur, and K. Takada. Poly[1-(trimethylsilyl)-1-propyne]—A New High Polymer Synthesized with Transition-Metal Catalysts and Characterized by Extremely High Gas Permeability. *Journal of the American Chemical Society*, 105(25):7473–7474, 1983.

[36] A.Y. Alentiev, Y.P. Yampolskii, V.P. Shantarovich, S.M. Nemser, and N.A. Plate. High transport parameters and free volume of perfluorodioxole copolymers. *Journal of Membrane Science*, 126(1):123–132, 1997.

[37] S.M. Nemser and I.C. Roman. Perfluorodioxole membranes. *U.S. Patent 5,051,114*, 1991.

[38] S.M. Nemser and I.C. Roman. Preparation and uses of permselective perfluorodimethyldioxole polymer membranes for gas separations. *World Patent 9,015,662*, 1990.

[39] T.C. Merkel, V. Bondar, K. Nagai, B.D. Freeman, and Y.P. Yampolskii. Gas sorption, diffusion, and permeation in poly(2,2-bis(trifluoromethyl)-4,5-difluoro-1,3-dioxole-co-tetrafluoroethylene). *Macromolecules*, 32(25):8427–8440, 1999.

[40] A.Y. Alentiev, V.P. Shantarovich, T.C. Merkel, V.I. Bondar, B.D. Freeman, and Y.P. Yampolskii. Gas and vapor sorption, permeation, and diffusion in glassy amorphous Teflon AF-1600. *Macromolecules*, 35(25):9513–9522, 2002.

[41] A.M. Polyakov, L.E. Starannikova, and Y.P. Yampolskii. Amorphous Teflon AF as organophilic pervaporation materials transport of individual components. *Journal of Membrane Science*, 216(1-2):241–256, 2003.

[42] H. Zhao, K. Ismail, and S.G. Weber. How fluorous is poly(2,2-bis(trifluoromethyl)-4,5-difluoro-1,3-dioxide-co-tetrafluoroethylene) (Teflon AF)? *Journal of the American Chemical Society*, 126(41):13184–13185, 2004.

[43] A.V. Tokarev, G.N. Bondarenko, and Y.P. Yampol'skii. Chain structure and stiffness of Teflon AF glassy amorphous fluoropolymers. *Polymer Science Series A*, 49(8):909–920, 2007.

Chapter 4

Fluoride and Hydroxide Ligands for Olefin Metathesis Catalysts

Ruthenium-based olefin metathesis catalysts were synthesized with varied halide ligands. The fast-initiating Piers-type catalysts were substituted with fluoride ligands, which gave deactivated catalysts. Moderate activity could be restored by the use of tris(pentafluorophenyl)boron and deprotonated triethylsilane. The Z-selective type catalysts were substituted with a series of halides, and a novel hydroxy-bridged ruthenium dimer was isolated. Initiation for the hydroxy-bridged dimer was more facile than for the other halides.

4.1 Introduction

The first well-defined ruthenium-based olefin metathesis catalyst to be reported had the general structure $L_2X_2Ru{=}CHR$ (Figure 4.1),[1] a structure that has remained constant in nearly all such catalysts that have been reported since.[2,3] However, within the context of that general structure, hundreds of compounds have been prepared with extensive variation of all ligands.[4] Early studies resulted in the optimization of the L-type ligand from PPh_3 to PCy_3 and then to an N-Heterocyclic Carbene (NHC) ligand, and the optimization of the alkylidene ligand from a diphenyl allylidene to a benzylidene. However, one ligand that has remained constant throughout is chloride as the X ligand.

Early studies on the first generation catalysts showed that the bromide and iodide analogs could be prepared by direct ligand exchange with halide salts (Figure 4.2).[5] It was shown that while the iodide-bearing catalyst initiates faster, the chloride-bearing catalyst is more active overall. For both parameters the bromide-bearing catalyst showed intermediate behavior. A similar study later done

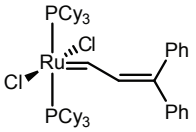

4.1

Figure 4.1: First well-defined ruthenium catalyst

on the second generation catalyst again showed the chloride-bearing catalyst to be more active while showing the iodide-bearing catalyst to initiate faster.[6] The second generation iodide catalyst can be prepared directly by exchange with sodium iodide (Figure 4.3).[7,8] The bromide-bearing catalyst cannot be prepared by direct ligand exchange with bromide salts, and was prepared from the first generation bromide catalyst (Figure 4.4).

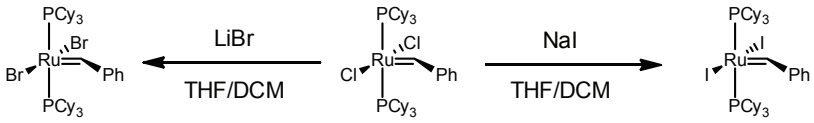

4.3 4.2 4.4

Figure 4.2: Synthesis of 4.3 and 4.4 from 4.2

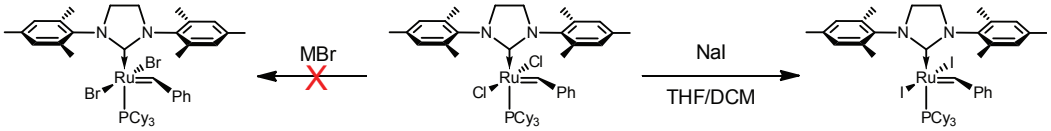

4.5 4.6 4.7

Figure 4.3: Synthesis of 4.7 from 4.6

The same study of halide ligands has been performed on the second generation Hoveyda-type complexes (Figure 4.5).[7] Due to the associative initiation mechanism in these catalysts, however, the trend is reversed and the iodide catalyst is the slowest to initiate.[8,9]

One seemingly obvious variation of the X ligand has never been prepared and studied. To the best of our knowledge, no ruthenium-based olefin metathesis catalyst with a directly bound fluoride ligand has ever been reported. This observation is consistent with the very limited number of ruthenium(II) fluoride complexes that have been reported in the literature. Low valent group VIII fluorides have only recently began to attract more study, due largely to the interest in catalysts for C-F bond formation.[10] The recent interest in the preparation of low valent late transition metal

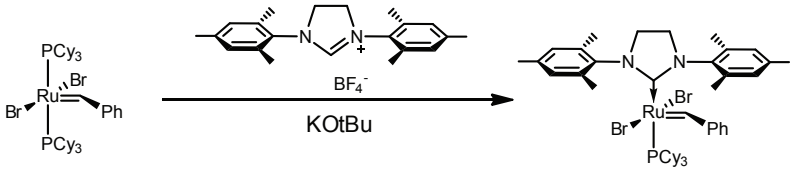

4.3 4.5

Figure 4.4: Synthesis of 4.5 from 4.3

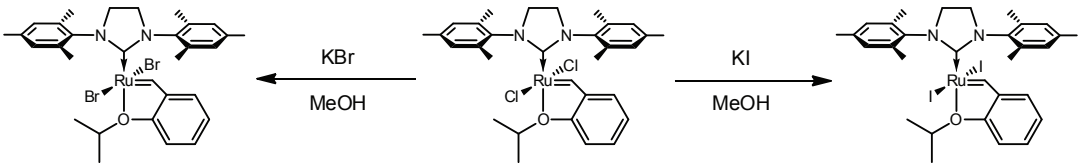

4.9 4.8 4.10

Figure 4.5: Synthesis of 4.9 and 4.10 from 4.8

fluorides, a line of research typically frustrated by the poor interaction between the soft metal centers and the hard fluoride ligand, is a theme found in group IX and group X metals, as well.[11–13]

For several decades ruthenium(II) fluorides were only known as simple ternary compounds of ruthenium, with fluoride and carbonyl ligands, most prominently the case of $[Ru(CO)_3F_2]_4$.[14–16] The use of strongly π-acid carbonyl ligands trans to the strongly π-basic fluoride helps to stabilize the poor interaction between the fluoride ligand and the filled d orbitals of ruthenium. The first ruthenium(II) fluorides to follow $[Ru(CO)_3F_2]_4$ were derivatives thereof, obtained by the addition of phosphine ligands which displace a carbonyl ligand and break up the tetramer.[10,17,18] These phosphino ruthenium fluorides retain two carbonyl ligands, which are again trans to the fluorides. The same exchange can be done with NHC ligands to give analogous structures[19,20] and the same structures can be obtained from ruthenium carbonyl hydrides by treatment with HF.[21] Ruthenium(II) fluoride complexes without carbonyl ligands have been prepared in three different ways: by exchanging out chloride ligands using thallium(I) fluoride,[22,23] by exchanging out hydride ligands using organofluorine compounds,[24] and by the displacement of carbonyl ligands by chelating phosphine ligands.[25] Carbonyl-free complexes are of particular interest in the context of olefin metathesis, since carbonyl ligands are known to lead to deactivated olefin metathesis catalysts.[26]

Unfortunately, even with the growing precedence for ruthenium(II) fluoride complexes in the

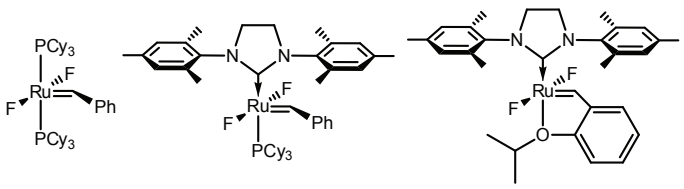

4.11 4.12 4.13

Figure 4.6: Hypothetical fluoride catalysts

literature, efforts to prepare fluoride-containing olefin metathesis catalysts have been consistently unsuccessful up to this point. Olefin metathesis catalysts have been subjected to a variety of fluoride sources by researchers in our group in an effort to prepare fluoride-bearing catalysts (Figure 4.6), but prior to this work catalyst decomposition has been the result.

4.2 Fluoride Piers-Type Catalysts

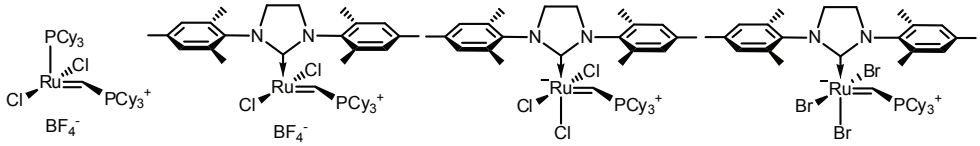

4.14[27] 4.15[27] 4.16[28,29] 4.17[28]

Figure 4.7: Piers-type catalysts 4.14 and 4.15, and derivatives 4.16 and 4.17

The first efforts to produce fluoride-containing catalysts began from the Piers-type catalysts 4.14 and 4.15 (Figure 4.7). These catalysts provide a unique platform for ligand exchange, since they are coordinatively unsaturated and readily bind a fifth ligand to form a sixteen electron complex. Both the trichloride (4.16) and tribromide (4.17) analogs of the second generation Piers catalyst have been reported.[28,29] These analogs are not active in olefin metathesis, as the vacant site occupied by the additional halide ligand precludes olefin coordination. The catalytic activity can be restored by removing one of the halide ligands with a halide-abstracting reagent, such as $B(C_6F_5)_3$.[30]

Guided by these results with chloride and bromide, we began to study the exchange with fluoride. It was quickly discovered that the use of tetrabutylammonium fluoride (TBAF) rapidly effects the exchange of the halide ligands, giving a complex with three fluoride ligands in place of two chlorides. This reaction is effective for both the first and second generation catalysts (Figures 4.8 and 4.9).

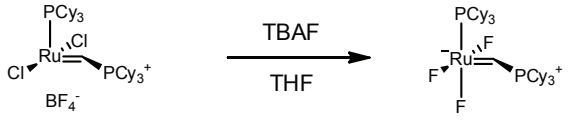

4.14 4.18

Figure 4.8: Synthesis of 4.18

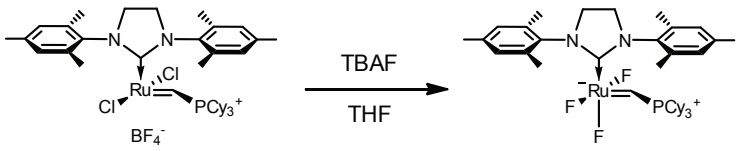

4.15 4.19

Figure 4.9: Synthesis of 4.19

The ligand exchange gives a mixture of chloride and halide ligands even under an excess of TBAF, and often requires that the intermediate product be isolated and subjected a second time to the reaction conditions. The difluoro and trifluoro derivatives are clearly distinguishable in the splitting pattern of the alkylidene proton in the ^{1}H NMR. The alkylidene proton is split into a doublet by ^{2}J-coupling with the ^{31}P nucleus, and is split again by ^{3}J-coupling with the ^{19}F nuclei. In the case of the second generation catalyst this gives a doublet of triplets, since two of the ^{19}F nuclei are coplanar with the alkylidene proton. Incomplete exchange can be observed when a doublet of doublet forms, indicating only one of the chloride ligands in the plane has been replaced.

A diffraction-quality crystal of 4.19 has been prepared and analyzed by X-ray crystallography. However, solving the crystal structure has been difficult due to the presence of chloride, hydroxide, and water ligands in the place of the fluorides. Even though the exact populations at each location

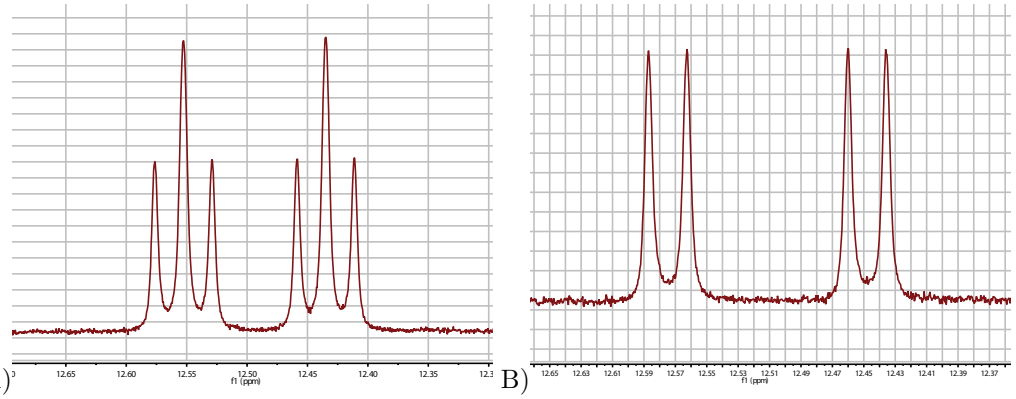

Figure 4.10: ^{1}H NMR splitting of the benzylidene peak in 4.18 (A) and 4.19 (B)

are difficult to calculate, the overall ligand geometry is clear and shows a strong deviation from the geometry of chloride and iodide-based catalysts. The X-Ru-X angle, which in most catalysts falls between 155° and 170°,[7,31,32] is 168.6° in the case of the analogous 4.16[28,29] but only 131.0° in the case of 4.19. This observation is consistent with all previously reported fluoride complexes of ruthenium(II), in that two fluoride ligands are never trans to each other. In all cases the π-basic fluoride is trans to a π-acidic ligand, either carbonyl[10,17–20] or a chelated phosphine.[22–25] In the case of 4.19 there is only one π-acidic ligand, the NHC ligand, which is already trans to the third fluoride. The remaining two fluoride ligands are forced trans to each other in the square planar complex but distort to a trigonal bipyramid to avoid such an unfavorable interaction.

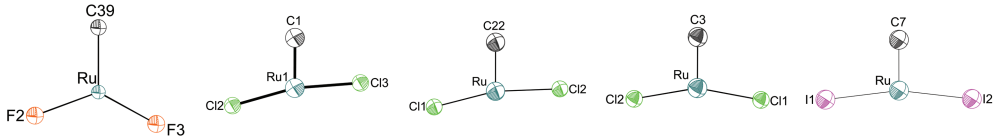

4.19	4.16	4.6	4.8	4.10
∠F-Ru-F: 131.0°	∠Cl-Ru-Cl: 168.6°[28,29]	∠Cl-Ru-Cl: 167.7°[31]	∠Cl-Ru-Cl: 156.5°[32]	∠I-Ru-I: 163.8°[7]

Figure 4.11: Comparison of various X-Ru-X angles from crystal structures

So far no crystal structure of 4.18 has been obtained. Efforts to isolate a diffraction-quality crystal were hampered by the formation of crystals of the decomposition product 4.20, which forms in the presence of residual TBAF. This decomposition product, which appears to be more crystalline than the desired product, has previously been characterized as a decomposition product formed in the presence of alcohols.[33] In this case the decomposition product was formed in THF, but the water present in TBAF may have induced the decomposition.

Both 4.18 and 4.19 were tested for activity as olefin metathesis catalysts. No activity was seen for the ring-opening metathesis polymerization (ROMP) of cyclooctene or for the ring-closing metathesis (RCM) of diethyl diallyl malonate. This is consistent with the studies of the analogous trichloride catalyst 4.16, which does not effectively catalyze olefin metathesis.[29]

Because catalytic activity may be induced in the case of 4.16 through the addition of chloride-abstracting $B(C_6F_5)_3$, the same strategy was tested in the case of 4.18 and 4.19. In addition to $B(C_6F_5)_3$, the combination of $C(C_6H_5)_3BF_4$ and $(C_2H_5)_3SiH$ was used, with the intention that the

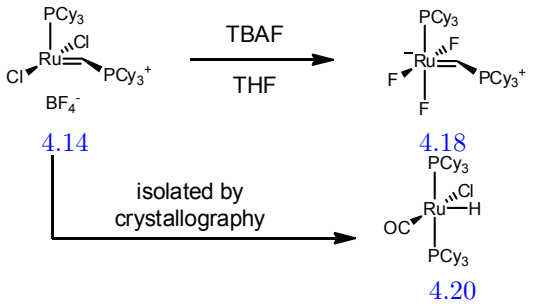

Figure 4.12: Decomposition to form 4.20

deprotonated silane would bind one of the fluoride ligands. However, no change was observed in the ^{1}H NMR upon addition of the $B(C_6F_5)_3$ or $(C_2H_5)_3Si^+$, which would be expected if one of the fluorides was removed. When one equivalent of $B(C_6F_5)_3$ and $(C_2H_5)_3Si^+$ were used with 4.19 at 50 °C in the presence diethyl diallylmalonate (DEDAM), RCM conversion over 24 hours reached 51.5% and 50.1%, respectively.

Because of the small but promising amount of activity achieved with halide-abstracting reagents, the synthesis of 4.13 was attempted from 4.19 (Figure 4.13). The reaction of 4.19 with 4.21 without any halide-abstracting reagent gave no reactivity until it was heated to complete decomposition. The same reaction in the presence of $B(C_6F_5)_3$ gives a very complex product mixture, with over ten species seen in the alkylidene region of the ^{1}H NMR spectrum. When a mixture of $(C_2H_5)_3SiH$ and $C(C_6H_5)_3BF_4$ was used the reaction yielded one product cleanly, with a diagnostic peak at 16.5 ppm. When this product was purified on a silica gel column, however, 4.8 was isolated cleanly. The putative fluoride complex, which was never fully characterized, underwent a halide exchange. The only available chloride source was the solvent, dichloromethane. Dichloromethane was present in the original reaction mixture as well, so the exchange would have had to occur after the reaction, during the purification on silica gel.

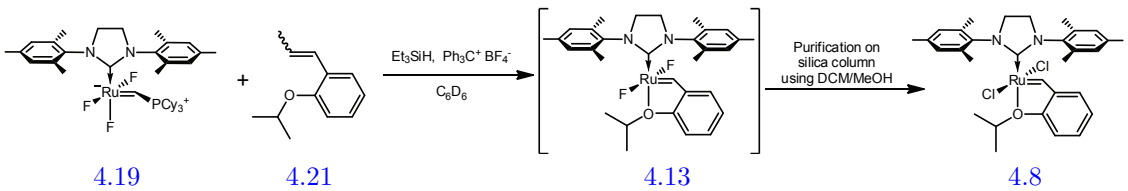

Figure 4.13: Synthesis of 4.13

The potential for these complexes to effect fluoride exchange with the solvent is an intriguing result. Such reactivity is not unprecedented for ruthenium, and in some cases can even be used to synthesize fluoride complexes.[24] These results, as they are outside the purview of the researched described herein, have not yet been pursued any further.

4.3 X-Ligand Variation on the Z-Selective Catalysts

The recent advances in Z-selective olefin metathesis have not only given organic chemists important control over product stereochemistry, but have also provided organometallic chemists a novel catalyst architecture with C-H activated NHC ligands. These C-H activated ligands, which contain one X-type ligand within themselves, have left only one X-type ligand remaining. Recent studies have focused on the use of chelating LX-type ligands to fill this remaining space, most notably the anionic nitrate ligand.[34]

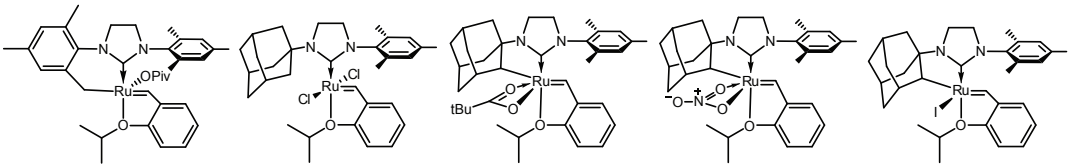

4.22 4.23 4.24 4.25 4.26

Figure 4.14: Important catalysts for Z-selective metathesis

The rigid ligand framework provided by the C-H activated NHC ligands enables unique substitutions for the remaining X-type ligand. A series of compounds with different X ligands were prepared, as described below.

4.26 can be prepared directly from 4.24 by direct ligand exchange with sodium iodide, as has

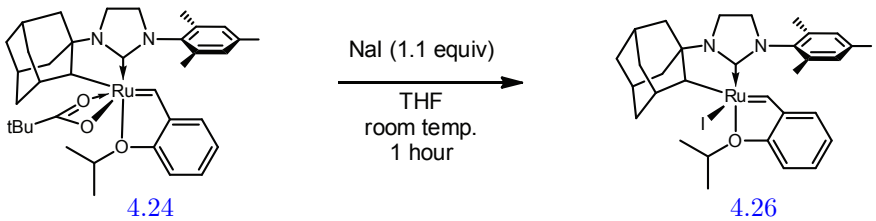

4.24 4.26

Figure 4.15: Synthesis of 4.26

been previously reported.[34]

The chloride and bromide analogs of 4.26 could not be prepared by direct exchange with simple halide salts. A combination of the ammonium salt and the tetrabutylammonium salt was required in both cases (Figures 4.16 and 4.17). With only tetrabutylammonium chloride incomplete conversion was observed, but with all other salts used individually no conversion was observed. Using an excess of both salts simultaneously gave clean and complete conversion for both the chloride and the bromide catalysts.

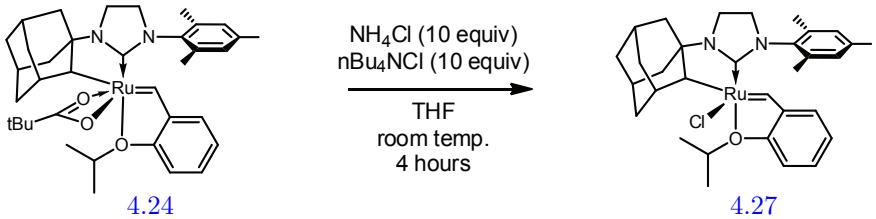

4.24 4.27

Figure 4.16: Synthesis of 4.27

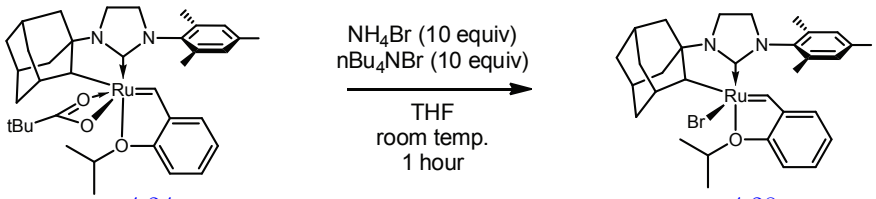

4.24 4.28

Figure 4.17: Synthesis of 4.28

When 4.24 is exposed to TBAF, the reaction mixture immediately turns from purple to red-orange. While the results were initially encouraging and suggested the formation of a fluoride-bearing catalyst, it was discovered upon rigorous purification that no signal was observable in the ^{19}F NMR and the high-resolution mass corresponded to the similar-massed hydroxy compound. X-ray crystallography showed the complex to be a dimer in the solid state, with bridging hydroxy ligands (Figure 4.21). The bridging hydroxy ligands freed up the normally chelated isopropoxy moiety, which was swung away from the metal center.

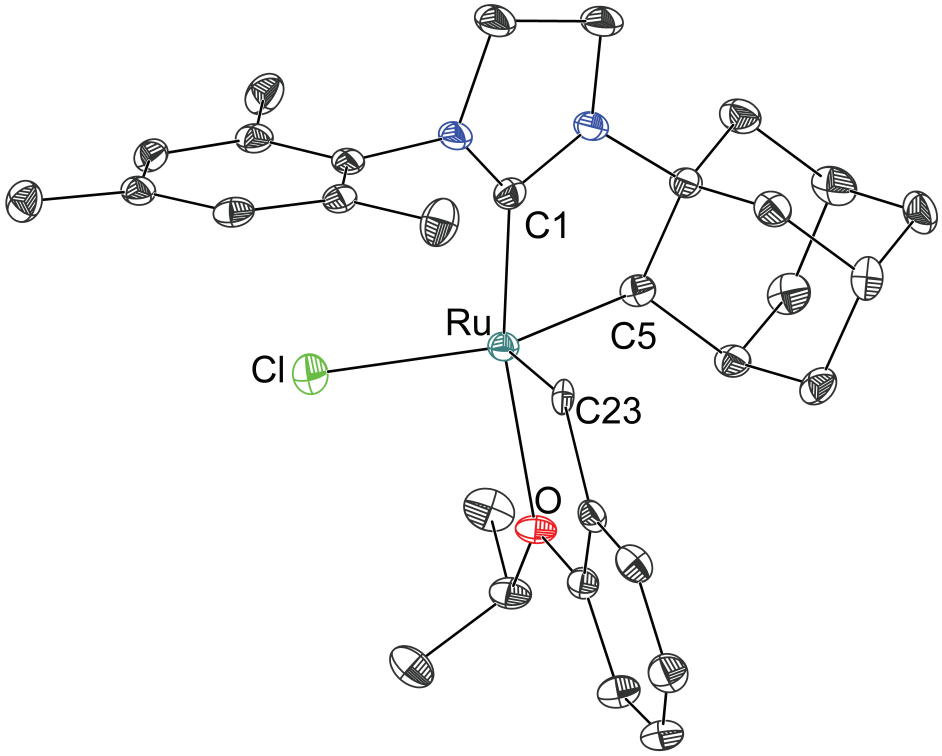

Figure 4.18: Crystal structure of 4.27 (hydrogens omitted for clarity)

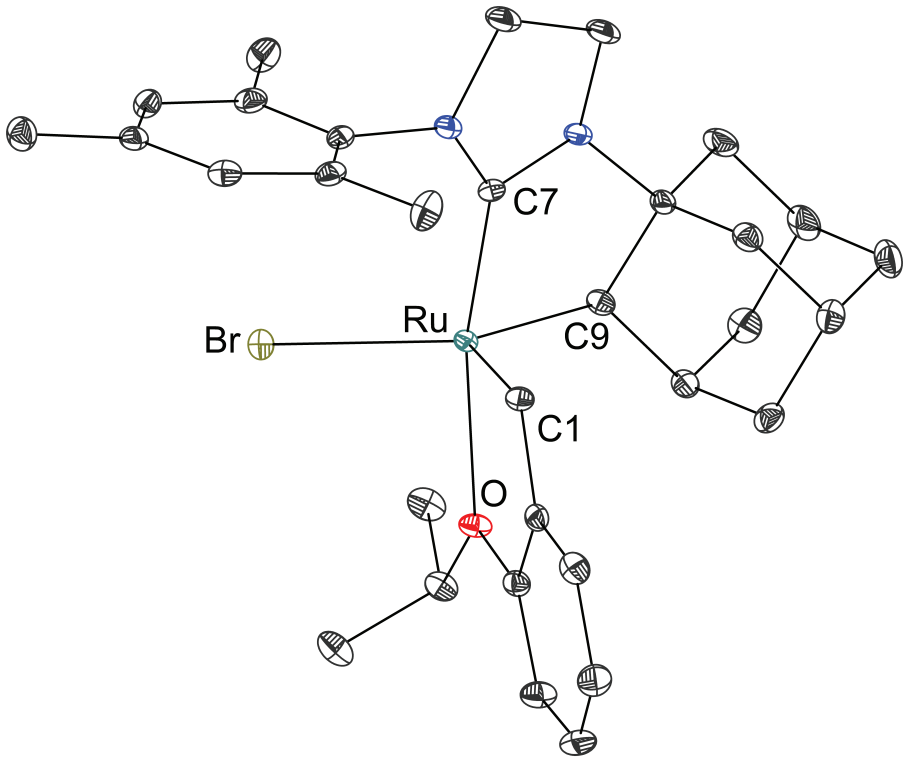

Figure 4.19: Crystal structure of 4.28 (hydrogens omitted for clarity)

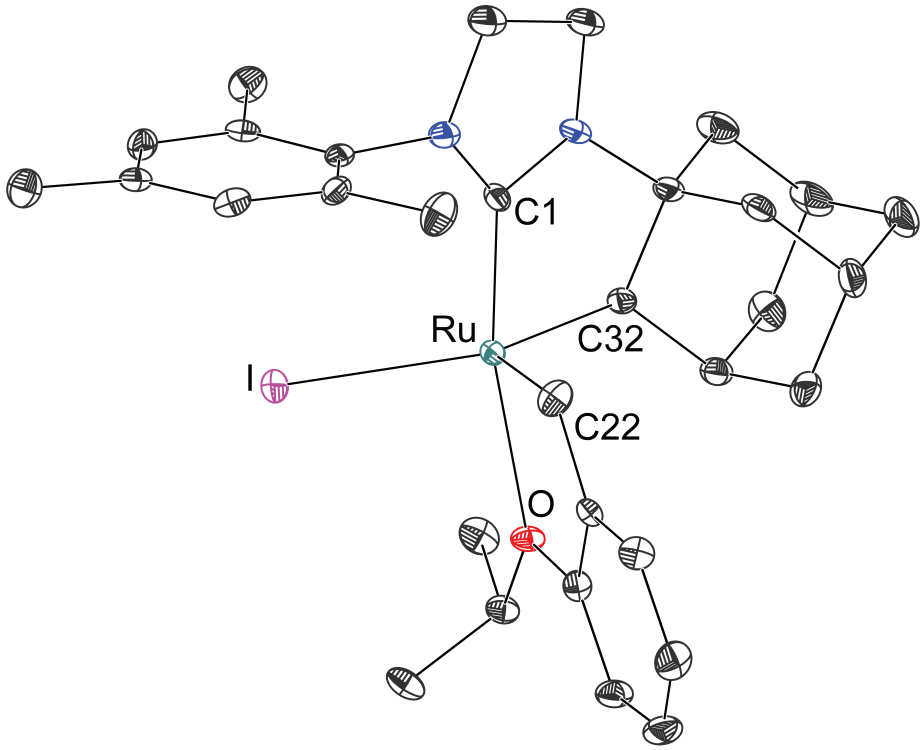

Figure 4.20: Crystal structure of 4.26 (hydrogens omitted for clarity)

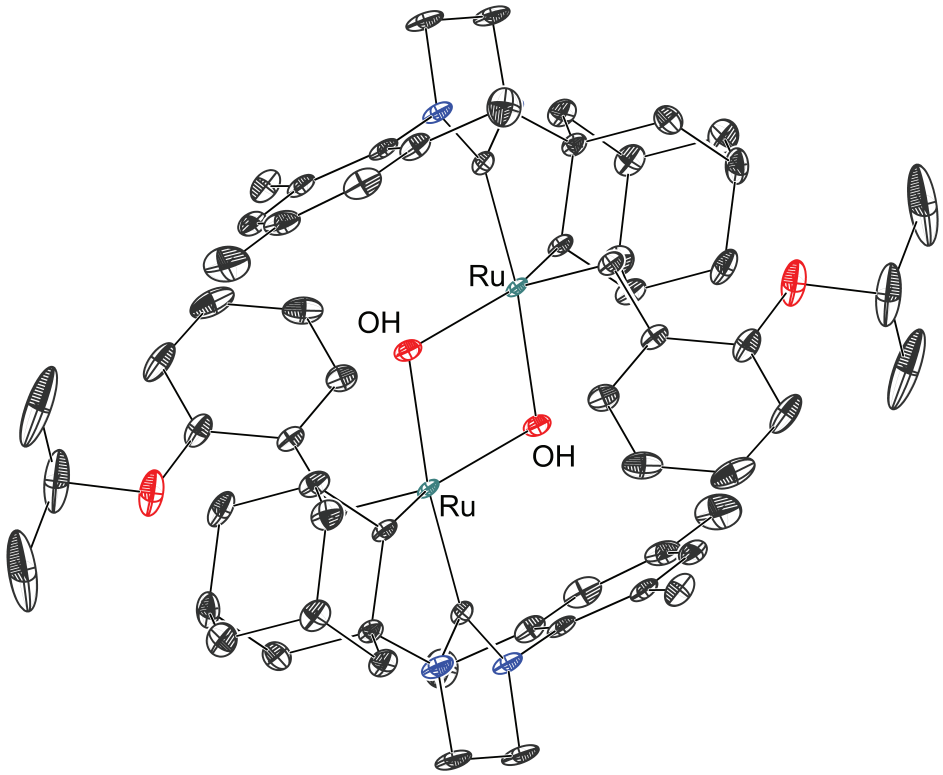

Figure 4.21: Crystal structure of 4.29 (hydrogens omitted for clarity)

Table 4.1: Comparison of bond lengths in Z-selective catalysts

	Iodide	**Bromide**	**Chloride**	**μ-OH**
	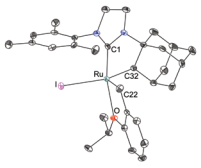	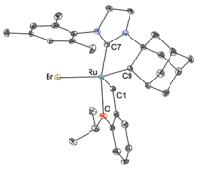	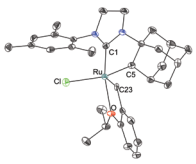	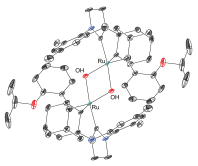
Initiation:	At 50 °C	Slowly at 60 °C	At 80 °C	At 50 °C
^{1}H NMR:	13.42 (s) - C_6D_6	13.68 (s) - C_6D_6	13.77 (s) - C_6D_6	12.73 (s) - C_6D_6
Ru-X:	2.7020	2.5301	2.3909	2.0468, 2.1485
Ru-Adm:	2.0302	2.0356	2.0452	2.0542
Ru-NHC:	1.9566	1.9623	1.9545	1.9418
Ru-O:	2.3359	2.3179	2.3086	———
Ru=C:	1.8308	1.8334	1.7989	1.8312

A comparison of the crystal structures of 4.26, 4.28, 4.27 and 4.29 reveals predictable trend in the ruthenium-halide (or hydroxide) bond length, with ruthenium-iodide being the longest and ruthenium-hydroxide being the shortest (Table 4.1). The ruthenium-NHC and ruthenium-ether bond distance show no appreciable trend, which agrees with previous observations that the X-type ligands do not have an appreciable electronic impact on the L-type ligands.[6] The ruthenium-carbon bond length for the CH-activated adamantyl moiety does show a trend, however. The ruthenium-carbon bond is longest in the case of the hydroxide ligand and shortest in the case of the iodide ligand.

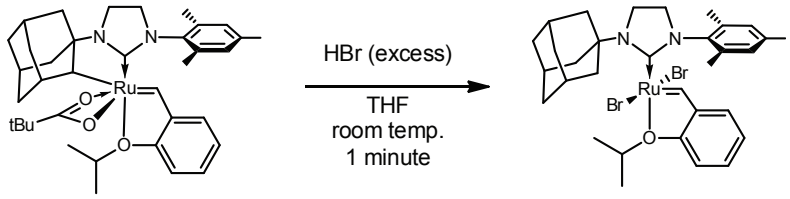

4.24 4.30

Figure 4.22: Synthesis of 4.30 from 4.24

In addition to the mono-halide series of catalysts that were synthesized, two di-halide analogs were synthesized. The dibromide analog 4.30 was prepared using a methanol solution of hydrogen bromide, which reacts completely in a matter of seconds with 4.24 (Figure 4.22). The hydrogen bromide protonates off both the pivalate and the CH-activated adamantyl ligand, opening up coordination sites for two bromide ligands. The overall series of transformations that gives 4.30 begins

with the dichloride 4.23, whose chloride ligands are removed in the first reaction (CH-activation with pivalate salts) and then replaced with bromide ligands in the second step. This two-step process efficiently yields a dibromide complex, which are typically difficult to prepare.

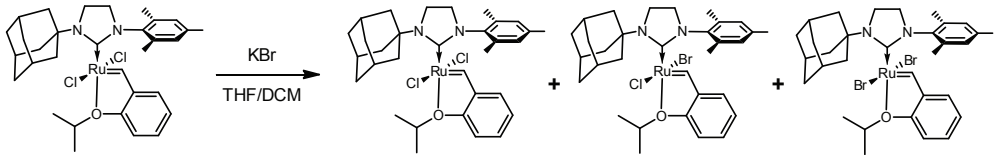

4.23 4.23 4.31 4.30

Figure 4.23: Synthesis of 4.30 from 4.23

The identity of 4.30 was confirmed by attempting the direct exchange of bromide for chloride in 4.23. This exchange, as expected, did not proceed to completion but rather gave a statistical mixture of 4.23, 4.31 and 4.30. The difficulty of forming the dibromide complex by direct ligand exchange highlights the synthetic utility of 4.24 used as an intermediate complex.

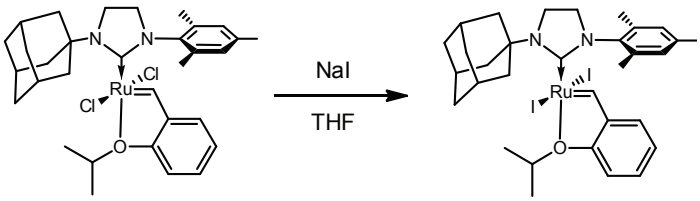

4.24 4.32

Figure 4.24: Synthesis of 4.32

The diiodide analog of 4.30 was also prepared (Figure 4.24). As is generally when preparing iodide catalysts,[5–8] the direct exchange was effected using an excess of sodium iodide at only slightly elevated temperature (40 °C).

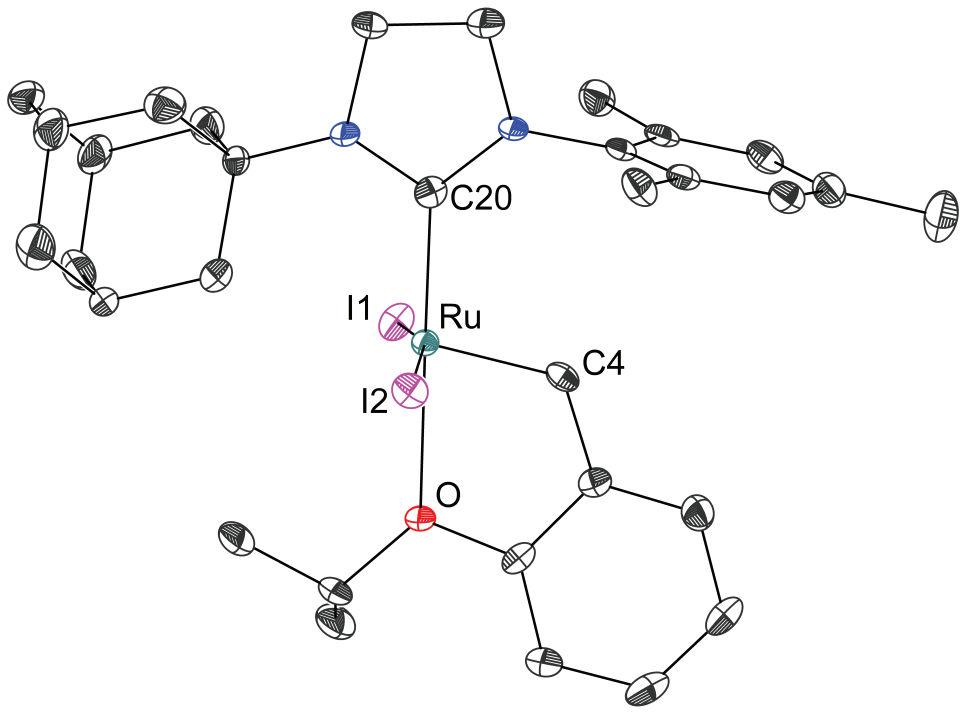

Figure 4.25: Crystal structure of 4.32 (hydrogens omitted for clarity)

4.4 Conclusion

Olefin metathesis catalysts with novel X-type ligands have been prepared. The fast-initiating Piers-type catalysts were substituted with fluoride ligands, giving deactivated, trifluoro structures. Activity was partially restored by the use of halide-abstracting reagents, but was still far below the activity of the analogous chloride catalysts. The chelated, Z-selective catalysts were substituted with a series of halides. When the Z-selective catalyst was exposed to fluoride sources a hydroxy-bridged dimer was formed, which showed an interesting dimeric structure with uncoordinated ether moieties. The novel addition of hydrogen bromide across the ligand-ruthenium bonds in Z-selective catalysts gives a dibromide structure, showing for the first time the potential for the Z-selective catalysts to be used as synthetic precursors for otherwise challenging catalyst structures.

4.5 Experimental Details

General Procedures: Manipulation of organometallic compounds was performed using standard Schlenk techniques under an atmosphere of dry argon or in a nitrogen-filled Vacuum Atmospheres drybox. All solvents used were purified by passing through alumina columns and, in the case of hydrocarbons, over a copper catalyst, as well.[35] All solvents were then freeze-pump-thawed and brought into the glove box in sealed flasks. Complexes 4.23, 4.24 and 4.26 were prepared according to the literature procedures.[36] All other reagents were used as purchased from Sigma-Aldrich. Standard NMR spectra were recorded on a Varian Inova 400 MHz spectrometer, while kinetic experiments were conducted on a Varian 500 MHz spectrometer equipped with an AutoX probe.

Preparation of 4.18: 740.5 mg 4.14 (0.889 mmol) was dissolved in 12 mL Genetron 113 in a 20 mL scintillation vial in a drybox. 1.721 g TBAF $\cdot$ H_{20} (6.16 mmol) were added and the reaction was set to stir. After 30 minutes the mixture was filtered through celite, and the filtrate was dried to an orange solid. The solid was extracted into a 1:1 pentane:ether mixture and dried again. 197.8 mg were collected for 30% yield. ^{1}H NMR (C_6D_6: δ 12.49 (dt, 1H), 2.4-0.9 (m, 60H, PCy_3).

Preparation of 4.19: 606.6 mg 4.15 (0.706 mmol) was dissolved in 12 mL Genetron 113 in a 20 mL scintillation vial in a drybox. 1.981 g TBAF $\cdot$ H_{20} (7.09 mmol) were added and the reaction was set to stir. After 30 minutes the mixture was filtered through celite, and the filtrate was dried to a dark red solid. The solid was extracted into benzene and dried again. 206 mg were collected for 38.4% yield. ^{1}H NMR (C_6D_6): δ 12.51 (dd, 1H), 6.89 (s, 4H), 3.43 (s, 4H), 2.67 (s, 6H), 2.18 (s, 6H), 2.0-1.0 (m, 30H, PCy_3). ^{19}F NMR (C_6D_6): δ -217.14

Preparation of 4.27: In a drybox a 20 mL scintillation vial was charged with 4.24 (150 mg, 0.229 mmol), NH_4Cl (122 mg, 2.28 mmol), nBu_4NCl (636 mg, 2.29 mmol) and THF (10 mL). The resulting purple suspension turned brown over the course of an hour. After 4 h the reaction mixture was filtered through celite and concentrated to a solid. The resulting residue was extracted into C_6H_6 (3 x 5 mL), filtered through celite, and concentrated to give 4.27 as a brown solid. ^{1}H NMR (C_6D_6): δ 13.77 (s, 1H), 7.36 (d, 1H), 6.96 (s, 1H), 6.92 (s, 1H), 6.84 (t, 1H), 6.76 (d, 1H), 6.63 (t, 1H), 4.76 (sep, 1H), 3.57 (t, 1H), 3.51 (m, 1H), 3.13 (t, 2H), 2.62 (s, 1H), 2.44 (s, 3H), 2.43 (s, 1H),

2.36 (s, 3H), 2.09 (s, 1H), 1.85 (d, 3H), 1.65-1.50 (m, 8H), 1.44-1.30 (m, 5H), 0.63 (d, 1H)

Preparation of 4.28: In a glovebox a 20 mL scintillation vial was charged with 4.24 (150 mg, 0.229 mmol), NH_4Br (224 mg, 2.28 mmol), nBu_4NBr (738 mg, 2.29 mmol) and THF (10 mL). The resulting purple suspension turned brown over the course of an hour. After 4 h the reaction mixture was filtered through celite and concentrated to a solid. The resulting residue was extracted into C_6H_6 (3 x 5 mL), filtered through celite, and concentrated to give 4.28 as a brown-green solid. ^{1}H NMR (C_6D_6): δ 13.68 (s, 1H), 7.42 (s, 1H), 7.36 (d, 1H), 6.92 (d, 1H), 6.83 (t, 1H), 6.70 (s, 1H), 6.64 (d, 1H), 4.77 (sep, 1H), 3.10 (t, 1H), 2.61 (s, 1H), 2.43 (s, 1H), 2.11 (s, 1H), 1.89 (d, 2H), 3.65-3.29 (m, 4H), 1.89 (d, 3H), 1.65-1.36 (m, 18H), 0.59 (d, 1H)

Preparation of 4.29: In a glovebox a 20 mL scintillation vial was charged with 4.24 (150 mg, 0.229 mmol) and THF (10 mL). 2.3 mL of a 1.0 M solution of nBu_4NF in THF The resulting purple suspension turned brown over the course of an hour. After 4 h the reaction mixture was filtered through celite and concentrated to a solid. The resulting residue was extracted into C_6H_6 (3 x 5 mL), filtered through celite, and concentrated to give 4.29 as an orange solid. ^{1}H NMR (C_6D_6): δ 12.73 (s, 1H), 7.44 (d, 1H), 7.08 (t, 1H), 6.93 (t, 1H), 6.71-6.63 (m, 2H), 6.51 (s, 1H), 4.83 (m, 1H), 3.40 (m, 1H), 3.35-3.26 (m, 1H), 3.20 (t, 2H), 2.49 (s, 1H), 2.39 (s, 3H), 2.27 (s, 3H), 2.25 (s, 1H), 2.18 (s, 3H), 2.10 (t, 1H), 1.99 (s, 3H), 1.89 (d, 4H), 1.56 (d, 2H), 1.40 (d, 3H), 1.31 (d, 3H), 1.22 (t, 1H), 1.14-1.10 (m, 1H)

Preparation of 4.30: The compound could be prepared either from 4.24 or 4.23. In the case of 4.24 the catalyst was dissolved in THF and a 10-20 fold excess of hydrogen bromide (in methanol solution) was added and the solution immediately changed from purple to brown. The benzylidene peak shifted cleanly from 14.87 ppm to 17.02 ppm (in C_6D_6). In the case of 4.23 the catalyst was again dissolved in THF and a 20 fold excess of lithium bromide was added and the solution was heated to 40 °C for 24 hours. The reaction was then dried, extracted into benzene, dried again, and fresh lithium bromide was added so the process could be repeated as needed. Intermediate reaction progress showed ^{1}H NMR peaks at 17.13 ppm, 17.06 ppm and 17.02 ppm (in C_6D_6).

Preparation of 4.32: In a glovebox a 20 mL scintillation vial was charged with 4.23 (50 mg, 77.8

μmol), NaI (357 mg, 1.56 mmol), THF (5 mL) and MeOH (5 mL). The resulting green solution was then stirred at 40 °C for 3 h. The yellowish-brown was dried to a solid under vacuum, then extracted into C_6H_6 (3 x 5mL) and dried again under vacuum to give 4.32 as a dark green solid. A crystal suitable for X-ray diffraction was prepared by slow diffusion of pentane into a concentrated solution of 4.32 in THF. ^{1}H NMR (C_6D_6): δ 16.38 (s, 1H), 7.14-7.10 (m, 2H), 6.83 (s, 2H), 6.66 (t, 1H), 6.48 (d, 1H), 4.68 (sep, 1H), 3.58 (t, 2H), 3.25 (t, 2H), 2.55 (s, 6H), 2.30 (br s, 3H), 2.23 (s, 3H), 1.93 (d, 3H), 1.66 (d, 9H), 1.42 (t, 2H) ^{13}C NMR (125 MHz, C_6D_6: δ 209.94, 170.35, 153.74, 145.36, 139.88, 138.41, 138.24, 131.12, 129.97, 124.61, 122.12, 113,87

References

[1] S.T. Nguyen, L.K. Johnson, R.H. Grubbs, and J.W. Ziller. Ring-Opening Metathesis Polymerization (ROMP) of Norbornene by a Group-VIII Carbene Complex in Protic Media. *Journal of the American Chemical Society*, 114(10):3974–3975, 1992.

[2] T.M. Trnka and R.H. Grubbs. The development of $L_2X_2Ru = CHR$ olefin metathesis catalysts: An organometallic success story. *Accounts of Chemical Research*, 34(1):18–29, 2001.

[3] R.H. Grubbs, editor. *Handbook of Metathesis*, volume 1–3. Wiley-VCH, Weinheim, 2003.

[4] G.C. Vougioukalakis and R.H. Grubbs. Ruthenium-Based Heterocyclic Carbene-Coordinated Olefin Metathesis Catalysts. *Chemical Reviews*, 110(3):1746–1787, 2010.

[5] E.L. Dias, S.T. Nguyen, and R.H. Grubbs. Well-defined ruthenium olefin metathesis catalysts: Mechanism and activity. *Journal of the American Chemical Society*, 119(17):3887–3897, 1997.

[6] M.S. Sanford, J.A. Love, and R.H. Grubbs. Mechanism and activity of ruthenium olefin metathesis catalysts. *Journal of the American Chemical Society*, 123(27):6543–6554, 2001.

[7] J. Wappel, C.A. Urbina-Blanco, M. Abbas, J.H. Albering, R. Saf, S.P. Nolan, and C. Slugovc. Halide exchanged Hoveyda-type complexes in olefin metathesis. *Beilstein Journal of Organic Chemistry*, 6:1091–1098, 2010.

[8] R.M. Thomas, A. Fedorov, B.K. Keitz, and R.H. Grubbs. Thermally Stable, Latent Olefin Metathesis Catalysts. *Organometallics*, 30(24):6713–6717, 2011.

[9] A. Hejl. *Controlling Olefin Metathesis Through Catalyst and Monomer Design*. PhD thesis, California Institute of Technology, 2007.

[10] K.S. Coleman, J. Fawcett, J.H. Holloway, E Hope, and D.R. Russell. Air-stable ruthenium(II) and osmium(II) fluoride complexes. Crystal structures of $[OC\text{-}6\text{-}13][MF_2(CO)_2(PR_3)_2]$ [M = Ru, $PR_3 = PEtPh_2$; M = Os, $PR_3 = PPh_3$ or $P(C_6H_{11})_3$]. *Journal of the Chemical Society-Dalton Transactions*, (19):3557–3562, 1997.

[11] V.V. Grushin. The Organometallic Fluorine Chemistry of Palladium and Rhodium: Studies toward Aromatic Fluorination. *Accounts of Chemical Research*, 43(1):160–171, 2010.

[12] N.D. Ball and M.S. Sanford. Synthesis and Reactivity of a Mono-σ-Aryl Palladium(IV) Fluoride Complex. *Journal of the American Chemical Society*, 131(11):3796–3797, 2009.

[13] J.M. Racowski, J.B. Gary, and M.S. Sanford. Carbon(sp(3))-Fluorine Bond-Forming Reductive Elimination from Palladium(IV) Complexes. *Angewandte Chemie—International Edition*, 51(14):3414–3417, 2012.

[14] R.D.W. Kemmitt, R.D. Peacock, and I.L. Wilson. Existence of Carbonyl Fluorides of Platinum Metals. *Chemical Communications*, (14):772–773, 1968.

[15] C.J. Marshall, R.D. Peacock, D.R. Russell, and I.L. Wilson. Preparation and Crystal Structure of a Ruthenium Carbonyl Fluoride $[Ru(CO)_3F_2]_4$. *Journal of the Chemical Society D—Chemical Communications*, (23):1643–1644, 1970.

[16] A.J. Hewitt, J.H. Holloway, R.D. Peacock, J.B. Raynor, and I.L. Wilson. Preparation and Characterization of tetrakis(tricarbonyldifluororuthenium), tricarbonyltrifluoruthenium, and bis(tricarbonyldifluororuthenium-ruthenium pentafluoride). *Journal of the Chemical Society—Dalton Transactions*, (7):579–583, 1976.

[17] S.A. Brewer, K.S. Coleman, J. Fawcett, J.H. Holloway, E.G. Hope, D.R. Russell, and P.G. Waston. Ruthenium and Osmium Acyl Fluoride Complexes—Crystal-Structure of $[OC\text{-}6\text{-}13][RUF_2(CO)_2(PPh_3)] \cdot CD_2CL_2$. *Journal of the Chemical Society—Dalton Transactions*, (7):1073–1076, 1995.

[18] D.A.J. Harding, E.G. Hope, J. Fawcett, and G.A. Solan. Alkynylphosphanes as supports for mixed-metal Co_4M (M = Ru, Os) fluoride complexes: Syntheses, structures and thermolysis studies. *Journal of Organometallic Chemistry*, 692(24):5474–5480, 2007.

[19] J. Fawcett, D.A.J. Harding, Eric G. Hope, K. Singh, and G.A. Solan. N-Heterocyclic carbene-

containing ruthenium difluoro complexes and their reactivity towards BF_3. *Dalton Transactions*, (34):6861–6870, 2009.

[20] K.S. Coleman, J. Fawcett, D.A.J. Harding, E.G. Hope, K. Singh, and G.A. Solan. Routes to Ruthenium-Fluoro Cations of the Type $[RuL_2(CO)_nF]^+$ (n=2,3; L = PR_3, NHC): A Play-Off between Solvent, L and Weakly Coordinating Anion. *European Journal of Inorganic Chemistry*, (26):4130–4138, 2010.

[21] K.S. Coleman, J.H. Holloway, E.G. Hope, and J. Langer. Reaction of ruthenium(II) and osmium(II) hydrides with anhydrous HF. *Journal of the Chemical Society-Dalton Transactions*, (23):4555–4559, 1997.

[22] P. Barthazy, R.M. Stoop, M. Worle, A. Togni, and A. Mezzetti. Toward metal-mediated C-F bond formation. Synthesis and reactivity of the 16-electron fluoro complex $[RuF(dppp)_2]PF_6$ (dppp=1,3-bis(diphenylphosphino)propane). *Organometallics*, 19(15):2844–2852, 2000.

[23] P. Barthazy, A. Togni, and A. Mezzetti. Catalytic fluorination by halide exchange with 16-electron ruthenium(II) complexes. X-ray structure of $[Tl(\mu\text{-}F)_2Ru(dppe)_2]PF_6$. *Organometallics*, 20(16):3472–3477, 2001.

[24] M.S. Kirkham, M.F. Mahon, and M.K. Whittlesey. C-F bond activation of perfluoroalkenes by ruthenium phosphine hydride complexes: X-ray crystal structures of *cis*-$Ru(dmpe)_2F(F\cdots HF)$ and $[Ru(dcpe)_2H]^+[(CF_3)_2C{=}C(O)CF_2CF_3]^-$. *Chemical Communications*, (9):813–814, 2001.

[25] D.A.J. Harding, E.G. Hope, G.A. Solan, and J. Fawcett. Bis[1,2-bis(diphenylphosphino)ethane-κ^2P,P′] difluoridoruthenium(II) trichloromethane disolvate. *Acta Crystallographica Section C—Crystal Structure Communications*, 63(Part 8):m383–m384, 2007.

[26] M.B. Herbert, Y. Lan, B.K. Keitz, P. Liu, K. Endo, M.W. Day, K.N. Houk, and R.H. Grubbs. Decomposition Pathways of Z-Selective Ruthenium Metathesis Catalysts. *Journal of the American Chemical Society*, 134(18):7861–7866, 2012.

[27] P.E. Romero, W.E. Piers, and R. McDonald. Rapidly initiating ruthenium olefin-metathesis catalysts. *Angewandte Chemie—International Edition*, 43(45):6161–6165, 2004.

[28] M.L. Macnaughtan, M.J.A. Johnson, and J.W. Kampf. Olefin metathesis reactions with vinyl halides: Formation, observation, interception, and fate of the ruthenium-monohalomethylidene moiety. *Journal of the American Chemical Society*, 129(25):7708–7709, 2007.

[29] E.F. van der Eide, P.E. Romero, and W.E. Piers. Generation and spectroscopic characterization of ruthenacyclobutane and ruthenium olefin carbene intermediates relevant to ring closing metathesis catalysis. *Journal of the American Chemical Society*, 130(13):4485–4491, 2008.

[30] E.M. Leitao, E.F. van der Eide, P.E. Romero, W.E. Piers, and R. McDonald. Kinetic and Thermodynamic Analysis of Processes Relevant to Initiation of Olefin Metathesis by Ruthenium Phosphonium Alkylidene Catalysts. *Journal of the American Chemical Society*, 132(8):2784–2794, 2010.

[31] S.E. Lehman and K.B. Wagener. Synthesis of ruthenium olefin metathesis catalysts with linear alkyl carbene complexes. *Organometallics*, 24(7):1477–1482, 2005.

[32] S.B. Garber, J.S. Kingsbury, B.L. Gray, and A.H. Hoveyda. Efficient and recyclable monomeric and dendritic ru-based metathesis catalysts. *Journal of the American Chemical Society*, 122(34):8168–8179, 2000.

[33] T.M. Trnka, J.P. Morgan, M.S. Sanford, T.E. Wilhelm, M. Scholl, T.L. Choi, S. Ding, M.W. Day, and R.H. Grubbs. Synthesis and activity of ruthenium alkylidene complexes coordinated with phosphine and N-heterocyclic carbene ligands. *Journal of the American Chemical Society*, 125(9):2546–2558, 2003.

[34] B.K. Keitz, K. Endo, P.R. Patel, M.B. Herbert, and R.H. Grubbs. Improved Ruthenium Catalysts for Z-Selective Olefin Metathesis. *Journal of the American Chemical Society*, 134(1):693–699, 2012.

[35] A.B. Pangborn, M.A. Giardello, R.H. Grubbs, R.K. Rosen, and F.J. Timmers. Safe and convenient procedure for solvent purification. *Organometallics*, 15(5):1518–1520, 1996.

[36] K. Endo and R.H. Grubbs. Chelated Ruthenium Catalysts for Z-Selective Olefin Metathesis. *Journal of the American Chemical Society*, 133(22):8525–8527, 2011.

Appendix A

Chelating Ligands for Model Ruthenium Complexes

Ever since the establishment of the metallacyclobutane mechanism for olefin metathesis, extensive research has focused on the isolation and characterization of reactive intermediates in the catalytic cycle. In particular, metallacyclobutanes and bound olefins have been of particular interest. Metallacyclobutanes have been isolated and characterized crystallographically for metathesis catalysts made from a number of early transition metal catalysts, including titanium,[1] tungsten[2] and molybdenum.[3] In the case of ruthenium no such structures have been isolated, although they have been observed at low temperatures by NMR spectroscopy.[4,5]

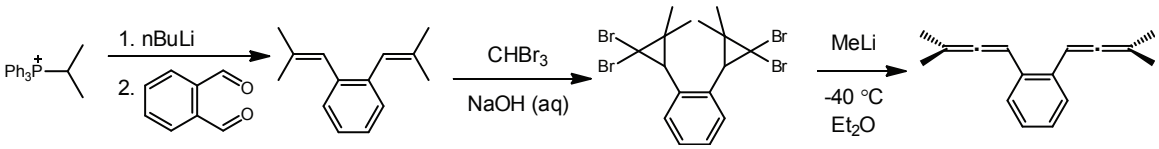

A.1 A.2 A.3 A.4

Figure A.1: Synthesis of diallene A.4

In an effort to isolate a ruthenacyclobutane, an *o*-diallenylbenzene was prepared following a literature precedent (Figure A.1).[6] The use of a diallene unit was designed to form a naphthalene unit upon olefin binding and metallacyclobutane formation, potentially stabilizing the otherwise elusive ruthenacyclobutane (Figure A.2).

Studies using fast-initiating catalyst A.5 and freshly prepared A.4 failed to produce an isolated ruthenacyclobutane. A complex mixture was formed in the reaction, and no metallacycles were

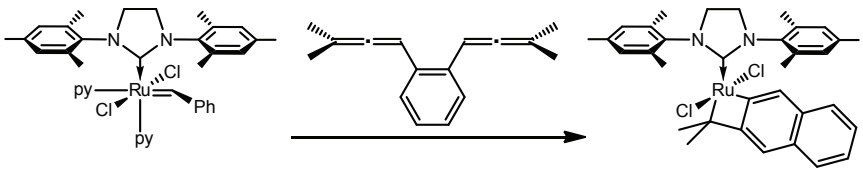

A.5 A.6

Figure A.2: Schematic of metallacyclobutane formation with ruthenium

observable by NMR. No complexes could be isolated by crystallization.

Ruthenium catalysts with bound olefins have been isolated and characterized crystallographically, but only using *o*-divinylbenzene, which cannot undergo RCM due to its constrained geometry.[7,8]

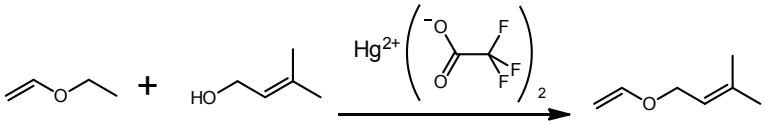

A.7 A.8 A.9

Figure A.3: Synthesis of vinyl ether A.9

To synthesize an improved model bound olefin complex, a vinyl ether with a pendant olefin was synthesized.[9] Instead of using a substrate which cannot complete RCM because of geometric constraints, a vinyl ether was used because they are known to deactivate ruthenium olefin metathesis catalysts by formation of a Fischer carbene. This deactivation does not completely preclude successful metathesis turnovers, as vinyl ethers have been shown to be successful substrates for RCM at elevated temperatures.[10]

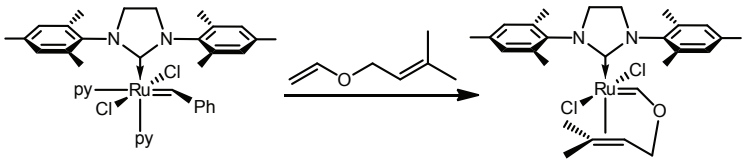

A.5 A.10

Figure A.4: Schematic of the formation of a ruthenium complex with a bound olefin

Studies using fast-initiating catalyst A.5 and A.9 failed to produce an isolated bound olefin compound. NMR scale studies showed that under a large excess of substrate no alkylidene peak is maintained in the ^{1}H NMR spectrum. When a 1:1 mixture was used in C_6D_6, however, peaks at 19.65 ppm and 14.03 ppm were observed. In CD_2Cl_2 no peaks were observed in the ^{1}H NMR past

9.0 ppm. The reaction was scaled up in C_6H_6 and the attempts were made to crystallize the product. The product resisted crystallization, however. A number of transparent crystals were formed from the reaction mixture, but X-ray crystallography revealed them to be the free NHC ligand.

References

[1] T.R. Howard, J.B. Lee, and R.H. Grubbs. Titanium metallacarbene-metallacyclobutane reactions: stepwise metathesis. *Journal of the American Chemical Society*, 102(22):6876–6878, 1980.

[2] A.J. Jiang, J.H. Simpson, P. Mueller, and R.R. Schrock. Fundamental Studies of Tungsten Alkylidene Imido Monoalkoxidepyrrolide Complexes. *Journal of the American Chemical Society*, 131(22):7770–7780, 2009.

[3] R.R. Schrock, A.J. Jiang, S.C. Marinescu, J.H. Simpson, and P. Mueller. Fundamental Studies of Molybdenum and Tungsten Methylidene and Metallacyclobutane Complexes. *Organometallics*, 29(21):5241–5251, 2010.

[4] A.G. Wenzel, G. Blake, D.G. VanderVelde, and R.H. Grubbs. Characterization and Dynamics of Substituted Ruthenacyclobutanes Relevant to the Olefin Cross-Metathesis Reaction. *Journal of the American Chemical Society*, 133(16):6429–6439, 2011.

[5] B.K. Keitz and R.H. Grubbs. Probing the Origin of Degenerate Metathesis Selectivity via Characterization and Dynamics of Ruthenacyclobutanes Containing Variable NHCs. *Journal of the American Chemical Society*, 133(40):16277–16284, 2011.

[6] S. Braverman and Y. Duar. Thermal Rearrangements of Allenes—Synthesis and Mechanism of Cycloaromatization of π-bridged and Heteroatom Bridged Diallenes. *Journal of the American Chemical Society*, 112(15):5830–5837, 1990.

[7] D.R. Anderson, D.D. Hickstein, D.J. O'Leary, and R.H. Grubbs. Model compounds of ruthenium-alkene intermediates in olefin metathesis reactions. *Journal of the American Chemical Society*, 128(26):8386–8387, 2006.

[8] D.R. Anderson, D.J. O'Leary, and R.H. Grubbs. Ruthenium-olefin complexes: Effect of ligand variation upon geometry. *Chemistry—A European Journal*, 14(25):7536–7544, 2008.

[9] R.K. Boeckman and S.S. Ko. Stereochemical Control in the Intramolecular Diels-Alder Reaction. 2. Structural and Electronic Effects on Reactivity and Selectivity. *Journal of the American Chemical Society*, 104(4):1033–1041, 1982.

[10] W.A.L. van Otterlo, E.L. Ngidi, and C.B. de Koning. Sequential isomerization and ring-closing metathesis: masked styryl and vinyloxyaryl groups for the synthesis of benzo-fused heterocycles. *Tetrahedron Letters*, 44(34):6483–6486, 2003.

Appendix B

Crystallographic Data

Table B.1: Crystal Data and Structure Analysis Details for 4.27

Empirical formula	C32 H41 Cl N2 O Ru
Formula weight	606.19
Crystallization solvent	
Crystal shape	rhomboidal
Crystal color	green
Crystal size	0.09 x 0.17 x 0.32 mm

Data Collection

Preliminary photograph(s)	rotation	
Type of diffractometer	Bruker APEX-II CCD	
Wavelength	0.71073 Å MoK	
Data collection temperature	100 K	
Theta range for 9323 reflections used in lattice determination	2.47 to 34.89°	
Unit cell dimensions	a = 10.2770(5) Å b = 25.1483(13) Å c = 10.9259(6) Å	α= 90° β= 90.518(3)° γ = 90°
Volume	2823.7(3) $Å^3$	
Z	4	
Crystal system	monoclinic	
Space group	P 1 21/n 1 (# 14)	
Density (calculated)	1.426 g/cm^3	
F(000)	1264	
Theta range for data collection	2.0 to 39.0°	
Completeness to theta = 25.00°	100.0%	
Index ranges	$-17 \le h \le 17$, $-44 \le k \le 44$, $-18 \le l \le 18$	
Data collection scan type	and scans	
Reflections collected	184727	
Independent reflections	15671 [R_{int}= 0.0769]	
Reflections > 2σ(I)	11838	
Average σ(I)/(net I)	0.0455	
Absorption coefficient	0.68 mm^{-1}	
Absorption correction	Semi-empirical from equivalents	
Max. and min. transmission	1.0000 and 0.9151	

Table B.1 (cont.):

Structure Solution and Refinement

Primary solution method	direct
Secondary solution method	difmap
Hydrogen placement	geom
Refinement method	Full-matrix least-squares on F^2
Data / restraints / parameters	15671 / 0 / 339
Treatment of hydrogen atoms	constr
Goodness-of-fit on F^2	2.62
Final R indices [I>2σ(I), 11838 reflections]	R1 = 0.0513, wR2 = 0.0788
R indices (all data)	R1 = 0.0772, wR2 = 0.0800
Type of weighting scheme used	calc
Weighting scheme used	calc w=1/[^2^(Fo^2^)]
Max shift/error	0.002
Average shift/error	0.000
Largest diff. peak and hole	2.31 and -1.77 e·$Å^{-3}$

Programs Used

Cell refinement	SAINT V8.18C (Bruker-AXS, 2007)
Data collection	APEX2 2012.2-0 (Bruker-AXS, 2007)
Data reduction	SAINT V8.18C (Bruker-AXS, 2007)
Structure solution	SHELXS-97 (Sheldrick, 1990)
Structure refinement	SHELXL-97 (Sheldrick, 1997)
Graphics	DIAMOND 3 (Crystal Impact, 1999)

Table B.2: Atomic coordinates (x 10^4) and equivalent isotropic displacement parameters ($Å^2$x 10^3) for 4.27. U(eq) is defined as one third of the trace of the orthogonalized U^{ij} tensor.

	x	y	z	U_{eq}
Ru(1)	2351(1)	6616(1)	9672(1)	13(1)
Cl(1)	1807(1)	7020(1)	11580(1)	25(1)
N(1)	624(1)	6724(1)	7614(1)	18(1)
N(2)	1107(1)	7529(1)	8242(1)	18(1)
O(1)	3845(1)	6087(1)	10682(1)	17(1)
C(1)	1288(2)	7008(1)	8490(2)	16(1)
C(2)	88(2)	7064(1)	6636(2)	25(1)
C(3)	213(2)	7617(1)	7197(2)	27(1)
C(4)	1105(2)	6185(1)	7393(2)	16(1)
C(5)	1654(2)	6001(1)	8638(2)	16(1)
C(6)	2277(2)	5450(1)	8479(2)	18(1)
C(7)	1208(2)	5062(1)	8052(2)	24(1)
C(8)	630(2)	5247(1)	6837(2)	24(1)
C(9)	1715(2)	5264(1)	5883(2)	27(1)
C(10)	2778(2)	5642(1)	6290(2)	22(1)
C(11)	2182(2)	6197(1)	6436(2)	19(1)
C(12)	39(2)	5804(1)	6977(2)	22(1)
C(13)	3346(2)	5469(1)	7526(2)	20(1)
C(14)	1325(2)	7962(1)	9073(2)	16(1)
C(15)	2364(2)	8311(1)	8866(2)	17(1)
C(16)	2463(2)	8756(1)	9621(2)	18(1)
C(17)	1592(2)	8859(1)	10546(2)	17(1)
C(18)	584(2)	8496(1)	10730(2)	18(1)
C(19)	418(2)	8051(1)	9997(2)	18(1)
C(20)	3341(2)	8225(1)	7868(2)	26(1)
C(21)	1674(2)	9353(1)	11326(2)	22(1)
C(22)	-725(2)	7685(1)	10173(2)	24(1)
C(23)	3829(2)	6806(1)	8906(2)	16(1)
C(24)	5092(2)	6577(1)	9310(2)	15(1)
C(25)	6290(2)	6721(1)	8806(2)	20(1)
C(26)	7424(2)	6462(1)	9159(2)	23(1)
C(27)	7366(2)	6057(1)	10001(2)	25(1)
C(28)	6197(2)	5912(1)	10541(2)	21(1)
C(29)	5071(2)	6178(1)	10203(2)	15(1)
C(30)	3703(2)	5717(1)	11717(2)	18(1)
C(31)	4227(2)	5961(1)	12872(2)	26(1)
C(32)	2270(2)	5588(1)	11818(2)	26(1)

Table B.3: Bond lengths [Å] and angles [°] for 4.27

Ru(1)-Cl(1)	2.3899(5)
Ru(1)-O(1)	2.3054(11)
Ru(1)-C(1)	1.9513(17)
Ru(1)-C(5)	2.0401(17)
Ru(1)-C(23)	1.8064(17)
N(1)-C(1)	1.370(2)
N(1)-C(2)	1.471(2)
N(1)-C(4)	1.465(2)
N(2)-C(1)	1.352(2)
N(2)-C(3)	1.476(2)
N(2)-C(14)	1.435(2)
O(1)-C(29)	1.3877(19)
O(1)-C(30)	1.472(2)
C(2)-H(2A)	0.9900
C(2)-H(2B)	0.9900
C(2)-C(3)	1.525(3)
C(3)-H(3A)	0.9900
C(3)-H(3B)	0.9900
C(4)-C(5)	1.538(2)
C(4)-C(11)	1.530(2)
C(4)-C(12)	1.522(2)
C(5)-H(5)	1.0000
C(5)-C(6)	1.538(2)
C(6)-H(6)	1.0000
C(6)-C(7)	1.538(2)
C(6)-C(13)	1.521(2)
C(7)-H(7A)	0.9900
C(7)-H(7B)	0.9900
C(7)-C(8)	1.521(3)
C(8)-H(8)	1.0000
C(8)-C(9)	1.534(3)
C(8)-C(12)	1.535(3)
C(9)-H(9A)	0.9900
C(9)-H(9B)	0.9900
C(9)-C(10)	1.512(3)
C(10)-H(10)	1.0000
C(10)-C(11)	1.534(2)
C(10)-C(13)	1.529(2)
C(11)-H(11A)	0.9900
C(11)-H(11B)	0.9900
C(12)-H(12A)	0.9900
C(12)-H(12B)	0.9900
C(13)-H(13A)	0.9900
C(13)-H(13B)	0.9900
C(14)-C(15)	1.401(2)
C(14)-C(19)	1.398(2)
C(15)-C(16)	1.394(2)
C(15)-C(20)	1.505(2)
C(16)-H(16)	0.9500
C(16)-C(17)	1.380(2)
C(17)-C(18)	1.397(2)

C(17)-C(21)	1.509(2)
C(18)-H(18)	0.9500
C(18)-C(19)	1.385(2)
C(19)-C(22)	1.505(2)
C(20)-H(20A)	0.9800
C(20)-H(20B)	0.9800
C(20)-H(20C)	0.9800
C(21)-H(21A)	0.9800
C(21)-H(21B)	0.9800
C(21)-H(21C)	0.9800
C(22)-H(22A)	0.9800
C(22)-H(22B)	0.9800
C(22)-H(22C)	0.9800
C(23)-H(23)	0.9500
C(23)-C(24)	1.484(2)
C(24)-C(25)	1.401(2)
C(24)-C(29)	1.399(2)
C(25)-H(25)	0.9500
C(25)-C(26)	1.387(3)
C(26)-H(26)	0.9500
C(26)-C(27)	1.373(3)
C(27)-H(27)	0.9500
C(27)-C(28)	1.391(2)
C(28)-H(28)	0.9500
C(28)-C(29)	1.385(2)
C(30)-H(30)	1.0000
C(30)-C(31)	1.500(3)
C(30)-C(32)	1.512(2)
C(31)-H(31A)	0.9800
C(31)-H(31B)	0.9800
C(31)-H(31C)	0.9800
C(32)-H(32A)	0.9800
C(32)-H(32B)	0.9800
C(32)-H(32C)	0.9800

O(1)-Ru(1)-Cl(1)	89.32(3)
C(1)-Ru(1)-Cl(1)	103.22(5)
C(1)-Ru(1)-O(1)	167.10(6)
C(1)-Ru(1)-C(5)	79.86(7)
C(5)-Ru(1)-Cl(1)	136.18(5)
C(5)-Ru(1)-O(1)	93.27(6)
C(23)-Ru(1)-Cl(1)	119.73(6)
C(23)-Ru(1)-O(1)	79.39(6)
C(23)-Ru(1)-C(1)	91.56(7)
C(23)-Ru(1)-C(5)	103.69(7)
C(1)-N(1)-C(2)	112.77(14)
C(1)-N(1)-C(4)	115.43(14)
C(4)-N(1)-C(2)	122.89(14)
C(1)-N(2)-C(3)	112.58(14)
C(1)-N(2)-C(14)	126.14(14)
C(14)-N(2)-C(3)	117.93(13)
C(29)-O(1)-Ru(1)	109.05(9)
C(29)-O(1)-C(30)	119.44(13)
C(30)-O(1)-Ru(1)	131.43(10)

N(1)-C(1)-Ru(1)	118.21(12)
N(2)-C(1)-Ru(1)	134.23(13)
N(2)-C(1)-N(1)	107.30(14)
N(1)-C(2)-H(2A)	111.4
N(1)-C(2)-H(2B)	111.4
N(1)-C(2)-C(3)	101.98(14)
H(2A)-C(2)-H(2B)	109.2
C(3)-C(2)-H(2A)	111.4
C(3)-C(2)-H(2B)	111.4
N(2)-C(3)-C(2)	102.96(14)
N(2)-C(3)-H(3A)	111.2
N(2)-C(3)-H(3B)	111.2
C(2)-C(3)-H(3A)	111.2
C(2)-C(3)-H(3B)	111.2
H(3A)-C(3)-H(3B)	109.1
N(1)-C(4)-C(5)	104.72(13)
N(1)-C(4)-C(11)	109.96(14)
N(1)-C(4)-C(12)	112.91(14)
C(11)-C(4)-C(5)	110.41(14)
C(12)-C(4)-C(5)	109.40(14)
C(12)-C(4)-C(11)	109.37(15)
Ru(1)-C(5)-H(5)	101.4
C(4)-C(5)-Ru(1)	112.75(11)
C(4)-C(5)-H(5)	101.4
C(6)-C(5)-Ru(1)	126.91(12)
C(6)-C(5)-C(4)	108.71(14)
C(6)-C(5)-H(5)	101.4
C(5)-C(6)-H(6)	109.6
C(5)-C(6)-C(7)	107.97(14)
C(7)-C(6)-H(6)	109.6
C(13)-C(6)-C(5)	110.67(14)
C(13)-C(6)-H(6)	109.6
C(13)-C(6)-C(7)	109.29(15)
C(6)-C(7)-H(7A)	109.6
C(6)-C(7)-H(7B)	109.6
H(7A)-C(7)-H(7B)	108.1
C(8)-C(7)-C(6)	110.13(15)
C(8)-C(7)-H(7A)	109.6
C(8)-C(7)-H(7B)	109.6
C(7)-C(8)-H(8)	109.5
C(7)-C(8)-C(9)	108.70(15)
C(7)-C(8)-C(12)	110.05(16)
C(9)-C(8)-H(8)	109.5
C(9)-C(8)-C(12)	109.43(15)
C(12)-C(8)-H(8)	109.5
C(8)-C(9)-H(9A)	109.6
C(8)-C(9)-H(9B)	109.6
H(9A)-C(9)-H(9B)	108.1
C(10)-C(9)-C(8)	110.22(15)
C(10)-C(9)-H(9A)	109.6
C(10)-C(9)-H(9B)	109.6
C(9)-C(10)-H(10)	109.8
C(9)-C(10)-C(11)	108.32(15)
C(9)-C(10)-C(13)	110.50(15)

C(11)-C(10)-H(10)	109.8
C(13)-C(10)-H(10)	109.8
C(13)-C(10)-C(11)	108.46(14)
C(4)-C(11)-C(10)	110.17(14)
C(4)-C(11)-H(11A)	109.6
C(4)-C(11)-H(11B)	109.6
C(10)-C(11)-H(11A)	109.6
C(10)-C(11)-H(11B)	109.6
H(11A)-C(11)-H(11B)	108.1
C(4)-C(12)-C(8)	108.68(14)
C(4)-C(12)-H(12A)	110.0
C(4)-C(12)-H(12B)	110.0
C(8)-C(12)-H(12A)	110.0
C(8)-C(12)-H(12B)	110.0
H(12A)-C(12)-H(12B)	108.3
C(6)-C(13)-C(10)	109.94(14)
C(6)-C(13)-H(13A)	109.7
C(6)-C(13)-H(13B)	109.7
C(10)-C(13)-H(13A)	109.7
C(10)-C(13)-H(13B)	109.7
H(13A)-C(13)-H(13B)	108.2
C(15)-C(14)-N(2)	119.17(15)
C(19)-C(14)-N(2)	118.45(15)
C(19)-C(14)-C(15)	122.10(16)
C(14)-C(15)-C(20)	122.79(16)
C(16)-C(15)-C(14)	117.30(16)
C(16)-C(15)-C(20)	119.91(16)
C(15)-C(16)-H(16)	118.7
C(17)-C(16)-C(15)	122.59(16)
C(17)-C(16)-H(16)	118.7
C(16)-C(17)-C(18)	118.05(16)
C(16)-C(17)-C(21)	122.31(15)
C(18)-C(17)-C(21)	119.61(15)
C(17)-C(18)-H(18)	118.9
C(19)-C(18)-C(17)	122.15(16)
C(19)-C(18)-H(18)	118.9
C(14)-C(19)-C(22)	121.39(16)
C(18)-C(19)-C(14)	117.79(16)
C(18)-C(19)-C(22)	120.80(16)
C(15)-C(20)-H(20A)	109.5
C(15)-C(20)-H(20B)	109.5
C(15)-C(20)-H(20C)	109.5
H(20A)-C(20)-H(20B)	109.5
H(20A)-C(20)-H(20C)	109.5
H(20B)-C(20)-H(20C)	109.5
C(17)-C(21)-H(21A)	109.5
C(17)-C(21)-H(21B)	109.5
C(17)-C(21)-H(21C)	109.5
H(21A)-C(21)-H(21B)	109.5
H(21A)-C(21)-H(21C)	109.5
H(21B)-C(21)-H(21C)	109.5
C(19)-C(22)-H(22A)	109.5
C(19)-C(22)-H(22B)	109.5
C(19)-C(22)-H(22C)	109.5

H(22A)-C(22)-H(22B)	109.5
H(22A)-C(22)-H(22C)	109.5
H(22B)-C(22)-H(22C)	109.5
Ru(1)-C(23)-H(23)	120.2
C(24)-C(23)-Ru(1)	119.69(12)
C(24)-C(23)-H(23)	120.2
C(25)-C(24)-C(23)	123.46(15)
C(29)-C(24)-C(23)	117.87(14)
C(29)-C(24)-C(25)	118.61(15)
C(24)-C(25)-H(25)	119.7
C(26)-C(25)-C(24)	120.54(17)
C(26)-C(25)-H(25)	119.7
C(25)-C(26)-H(26)	120.2
C(27)-C(26)-C(25)	119.53(17)
C(27)-C(26)-H(26)	120.2
C(26)-C(27)-H(27)	119.3
C(26)-C(27)-C(28)	121.41(17)
C(28)-C(27)-H(27)	119.3
C(27)-C(28)-H(28)	120.6
C(29)-C(28)-C(27)	118.89(17)
C(29)-C(28)-H(28)	120.6
O(1)-C(29)-C(24)	113.72(14)
C(28)-C(29)-O(1)	125.35(15)
C(28)-C(29)-C(24)	120.93(15)
O(1)-C(30)-H(30)	109.2
O(1)-C(30)-C(31)	110.50(14)
O(1)-C(30)-C(32)	107.16(14)
C(31)-C(30)-H(30)	109.2
C(31)-C(30)-C(32)	111.60(15)
C(32)-C(30)-H(30)	109.2
C(30)-C(31)-H(31A)	109.5
C(30)-C(31)-H(31B)	109.5
C(30)-C(31)-H(31C)	109.5
H(31A)-C(31)-H(31B)	109.5
H(31A)-C(31)-H(31C)	109.5
H(31B)-C(31)-H(31C)	109.5
C(30)-C(32)-H(32A)	109.5
C(30)-C(32)-H(32B)	109.5
C(30)-C(32)-H(32C)	109.5
H(32A)-C(32)-H(32B)	109.5
H(32A)-C(32)-H(32C)	109.5
H(32B)-C(32)-H(32C)	109.5

Table B.4: Anisotropic displacement parameters ($Å^2 x\ 10^4$) for 4.27. The anisotropic displacement factor exponent takes the form: $-2\pi^2 [h^2 a^{*2} U^{11} + ... + 2 h k a^* b^* U^{12}]$.

	U^{11}	U^{22}	U^{33}	U^{23}	U^{13}	U^{12}
Ru(1)	136(1)	121(1)	136(1)	3(1)	-14(1)	6(1)
Cl(1)	283(2)	262(2)	193(2)	-34(2)	0(2)	57(2)
N(1)	187(7)	145(7)	193(7)	-20(6)	-68(6)	28(5)
N(2)	227(8)	130(7)	173(7)	-9(6)	-71(6)	43(6)
O(1)	154(6)	174(6)	172(6)	70(5)	-28(5)	-10(4)
C(1)	135(8)	153(8)	177(8)	-13(7)	4(6)	13(6)
C(2)	304(11)	196(9)	242(10)	-4(8)	-129(8)	68(7)
C(3)	363(11)	180(9)	254(10)	-15(8)	-155(8)	80(8)
C(4)	188(8)	118(8)	185(9)	-18(6)	-51(7)	6(6)
C(5)	144(8)	131(8)	192(8)	15(6)	-11(6)	-11(6)
C(6)	204(9)	121(8)	200(9)	14(7)	-27(7)	1(6)
C(7)	256(10)	137(8)	310(11)	2(8)	-21(8)	-43(7)
C(8)	256(10)	165(9)	311(11)	-20(8)	-83(8)	-73(7)
C(9)	393(12)	182(9)	238(10)	-72(8)	-73(9)	20(8)
C(10)	260(10)	191(9)	204(9)	-32(7)	38(8)	11(7)
C(11)	244(9)	147(8)	180(9)	5(7)	-24(7)	2(7)
C(12)	197(9)	213(9)	260(10)	-12(8)	-63(7)	-23(7)
C(13)	222(9)	126(8)	254(10)	-8(7)	-3(7)	28(6)
C(14)	210(9)	106(7)	167(8)	-1(6)	-56(7)	45(6)
C(15)	208(9)	134(8)	179(8)	16(6)	-28(7)	46(6)
C(16)	185(9)	130(7)	222(9)	32(7)	-29(7)	0(6)
C(17)	193(9)	127(8)	188(9)	5(6)	-44(7)	21(6)
C(18)	194(9)	157(8)	193(9)	-5(6)	3(7)	35(6)
C(19)	186(9)	132(8)	212(9)	26(7)	-29(7)	23(6)
C(20)	307(11)	194(9)	285(11)	-4(8)	84(9)	10(8)
C(21)	243(10)	164(9)	256(10)	-31(7)	13(8)	-6(7)
C(22)	224(10)	162(9)	338(11)	-24(8)	25(8)	5(7)
C(23)	292(10)	95(7)	96(7)	34(6)	41(7)	80(6)
C(24)	156(8)	153(8)	147(7)	-21(7)	-14(6)	-17(6)
C(25)	208(9)	206(9)	176(9)	-2(7)	1(7)	-44(7)
C(26)	160(9)	285(10)	241(10)	-17(8)	13(7)	-28(7)
C(27)	157(9)	309(11)	277(10)	3(8)	-43(8)	57(7)
C(28)	176(9)	200(9)	247(10)	54(7)	-25(7)	21(7)
C(29)	127(8)	162(8)	163(8)	-8(6)	-8(6)	-18(6)
C(30)	209(9)	151(8)	195(9)	68(7)	-33(7)	-12(6)
C(31)	308(11)	289(11)	176(9)	35(8)	-28(8)	-52(8)
C(32)	245(10)	287(11)	234(10)	102(8)	15(8)	-82(8)

Table B.5: Hydrogen coordinates (x 10^3) and isotropic displacement parameters ($Å^2$x 10^3) for 4.27

	x	y	z	U_{iso}
H(2A)	-83	698	645	30
H(2B)	60	703	588	30
H(3A)	58	787	661	32
H(3B)	-64	775	747	32
H(5)	84	591	908	19
H(6)	265	533	928	21
H(7A)	158	470	796	28
H(7B)	52	504	868	28
H(8)	-6	499	656	29
H(9A)	208	490	578	33
H(9B)	135	538	509	33
H(10)	348	565	566	26
H(11A)	287	645	669	23
H(11B)	182	632	564	23
H(12A)	-33	592	618	27
H(12B)	-67	580	759	27
H(13A)	375	511	745	24
H(13B)	403	572	779	24
H(16)	316	900	949	22
H(18)	-1	856	1138	22
H(20A)	405	800	817	39
H(20B)	370	857	761	39
H(20C)	292	805	717	39
H(21A)	252	953	1120	33
H(21B)	158	926	1219	33
H(21C)	97	960	1109	33
H(22A)	-114	777	1095	36
H(22B)	-42	732	1018	36
H(22C)	-135	774	950	36
H(23)	380	705	825	19
H(25)	633	700	822	24
H(26)	824	656	882	27
H(27)	814	587	1022	30
H(28)	617	564	1113	25
H(30)	420	538	1154	22
H(31A)	513	607	1275	39
H(31B)	419	570	1354	39
H(31C)	370	627	1308	39
H(32A)	178	591	1199	38
H(32B)	214	533	1248	38
H(32C)	196	543	1105	38

Table B.6: Crystal Data and Structure Analysis Details for 4.28

Empirical formula	C32 H41 Br N2 O Ru
Formula weight	650.65
Crystallization solvent	dichloromethane
Crystal shape	tapered
Crystal color	brown
Crystal size	0.17 x 0.34 x 0.37 mm

Data Collection

Preliminary photograph(s)	rotation	
Type of diffractometer	Bruker SMART 1000 CCD	
Wavelength	0.71073 Å MoK	
Data collection temperature	100 K	
Theta range for 9886 reflections used in lattice determination	2.47 to 42.48°	
Unit cell dimensions	a = 10.3707(2) Å b = 25.2528(6) Å c = 10.9022(2) Å	α= 90° β= 90.548(1)° γ = 90°
Volume	2855.04(10) $Å^3$	
Z	4	
Crystal system	monoclinic	
Space group	P 1 21/n 1 (# 14)	
Density (calculated)	1.514 g/cm^3	
F(000)	1336	
Theta range for data collection	1.6 to 43.7°	
Completeness to theta = 25.00°	100.0%	
Index ranges	$-19 \le h \le 19$, $-48 \le k \le 48$, $-21 \le l \le 21$	
Data collection scan type	and scans	
Reflections collected	125464	
Independent reflections	21422 [R_{int}= 0.0469]	
Reflections > 2σ(I)	16363	
Average σ(I)/(net I)	0.0402	
Absorption coefficient	1.98 mm^{-1}	
Absorption correction	Semi-empirical from equivalents	
Max. and min. transmission	1.0000 and 0.8260	

Table B6 (cont.):

Structure Solution and Refinement

Primary solution method	direct
Secondary solution method	difmap
Hydrogen placement	geom
Refinement method	Full-matrix least-squares on F^2
Data / restraints / parameters	21422 / 0 / 339
Treatment of hydrogen atoms	constr
Goodness-of-fit on F^2	1.68
Final R indices [I>2σ(I), 16363 reflections]	R1 = 0.0339, wR2 = 0.0503
R indices (all data)	R1 = 0.0565, wR2 = 0.0520
Type of weighting scheme used	calc
Weighting scheme used	calc w=1/[^2^(Fo^2^)]
Max shift/error	0.004
Average shift/error	0.000
Largest diff. peak and hole	1.39 and -0.73 e·$Å^{-3}$

Programs Used

Cell refinement	SAINT V8.18C (Bruker-AXS, 2007)
Data collection	SMART v5.054 (Bruker, 2001)
Data reduction	SAINT V8.18C (Bruker-AXS, 2007)
Structure solution	SHELXS-97 (Sheldrick, 1990)
Structure refinement	SHELXL-97 (Sheldrick, 1997)
Graphics	DIAMOND 3 (Crystal Impact, 1999)

Table B.7: Atomic coordinates (x 10^4) and equivalent isotropic displacement parameters ($Å^2$x 10^3) for 4.28. U(eq) is defined as one third of the trace of the orthogonalized U^{ij} tensor

	x	y	z	U_{eq}
Ru(1)	2353(1)	6607(1)	9674(1)	8(1)
Br(1)	1777(1)	7032(1)	11699(1)	15(1)
N(1)	632(1)	6718(1)	7613(1)	12(1)
N(2)	1123(1)	7520(1)	8238(1)	12(1)
O(1)	3843(1)	6075(1)	10681(1)	11(1)
C(1)	1293(1)	7001(1)	8486(1)	10(1)
C(2)	87(1)	7054(1)	6635(1)	18(1)
C(3)	260(1)	7611(1)	7167(1)	20(1)
C(4)	1103(1)	6180(1)	7395(1)	11(1)
C(5)	1656(1)	5994(1)	8637(1)	10(1)
C(6)	2275(1)	5446(1)	8477(1)	11(1)
C(7)	1211(1)	5055(1)	8058(1)	16(1)
C(8)	622(1)	5243(1)	6833(1)	17(1)
C(9)	1693(1)	5255(1)	5870(1)	18(1)
C(10)	2759(1)	5640(1)	6274(1)	14(1)
C(11)	2170(1)	6192(1)	6424(1)	13(1)
C(12)	33(1)	5799(1)	6977(1)	15(1)
C(13)	3334(1)	5463(1)	7508(1)	14(1)
C(14)	1324(1)	7956(1)	9064(1)	11(1)
C(15)	2354(1)	8301(1)	8877(1)	12(1)
C(16)	2454(1)	8748(1)	9633(1)	12(1)
C(17)	1564(1)	8854(1)	10545(1)	11(1)
C(18)	552(1)	8497(1)	10706(1)	12(1)
C(19)	396(1)	8052(1)	9967(1)	12(1)
C(20)	3342(1)	8212(1)	7892(1)	19(1)
C(21)	1645(1)	9348(1)	11323(1)	15(1)
C(22)	-759(1)	7696(1)	10112(1)	16(1)
C(23)	3847(1)	6809(1)	8918(1)	10(1)
C(24)	5072(1)	6570(1)	9308(1)	10(1)
C(25)	6258(1)	6716(1)	8800(1)	13(1)
C(26)	7392(1)	6460(1)	9152(1)	16(1)
C(27)	7342(1)	6053(1)	10006(1)	18(1)
C(28)	6179(1)	5906(1)	10550(1)	15(1)
C(29)	5056(1)	6169(1)	10209(1)	10(1)
C(30)	3720(1)	5702(1)	11709(1)	12(1)
C(31)	4253(1)	5947(1)	12881(1)	18(1)
C(32)	2300(1)	5568(1)	11831(1)	17(1)

Table B.8: Bond lengths [Å] and angles [°] for 4.28

Ru(1)-Br(1)	2.53136(13)
Ru(1)-O(1)	2.3164(7)
Ru(1)-C(1)	1.9623(9)
Ru(1)-C(5)	2.0429(9)
Ru(1)-C(23)	1.8349(10)
N(1)-C(1)	1.3688(12)
N(1)-C(2)	1.4724(13)
N(1)-C(4)	1.4638(12)
N(2)-C(1)	1.3498(12)
N(2)-C(3)	1.4821(12)
N(2)-C(14)	1.4364(12)
O(1)-C(29)	1.3847(11)
O(1)-C(30)	1.4701(11)
C(2)-H(2A)	0.9900
C(2)-H(2B)	0.9900
C(2)-C(3)	1.5312(15)
C(3)-H(3A)	0.9900
C(3)-H(3B)	0.9900
C(4)-C(5)	1.5382(12)
C(4)-C(11)	1.5384(13)
C(4)-C(12)	1.5347(13)
C(5)-H(5)	1.0000
C(5)-C(6)	1.5382(13)
C(6)-H(6)	1.0000
C(6)-C(7)	1.5463(14)
C(6)-C(13)	1.5313(14)
C(7)-H(7A)	0.9900
C(7)-H(7B)	0.9900
C(7)-C(8)	1.5384(14)
C(8)-H(8)	1.0000
C(8)-C(9)	1.5361(15)
C(8)-C(12)	1.5404(15)
C(9)-H(9A)	0.9900
C(9)-H(9B)	0.9900
C(9)-C(10)	1.5327(15)
C(10)-H(10)	1.0000
C(10)-C(11)	1.5321(14)
C(10)-C(13)	1.5331(14)
C(11)-H(11A)	0.9900
C(11)-H(11B)	0.9900
C(12)-H(12A)	0.9900
C(12)-H(12B)	0.9900
C(13)-H(13A)	0.9900
C(13)-H(13B)	0.9900
C(14)-C(15)	1.3943(14)
C(14)-C(19)	1.4046(14)
C(15)-C(16)	1.4023(14)
C(15)-C(20)	1.5086(14)
C(16)-H(16)	0.9500
C(16)-C(17)	1.3888(13)
C(17)-C(18)	1.3955(14)

C(17)-C(21)	1.5093(13)
C(18)-H(18)	0.9500
C(18)-C(19)	1.3930(14)
C(19)-C(22)	1.5078(14)
C(20)-H(20A)	0.9800
C(20)-H(20B)	0.9800
C(20)-H(20C)	0.9800
C(21)-H(21A)	0.9800
C(21)-H(21B)	0.9800
C(21)-H(21C)	0.9800
C(22)-H(22A)	0.9800
C(22)-H(22B)	0.9800
C(22)-H(22C)	0.9800
C(23)-H(23)	0.9500
C(23)-C(24)	1.4655(13)
C(24)-C(25)	1.4031(13)
C(24)-C(29)	1.4107(13)
C(25)-H(25)	0.9500
C(25)-C(26)	1.3935(14)
C(26)-H(26)	0.9500
C(26)-C(27)	1.3878(15)
C(27)-H(27)	0.9500
C(27)-C(28)	1.3990(14)
C(28)-H(28)	0.9500
C(28)-C(29)	1.3876(13)
C(30)-H(30)	1.0000
C(30)-C(31)	1.5191(14)
C(30)-C(32)	1.5177(14)
C(31)-H(31A)	0.9800
C(31)-H(31B)	0.9800
C(31)-H(31C)	0.9800
C(32)-H(32A)	0.9800
C(32)-H(32B)	0.9800
C(32)-H(32C)	0.9800

O(1)-Ru(1)-Br(1)	89.683(18)
C(1)-Ru(1)-Br(1)	103.01(3)
C(1)-Ru(1)-O(1)	166.94(3)
C(1)-Ru(1)-C(5)	79.97(4)
C(5)-Ru(1)-Br(1)	135.93(3)
C(5)-Ru(1)-O(1)	93.12(3)
C(23)-Ru(1)-Br(1)	118.71(3)
C(23)-Ru(1)-O(1)	79.16(3)
C(23)-Ru(1)-C(1)	91.84(4)
C(23)-Ru(1)-C(5)	104.97(4)
C(1)-N(1)-C(2)	112.85(8)
C(1)-N(1)-C(4)	115.61(8)
C(4)-N(1)-C(2)	122.96(8)
C(1)-N(2)-C(3)	112.66(8)
C(1)-N(2)-C(14)	126.92(8)
C(14)-N(2)-C(3)	117.25(8)
C(29)-O(1)-Ru(1)	109.18(5)
C(29)-O(1)-C(30)	118.65(7)
C(30)-O(1)-Ru(1)	132.08(6)

N(1)-C(1)-Ru(1)	117.84(7)
N(2)-C(1)-Ru(1)	134.16(7)
N(2)-C(1)-N(1)	107.73(8)
N(1)-C(2)-H(2A)	111.3
N(1)-C(2)-H(2B)	111.3
N(1)-C(2)-C(3)	102.27(8)
H(2A)-C(2)-H(2B)	109.2
C(3)-C(2)-H(2A)	111.3
C(3)-C(2)-H(2B)	111.3
N(2)-C(3)-C(2)	102.93(8)
N(2)-C(3)-H(3A)	111.2
N(2)-C(3)-H(3B)	111.2
C(2)-C(3)-H(3A)	111.2
C(2)-C(3)-H(3B)	111.2
H(3A)-C(3)-H(3B)	109.1
N(1)-C(4)-C(5)	105.16(7)
N(1)-C(4)-C(11)	109.69(8)
N(1)-C(4)-C(12)	112.85(8)
C(5)-C(4)-C(11)	110.31(8)
C(12)-C(4)-C(5)	109.44(8)
C(12)-C(4)-C(11)	109.32(8)
Ru(1)-C(5)-H(5)	101.4
C(4)-C(5)-Ru(1)	112.56(6)
C(4)-C(5)-H(5)	101.4
C(6)-C(5)-Ru(1)	126.78(6)
C(6)-C(5)-C(4)	109.09(8)
C(6)-C(5)-H(5)	101.4
C(5)-C(6)-H(6)	109.6
C(5)-C(6)-C(7)	108.11(8)
C(7)-C(6)-H(6)	109.6
C(13)-C(6)-C(5)	110.81(8)
C(13)-C(6)-H(6)	109.6
C(13)-C(6)-C(7)	109.21(8)
C(6)-C(7)-H(7A)	109.7
C(6)-C(7)-H(7B)	109.7
H(7A)-C(7)-H(7B)	108.2
C(8)-C(7)-C(6)	109.66(8)
C(8)-C(7)-H(7A)	109.7
C(8)-C(7)-H(7B)	109.7
C(7)-C(8)-H(8)	109.4
C(7)-C(8)-C(12)	110.28(8)
C(9)-C(8)-C(7)	108.38(9)
C(9)-C(8)-H(8)	109.4
C(9)-C(8)-C(12)	109.96(9)
C(12)-C(8)-H(8)	109.4
C(8)-C(9)-H(9A)	109.7
C(8)-C(9)-H(9B)	109.7
H(9A)-C(9)-H(9B)	108.2
C(10)-C(9)-C(8)	109.94(8)
C(10)-C(9)-H(9A)	109.7
C(10)-C(9)-H(9B)	109.7
C(9)-C(10)-H(10)	109.8
C(9)-C(10)-C(13)	109.94(9)
C(11)-C(10)-C(9)	108.69(9)

C(11)-C(10)-H(10)	109.8
C(11)-C(10)-C(13)	108.86(8)
C(13)-C(10)-H(10)	109.8
C(4)-C(11)-H(11A)	109.6
C(4)-C(11)-H(11B)	109.6
C(10)-C(11)-C(4)	110.22(8)
C(10)-C(11)-H(11A)	109.6
C(10)-C(11)-H(11B)	109.6
H(11A)-C(11)-H(11B)	108.1
C(4)-C(12)-C(8)	108.42(8)
C(4)-C(12)-H(12A)	110.0
C(4)-C(12)-H(12B)	110.0
C(8)-C(12)-H(12A)	110.0
C(8)-C(12)-H(12B)	110.0
H(12A)-C(12)-H(12B)	108.4
C(6)-C(13)-C(10)	109.76(8)
C(6)-C(13)-H(13A)	109.7
C(6)-C(13)-H(13B)	109.7
C(10)-C(13)-H(13A)	109.7
C(10)-C(13)-H(13B)	109.7
H(13A)-C(13)-H(13B)	108.2
C(15)-C(14)-N(2)	119.59(9)
C(15)-C(14)-C(19)	121.75(9)
C(19)-C(14)-N(2)	118.36(9)
C(14)-C(15)-C(16)	118.03(9)
C(14)-C(15)-C(20)	122.55(9)
C(16)-C(15)-C(20)	119.42(9)
C(15)-C(16)-H(16)	119.0
C(17)-C(16)-C(15)	121.98(9)
C(17)-C(16)-H(16)	119.0
C(16)-C(17)-C(18)	118.17(9)
C(16)-C(17)-C(21)	121.81(9)
C(18)-C(17)-C(21)	119.99(9)
C(17)-C(18)-H(18)	118.9
C(19)-C(18)-C(17)	122.15(9)
C(19)-C(18)-H(18)	118.9
C(14)-C(19)-C(22)	121.46(9)
C(18)-C(19)-C(14)	117.89(9)
C(18)-C(19)-C(22)	120.62(9)
C(15)-C(20)-H(20A)	109.5
C(15)-C(20)-H(20B)	109.5
C(15)-C(20)-H(20C)	109.5
H(20A)-C(20)-H(20B)	109.5
H(20A)-C(20)-H(20C)	109.5
H(20B)-C(20)-H(20C)	109.5
C(17)-C(21)-H(21A)	109.5
C(17)-C(21)-H(21B)	109.5
C(17)-C(21)-H(21C)	109.5
H(21A)-C(21)-H(21B)	109.5
H(21A)-C(21)-H(21C)	109.5
H(21B)-C(21)-H(21C)	109.5
C(19)-C(22)-H(22A)	109.5
C(19)-C(22)-H(22B)	109.5
C(19)-C(22)-H(22C)	109.5

H(22A)-C(22)-H(22B)	109.5
H(22A)-C(22)-H(22C)	109.5
H(22B)-C(22)-H(22C)	109.5
Ru(1)-C(23)-H(23)	120.4
C(24)-C(23)-Ru(1)	119.22(7)
C(24)-C(23)-H(23)	120.4
C(25)-C(24)-C(23)	122.56(9)
C(25)-C(24)-C(29)	118.60(9)
C(29)-C(24)-C(23)	118.83(8)
C(24)-C(25)-H(25)	119.6
C(26)-C(25)-C(24)	120.72(9)
C(26)-C(25)-H(25)	119.6
C(25)-C(26)-H(26)	120.3
C(27)-C(26)-C(25)	119.41(10)
C(27)-C(26)-H(26)	120.3
C(26)-C(27)-H(27)	119.4
C(26)-C(27)-C(28)	121.24(10)
C(28)-C(27)-H(27)	119.4
C(27)-C(28)-H(28)	120.5
C(29)-C(28)-C(27)	118.97(9)
C(29)-C(28)-H(28)	120.5
O(1)-C(29)-C(24)	113.50(8)
O(1)-C(29)-C(28)	125.51(9)
C(28)-C(29)-C(24)	120.99(9)
O(1)-C(30)-H(30)	109.3
O(1)-C(30)-C(31)	110.31(8)
O(1)-C(30)-C(32)	107.48(8)
C(31)-C(30)-H(30)	109.3
C(32)-C(30)-H(30)	109.3
C(32)-C(30)-C(31)	111.25(9)
C(30)-C(31)-H(31A)	109.5
C(30)-C(31)-H(31B)	109.5
C(30)-C(31)-H(31C)	109.5
H(31A)-C(31)-H(31B)	109.5
H(31A)-C(31)-H(31C)	109.5
H(31B)-C(31)-H(31C)	109.5
C(30)-C(32)-H(32A)	109.5
C(30)-C(32)-H(32B)	109.5
C(30)-C(32)-H(32C)	109.5
H(32A)-C(32)-H(32B)	109.5
H(32A)-C(32)-H(32C)	109.5
H(32B)-C(32)-H(32C)	109.5

Table B.9: Anisotropic displacement parameters ($Å^2 x\ 10^4$) for 4.28. The anisotropic displacement factor exponent takes the form: $-2\pi^2 [h^2 a^{*2} U^{11} + ... + 2 h k a^* b^* U^{12}]$

	U^{11}	U^{22}	U^{33}	U^{23}	U^{13}	U^{12}
Ru(1)	82(1)	75(1)	74(1)	-5(1)	-8(1)	1(1)
Br(1)	168(1)	166(1)	110(1)	-35(1)	6(1)	39(1)
N(1)	130(3)	103(3)	123(3)	-17(3)	-47(3)	27(3)
N(2)	149(4)	94(3)	117(3)	-8(3)	-37(3)	31(3)
O(1)	101(3)	126(3)	105(3)	44(2)	1(2)	-4(2)
C(1)	92(4)	96(4)	107(3)	-17(3)	-5(3)	12(3)
C(2)	240(5)	139(4)	161(4)	-20(4)	-108(4)	65(4)
C(3)	264(5)	136(5)	187(5)	-12(4)	-120(4)	65(4)
C(4)	114(4)	91(4)	111(4)	-19(3)	-25(3)	4(3)
C(5)	100(4)	92(4)	105(4)	-2(3)	-3(3)	-17(3)
C(6)	147(4)	78(4)	114(4)	-3(3)	-12(3)	1(3)
C(7)	193(5)	100(4)	185(4)	6(4)	-1(4)	-36(4)
C(8)	195(5)	120(4)	192(5)	-37(4)	-51(4)	-44(4)
C(9)	283(6)	131(4)	137(4)	-49(4)	-27(4)	8(4)
C(10)	188(5)	123(4)	121(4)	-14(3)	28(3)	13(4)
C(11)	160(4)	108(4)	110(4)	6(3)	-6(3)	-4(3)
C(12)	134(4)	148(4)	174(4)	-21(4)	-51(3)	-21(4)
C(13)	155(4)	99(4)	157(4)	-12(3)	11(3)	27(3)
C(14)	130(4)	81(4)	113(4)	-5(3)	-16(3)	27(3)
C(15)	128(4)	102(4)	123(4)	10(3)	4(3)	30(3)
C(16)	115(4)	98(4)	148(4)	8(3)	-3(3)	1(3)
C(17)	130(4)	90(4)	118(4)	-3(3)	-15(3)	14(3)
C(18)	122(4)	109(4)	136(4)	-3(3)	21(3)	16(3)
C(19)	119(4)	96(4)	141(4)	9(3)	-7(3)	13(3)
C(20)	216(5)	157(5)	199(5)	-12(4)	90(4)	2(4)
C(21)	172(5)	120(4)	165(4)	-32(4)	8(3)	-8(4)
C(22)	142(4)	121(4)	232(5)	-20(4)	22(4)	-17(4)
C(23)	120(4)	94(4)	97(3)	17(3)	-4(3)	3(3)
C(24)	103(3)	96(4)	95(3)	-7(3)	-7(3)	-11(3)
C(25)	136(4)	133(4)	118(4)	10(3)	10(3)	-19(3)
C(26)	106(4)	207(5)	173(4)	-9(4)	22(3)	-17(4)
C(27)	107(4)	217(5)	207(5)	21(4)	-8(4)	40(4)
C(28)	131(4)	161(5)	156(4)	48(4)	-11(3)	25(4)
C(29)	97(4)	106(4)	105(4)	3(3)	-4(3)	-13(3)
C(30)	150(4)	114(4)	106(4)	45(3)	-2(3)	-16(3)
C(31)	215(5)	214(5)	117(4)	22(4)	-27(4)	-36(4)
C(32)	163(4)	181(5)	152(4)	46(4)	10(3)	-49(4)

Table B.10: Hydrogen coordinates (x 10^3) and isotropic displacement parameters ($Å^2$x 10^3) for 4.28

	x	y	z	U_{iso}
H(2A)	-84	697	648	22
H(2B)	57	701	586	22
H(3A)	66	785	656	24
H(3B)	-58	776	742	24
H(5)	85	590	909	12
H(6)	265	532	928	14
H(7A)	158	470	796	19
H(7B)	53	504	869	19
H(8)	-7	499	656	20
H(9A)	206	490	577	22
H(9B)	133	537	507	22
H(10)	345	565	564	17
H(11A)	180	631	563	15
H(11B)	285	645	668	15
H(12A)	-34	592	619	18
H(12B)	-66	579	759	18
H(13A)	373	511	742	16
H(13B)	402	571	777	16
H(16)	315	899	952	14
H(18)	-5	856	1134	15
H(20A)	404	799	822	29
H(20B)	369	855	763	29
H(20C)	294	804	719	29
H(21A)	249	952	1121	23
H(21B)	154	925	1219	23
H(21C)	96	960	1107	23
H(22A)	-117	777	1090	25
H(22B)	-48	732	1009	25
H(22C)	-138	776	944	25
H(23)	383	707	828	12
H(25)	629	699	821	15
H(26)	819	656	881	19
H(27)	811	587	1023	21
H(28)	616	563	1114	18
H(30)	421	537	1152	15
H(31A)	515	606	1276	27
H(31B)	422	569	1355	27
H(31C)	374	626	1310	27
H(32A)	181	589	1198	25
H(32B)	218	532	1252	25
H(32C)	199	540	1107	25

Table B.11: Crystal Data and Structure Analysis Details for 4.26

Empirical formula	C32 H41 I N2 O Ru
Formula weight	697.64
Crystallization solvent	diethyl ether
Crystal shape	plate
Crystal color	brown
Crystal size	0.08 x 0.08 x 0.20 mm

Data Collection

Preliminary photograph(s)	rotation	
Type of diffractometer	Bruker APEX-II CCD	
Wavelength	0.71073 Å MoK	
Data collection temperature	100 K	
Theta range for 9907 reflections used in lattice determination	2.46 to 30.44°	
Unit cell dimensions	a = 10.5392(6) Å b = 25.1821(14) Å c = 10.9470(6) Å	α= 90° β= 91.365(3)° γ = 90°
Volume	2904.5(3) $Å^3$	
Z	4	
Crystal system	monoclinic	
Space group	P 1 21/n 1 (# 14)	
Density (calculated)	1.595 g/cm^3	
F(000)	1408	
Theta range for data collection	2.0 to 37.0°	
Completeness to theta = 25.00°	99.8%	
Index ranges	$-17 \le h \le 17$, $-41 \le k \le 42$, $-18 \le l \le 18$	
Data collection scan type	and scans	
Reflections collected	109331	
Independent reflections	14174 [R_{int}= 0.1025]	
Reflections > 2σ(I)	9643	
Average σ(I)/(net I)	0.0737	
Absorption coefficient	1.63 mm^{-1}	
Absorption correction	Semi-empirical from equivalents	
Max. and min. transmission	1.0000 and 0.8886	

Table B.11 (cont.):

Structure Solution and Refinement

Primary solution method	direct
Secondary solution method	difmap
Hydrogen placement	geom
Refinement method	Full-matrix least-squares on F^2
Data / restraints / parameters	14174 / 0 / 339
Treatment of hydrogen atoms	constr
Goodness-of-fit on F^2	1.58
Final R indices [I>2σ(I), 9643 reflections]	R1 = 0.0497, wR2 = 0.0705
R indices (all data)	R1 = 0.0927, wR2 = 0.0745
Type of weighting scheme used	calc
Weighting scheme used	calc w=1/[^2^(Fo^2^)]
Max shift/error	0.004
Average shift/error	0.000
Largest diff. peak and hole	2.40 and -1.25 e·$Å^{-3}$

Programs Used

Cell refinement	SAINT V8.18C (Bruker-AXS, 2007)
Data collection	APEX2 2012.2-0 (Bruker-AXS, 2007)
Data reduction	SAINT V8.18C (Bruker-AXS, 2007)
Structure solution	SHELXS-97 (Sheldrick, 1990)
Structure refinement	SHELXL-97 (Sheldrick, 1997)
Graphics	DIAMOND 3 (Crystal Impact, 1999)

Table B.12: Atomic coordinates (x 10^4) and equivalent isotropic displacement parameters ($Å^2$x 10^3) for 4.26. U(eq) is defined as one third of the trace of the orthogonalized U^{ij} tensor

	x	y	z	U_{eq}
Ru(1)	2297(1)	6573(1)	9653(1)	10(1)
I(1)	1656(1)	7012(1)	11804(1)	17(1)
N(1)	594(2)	6686(1)	7590(2)	16(1)
N(2)	1032(2)	7490(1)	8240(2)	15(1)
O(1)	3790(2)	6036(1)	10666(2)	13(1)
C(1)	1242(2)	6970(1)	8474(2)	12(1)
C(2)	20(3)	7022(1)	6627(3)	24(1)
C(3)	218(3)	7580(1)	7144(3)	23(1)
C(4)	1075(2)	6151(1)	7362(2)	15(1)
C(5)	1637(2)	5964(1)	8595(2)	12(1)
C(6)	2266(2)	5419(1)	8425(2)	16(1)
C(7)	1234(3)	5024(1)	7993(3)	21(1)
C(8)	635(3)	5214(1)	6781(3)	23(1)
C(9)	1671(3)	5239(1)	5826(3)	26(1)
C(10)	2708(3)	5627(1)	6244(2)	20(1)
C(11)	2108(2)	6176(1)	6402(2)	16(1)
C(12)	34(3)	5767(1)	6933(3)	21(1)
C(13)	3291(2)	5448(1)	7466(2)	17(1)
C(14)	1218(2)	7933(1)	9054(2)	13(1)
C(15)	2246(2)	8271(1)	8892(2)	15(1)
C(16)	2340(2)	8719(1)	9646(2)	15(1)
C(17)	1456(2)	8833(1)	10516(2)	14(1)
C(18)	440(2)	8486(1)	10648(2)	15(1)
C(19)	293(2)	8038(1)	9921(2)	14(1)
C(20)	3226(3)	8177(1)	7942(3)	24(1)
C(21)	1547(3)	9328(1)	11292(3)	20(1)
C(22)	-870(2)	7692(1)	10023(3)	19(1)
C(23)	3769(2)	6778(1)	8936(2)	15(1)
C(24)	4968(2)	6542(1)	9314(2)	12(1)
C(25)	6128(2)	6685(1)	8812(2)	16(1)
C(26)	7244(2)	6435(1)	9155(3)	19(1)
C(27)	7219(3)	6033(1)	10011(3)	21(1)
C(28)	6085(2)	5882(1)	10554(2)	18(1)
C(29)	4977(2)	6140(1)	10204(2)	13(1)
C(30)	3697(2)	5655(1)	11674(2)	14(1)
C(31)	4205(3)	5899(1)	12849(2)	19(1)
C(32)	2319(2)	5496(1)	11769(2)	19(1)

Table B.13: Bond lengths [Å] and angles [°] for 4.26

Ru(1)-I(1)	2.7021(3)
Ru(1)-O(1)	2.3346(16)
Ru(1)-C(1)	1.958(2)
Ru(1)-C(5)	2.035(2)
Ru(1)-C(23)	1.830(3)
N(1)-C(1)	1.373(3)
N(1)-C(2)	1.470(3)
N(1)-C(4)	1.464(3)
N(2)-C(1)	1.351(3)
N(2)-C(3)	1.476(3)
N(2)-C(14)	1.437(3)
O(1)-C(29)	1.385(3)
O(1)-C(30)	1.467(3)
C(2)-H(2A)	0.9900
C(2)-H(2B)	0.9900
C(2)-C(3)	1.527(4)
C(3)-H(3A)	0.9900
C(3)-H(3B)	0.9900
C(4)-C(5)	1.535(3)
C(4)-C(11)	1.532(4)
C(4)-C(12)	1.528(3)
C(5)-H(5)	1.0000
C(5)-C(6)	1.536(3)
C(6)-H(6)	1.0000
C(6)-C(7)	1.539(4)
C(6)-C(13)	1.526(4)
C(7)-H(7A)	0.9900
C(7)-H(7B)	0.9900
C(7)-C(8)	1.532(4)
C(8)-H(8)	1.0000
C(8)-C(9)	1.530(4)
C(8)-C(12)	1.541(4)
C(9)-H(9A)	0.9900
C(9)-H(9B)	0.9900
C(9)-C(10)	1.529(4)
C(10)-H(10)	1.0000
C(10)-C(11)	1.530(3)
C(10)-C(13)	1.527(4)
C(11)-H(11A)	0.9900
C(11)-H(11B)	0.9900
C(12)-H(12A)	0.9900
C(12)-H(12B)	0.9900
C(13)-H(13A)	0.9900
C(13)-H(13B)	0.9900
C(14)-C(15)	1.392(3)
C(14)-C(19)	1.402(3)
C(15)-C(16)	1.401(3)
C(15)-C(20)	1.501(4)
C(16)-H(16)	0.9500
C(16)-C(17)	1.378(3)
C(17)-C(18)	1.392(3)

C(17)-C(21)	1.510(3)
C(18)-H(18)	0.9500
C(18)-C(19)	1.387(3)
C(19)-C(22)	1.510(3)
C(20)-H(20A)	0.9800
C(20)-H(20B)	0.9800
C(20)-H(20C)	0.9800
C(21)-H(21A)	0.9800
C(21)-H(21B)	0.9800
C(21)-H(21C)	0.9800
C(22)-H(22A)	0.9800
C(22)-H(22B)	0.9800
C(22)-H(22C)	0.9800
C(23)-H(23)	0.9500
C(23)-C(24)	1.449(3)
C(24)-C(25)	1.400(3)
C(24)-C(29)	1.406(3)
C(25)-H(25)	0.9500
C(25)-C(26)	1.379(4)
C(26)-H(26)	0.9500
C(26)-C(27)	1.381(4)
C(27)-H(27)	0.9500
C(27)-C(28)	1.400(4)
C(28)-H(28)	0.9500
C(28)-C(29)	1.382(3)
C(30)-H(30)	1.0000
C(30)-C(31)	1.512(3)
C(30)-C(32)	1.512(3)
C(31)-H(31A)	0.9800
C(31)-H(31B)	0.9800
C(31)-H(31C)	0.9800
C(32)-H(32A)	0.9800
C(32)-H(32B)	0.9800
C(32)-H(32C)	0.9800

O(1)-Ru(1)-I(1)	90.17(4)
C(1)-Ru(1)-I(1)	102.40(7)
C(1)-Ru(1)-O(1)	167.08(8)
C(1)-Ru(1)-C(5)	80.16(10)
C(5)-Ru(1)-I(1)	135.72(7)
C(5)-Ru(1)-O(1)	92.95(8)
C(23)-Ru(1)-I(1)	119.32(8)
C(23)-Ru(1)-O(1)	78.40(9)
C(23)-Ru(1)-C(1)	92.66(11)
C(23)-Ru(1)-C(5)	104.53(11)
C(1)-N(1)-C(2)	113.3(2)
C(1)-N(1)-C(4)	115.6(2)
C(4)-N(1)-C(2)	123.1(2)
C(1)-N(2)-C(3)	113.1(2)
C(1)-N(2)-C(14)	127.9(2)
C(14)-N(2)-C(3)	116.9(2)
C(29)-O(1)-Ru(1)	108.76(14)
C(29)-O(1)-C(30)	118.37(18)
C(30)-O(1)-Ru(1)	132.80(14)

N(1)-C(1)-Ru(1)	117.61(17)
N(2)-C(1)-Ru(1)	135.07(18)
N(2)-C(1)-N(1)	107.2(2)
N(1)-C(2)-H(2A)	111.3
N(1)-C(2)-H(2B)	111.3
N(1)-C(2)-C(3)	102.3(2)
H(2A)-C(2)-H(2B)	109.2
C(3)-C(2)-H(2A)	111.3
C(3)-C(2)-H(2B)	111.3
N(2)-C(3)-C(2)	103.4(2)
N(2)-C(3)-H(3A)	111.1
N(2)-C(3)-H(3B)	111.1
C(2)-C(3)-H(3A)	111.1
C(2)-C(3)-H(3B)	111.1
H(3A)-C(3)-H(3B)	109.1
N(1)-C(4)-C(5)	105.11(19)
N(1)-C(4)-C(11)	109.5(2)
N(1)-C(4)-C(12)	112.7(2)
C(11)-C(4)-C(5)	110.5(2)
C(12)-C(4)-C(5)	109.6(2)
C(12)-C(4)-C(11)	109.4(2)
Ru(1)-C(5)-H(5)	101.2
C(4)-C(5)-Ru(1)	112.90(16)
C(4)-C(5)-H(5)	101.2
C(4)-C(5)-C(6)	109.0(2)
C(6)-C(5)-Ru(1)	126.82(18)
C(6)-C(5)-H(5)	101.2
C(5)-C(6)-H(6)	109.6
C(5)-C(6)-C(7)	108.1(2)
C(7)-C(6)-H(6)	109.6
C(13)-C(6)-C(5)	110.8(2)
C(13)-C(6)-H(6)	109.6
C(13)-C(6)-C(7)	109.0(2)
C(6)-C(7)-H(7A)	109.7
C(6)-C(7)-H(7B)	109.7
H(7A)-C(7)-H(7B)	108.2
C(8)-C(7)-C(6)	109.8(2)
C(8)-C(7)-H(7A)	109.7
C(8)-C(7)-H(7B)	109.7
C(7)-C(8)-H(8)	109.3
C(7)-C(8)-C(12)	110.5(2)
C(9)-C(8)-C(7)	108.6(2)
C(9)-C(8)-H(8)	109.3
C(9)-C(8)-C(12)	109.8(2)
C(12)-C(8)-H(8)	109.3
C(8)-C(9)-H(9A)	109.7
C(8)-C(9)-H(9B)	109.7
H(9A)-C(9)-H(9B)	108.2
C(10)-C(9)-C(8)	109.8(2)
C(10)-C(9)-H(9A)	109.7
C(10)-C(9)-H(9B)	109.7
C(9)-C(10)-H(10)	109.7
C(9)-C(10)-C(11)	108.4(2)
C(11)-C(10)-H(10)	109.7

C(13)-C(10)-C(9)	110.0(2)
C(13)-C(10)-H(10)	109.7
C(13)-C(10)-C(11)	109.1(2)
C(4)-C(11)-H(11A)	109.6
C(4)-C(11)-H(11B)	109.6
C(10)-C(11)-C(4)	110.1(2)
C(10)-C(11)-H(11A)	109.6
C(10)-C(11)-H(11B)	109.6
H(11A)-C(11)-H(11B)	108.2
C(4)-C(12)-C(8)	108.1(2)
C(4)-C(12)-H(12A)	110.1
C(4)-C(12)-H(12B)	110.1
C(8)-C(12)-H(12A)	110.1
C(8)-C(12)-H(12B)	110.1
H(12A)-C(12)-H(12B)	108.4
C(6)-C(13)-C(10)	109.9(2)
C(6)-C(13)-H(13A)	109.7
C(6)-C(13)-H(13B)	109.7
C(10)-C(13)-H(13A)	109.7
C(10)-C(13)-H(13B)	109.7
H(13A)-C(13)-H(13B)	108.2
C(15)-C(14)-N(2)	119.4(2)
C(15)-C(14)-C(19)	121.8(2)
C(19)-C(14)-N(2)	118.6(2)
C(14)-C(15)-C(16)	117.5(2)
C(14)-C(15)-C(20)	122.8(2)
C(16)-C(15)-C(20)	119.7(2)
C(15)-C(16)-H(16)	118.8
C(17)-C(16)-C(15)	122.4(2)
C(17)-C(16)-H(16)	118.8
C(16)-C(17)-C(18)	118.4(2)
C(16)-C(17)-C(21)	121.7(2)
C(18)-C(17)-C(21)	119.9(2)
C(17)-C(18)-H(18)	119.1
C(19)-C(18)-C(17)	121.8(2)
C(19)-C(18)-H(18)	119.1
C(14)-C(19)-C(22)	121.3(2)
C(18)-C(19)-C(14)	118.2(2)
C(18)-C(19)-C(22)	120.5(2)
C(15)-C(20)-H(20A)	109.5
C(15)-C(20)-H(20B)	109.5
C(15)-C(20)-H(20C)	109.5
H(20A)-C(20)-H(20B)	109.5
H(20A)-C(20)-H(20C)	109.5
H(20B)-C(20)-H(20C)	109.5
C(17)-C(21)-H(21A)	109.5
C(17)-C(21)-H(21B)	109.5
C(17)-C(21)-H(21C)	109.5
H(21A)-C(21)-H(21B)	109.5
H(21A)-C(21)-H(21C)	109.5
H(21B)-C(21)-H(21C)	109.5
C(19)-C(22)-H(22A)	109.5
C(19)-C(22)-H(22B)	109.5
C(19)-C(22)-H(22C)	109.5

H(22A)-C(22)-H(22B)	109.5
H(22A)-C(22)-H(22C)	109.5
H(22B)-C(22)-H(22C)	109.5
Ru(1)-C(23)-H(23)	119.9
C(24)-C(23)-Ru(1)	120.28(19)
C(24)-C(23)-H(23)	119.9
C(25)-C(24)-C(23)	123.1(2)
C(25)-C(24)-C(29)	117.9(2)
C(29)-C(24)-C(23)	119.0(2)
C(24)-C(25)-H(25)	119.3
C(26)-C(25)-C(24)	121.5(2)
C(26)-C(25)-H(25)	119.3
C(25)-C(26)-H(26)	120.3
C(25)-C(26)-C(27)	119.4(2)
C(27)-C(26)-H(26)	120.3
C(26)-C(27)-H(27)	119.4
C(26)-C(27)-C(28)	121.2(2)
C(28)-C(27)-H(27)	119.4
C(27)-C(28)-H(28)	120.7
C(29)-C(28)-C(27)	118.6(2)
C(29)-C(28)-H(28)	120.7
O(1)-C(29)-C(24)	113.5(2)
C(28)-C(29)-O(1)	125.1(2)
C(28)-C(29)-C(24)	121.5(2)
O(1)-C(30)-H(30)	109.0
O(1)-C(30)-C(31)	110.2(2)
O(1)-C(30)-C(32)	107.82(19)
C(31)-C(30)-H(30)	109.0
C(31)-C(30)-C(32)	111.7(2)
C(32)-C(30)-H(30)	109.0
C(30)-C(31)-H(31A)	109.5
C(30)-C(31)-H(31B)	109.5
C(30)-C(31)-H(31C)	109.5
H(31A)-C(31)-H(31B)	109.5
H(31A)-C(31)-H(31C)	109.5
H(31B)-C(31)-H(31C)	109.5
C(30)-C(32)-H(32A)	109.5
C(30)-C(32)-H(32B)	109.5
C(30)-C(32)-H(32C)	109.5
H(32A)-C(32)-H(32B)	109.5
H(32A)-C(32)-H(32C)	109.5
H(32B)-C(32)-H(32C)	109.5

Table B.14: Anisotropic displacement parameters ($Å^2 x\ 10^4$) for 4.26. The anisotropic displacement factor exponent takes the form: $-2\pi^2 [h^2 a^{*2} U^{11} + ... + 2 h k a^* b^* U^{12}]$

	U^{11}	U^{22}	U^{33}	U^{23}	U^{13}	U^{12}
Ru(1)	94(1)	110(1)	90(1)	-10(1)	-3(1)	3(1)
I(1)	175(1)	210(1)	130(1)	-40(1)	14(1)	43(1)
N(1)	164(11)	167(11)	144(11)	-27(8)	-66(9)	39(8)
N(2)	163(11)	134(10)	144(11)	-8(8)	-45(9)	36(8)
O(1)	119(8)	145(9)	115(9)	54(7)	5(7)	9(7)
C(1)	118(11)	152(12)	99(11)	-13(9)	-5(9)	8(9)
C(2)	293(16)	206(14)	217(15)	-37(12)	-136(12)	84(12)
C(3)	263(15)	207(14)	222(15)	-21(11)	-86(12)	74(11)
C(4)	160(12)	134(12)	146(13)	-26(10)	-56(10)	18(10)
C(5)	101(11)	142(12)	132(12)	-4(9)	-2(9)	5(9)
C(6)	181(13)	113(11)	168(13)	-6(9)	-38(10)	23(10)
C(7)	245(15)	155(13)	220(15)	-13(11)	-25(12)	-52(11)
C(8)	253(15)	192(14)	252(16)	-37(12)	-121(12)	-71(11)
C(9)	394(18)	172(14)	195(15)	-68(11)	-87(13)	16(12)
C(10)	258(15)	198(14)	140(14)	-32(10)	33(11)	30(11)
C(11)	197(13)	155(12)	134(13)	12(10)	-33(10)	16(10)
C(12)	194(14)	224(14)	220(15)	-13(11)	-85(11)	-30(11)
C(13)	190(13)	130(12)	192(14)	-16(10)	9(11)	33(10)
C(14)	146(11)	101(11)	140(12)	-4(9)	-27(9)	37(9)
C(15)	144(12)	143(12)	153(13)	8(9)	25(10)	42(9)
C(16)	130(11)	115(11)	209(13)	27(10)	1(10)	11(9)
C(17)	133(12)	140(12)	154(13)	4(10)	-23(10)	24(9)
C(18)	139(12)	171(13)	151(13)	9(10)	33(10)	16(10)
C(19)	120(11)	148(12)	145(12)	20(10)	-40(9)	15(9)
C(20)	226(15)	212(14)	278(17)	-11(11)	104(13)	13(11)
C(21)	208(14)	172(13)	212(15)	-26(11)	24(11)	-17(10)
C(22)	162(13)	178(13)	229(15)	5(11)	25(11)	-25(10)
C(23)	199(13)	80(11)	180(14)	21(9)	5(10)	13(10)
C(24)	121(11)	123(11)	107(11)	-12(9)	-6(9)	-19(9)
C(25)	160(12)	159(13)	171(13)	25(10)	25(10)	-23(10)
C(26)	131(12)	246(14)	205(14)	5(11)	46(11)	-23(10)
C(27)	120(12)	295(16)	228(15)	18(12)	2(11)	49(11)
C(28)	146(12)	212(13)	178(14)	51(11)	-5(10)	27(10)
C(29)	111(11)	133(12)	145(13)	-1(9)	20(9)	-23(9)
C(30)	171(12)	134(12)	120(12)	46(9)	5(10)	2(9)
C(31)	223(14)	240(14)	113(13)	39(10)	-25(11)	-20(11)
C(32)	202(14)	205(14)	166(14)	60(10)	35(11)	-45(11)

Table B.15: Hydrogen coordinates (x 10^3) and isotropic displacement parameters ($Å^2$x 10^3) for 4.26

	x	y	z	U_{iso}
H(2A)	-89	694	650	29
H(2B)	46	698	584	29
H(3A)	64	781	655	28
H(3B)	-60	774	736	28
H(5)	85	586	903	15
H(6)	265	530	922	19
H(7A)	161	467	788	25
H(7B)	57	500	862	25
H(8)	-3	496	651	28
H(9A)	204	488	571	31
H(9B)	130	536	503	31
H(10)	338	565	562	24
H(11A)	173	630	561	20
H(11B)	277	643	666	20
H(12A)	-34	589	614	26
H(12B)	-64	575	754	26
H(13A)	369	509	737	20
H(13B)	396	570	773	20
H(16)	304	895	956	18
H(18)	-17	856	1125	18
H(20A)	393	797	830	36
H(20B)	354	852	765	36
H(20C)	284	798	725	36
H(21A)	238	949	1120	30
H(21B)	143	923	1215	30
H(21C)	88	958	1103	30
H(22A)	-128	776	1080	28
H(22B)	-62	732	999	28
H(22C)	-147	777	935	28
H(23)	375	704	831	18
H(25)	615	696	822	20
H(26)	802	654	880	23
H(27)	798	586	1024	26
H(28)	608	561	1115	21
H(30)	421	533	1148	17
H(31A)	507	603	1273	29
H(31B)	422	563	1350	29
H(31C)	366	620	1308	29
H(32A)	181	581	1193	29
H(32B)	223	524	1244	29
H(32C)	203	533	1100	29

Table B.16: Crystal Data and Structure Analysis Details for 4.29

Empirical formula	C35.94 H51.44 N2 O2 Ru
Formula weight	644.53
Crystallization solvent	
Crystal shape	block
Crystal color	orange
Crystal size	0.23 x 0.23 x 0.34 mm

Data Collection

Preliminary photograph(s)	rotation	
Type of diffractometer	Bruker APEX-II CCD	
Wavelength	0.71073 Å MoK	
Data collection temperature	100 K	
Theta range for 9785 reflections used in lattice determination	2.31 to 36.37°	
Unit cell dimensions	a = 10.6947(6) Å b = 11.1949(5) Å c = 15.3408(8) Å	α= 104.669(3)° β= 90.646(3)° γ = 108.874(3)°
Volume	1672.55(15) $Å^3$	
Z	2	
Crystal system	triclinic	
Space group	P -1 (# 2)	
Density (calculated)	1.280 g/cm^3	
F(000)	682	
Theta range for data collection	2.0 to 37.5°	
Completeness to theta = 25.00°	100.0%	
Index ranges	$-18 \le h \le 17$, $-18 \le k \le 18$, $-25 \le l \le 26$	
Data collection scan type	and scans	
Reflections collected	119236	
Independent reflections	16793 [R_{int}= 0.0442]	
Reflections > 2σ(I)	14725	
Average σ(I)/(net I)	0.0309	
Absorption coefficient	0.50 mm^{-1}	
Absorption correction	Semi-empirical from equivalents	
Max. and min. transmission	1.0000 and 0.9043	

Table B.16 (cont.):

Structure Solution and Refinement

Primary solution method	direct
Secondary solution method	difmap
Hydrogen placement	geom
Refinement method	Full-matrix least-squares on F^2
Data / restraints / parameters	16793 / 0 / 413
Treatment of hydrogen atoms	mixed
Goodness-of-fit on F^2	3.18
Final R indices [I>2σ(I), 14725 reflections]	R1 = 0.0440, wR2 = 0.0788
R indices (all data)	R1 = 0.0532, wR2 = 0.0794
Type of weighting scheme used	calc
Weighting scheme used	calc w=1/[^2^(Fo^2^)]
Max shift/error	0.002
Average shift/error	0.000
Largest diff. peak and hole	3.99 and -2.27 e·$Å^{-3}$

Programs Used

Cell refinement	SAINT V8.18C (Bruker-AXS, 2007)
Data collection	APEX2 2012.2-0 (Bruker-AXS, 2007)
Data reduction	SAINT V8.18C (Bruker-AXS, 2007)
Structure solution	SHELXS-97 (Sheldrick, 1990)
Structure refinement	SHELXL-97 (Sheldrick, 1997)
Graphics	DIAMOND 3 (Crystal Impact, 1999)

Table B.17: Atomic coordinates (x 10^4) and equivalent isotropic displacement parameters ($Å^2$x 10^3) for 4.29. U(eq) is defined as one third of the trace of the orthogonalized U^{ij} tensor

	x	y	z	U_{eq}
Ru(1)	4032(1)	3849(1)	4114(1)	11(1)
O(2)	4243(1)	4432(1)	5490(1)	15(1)
N(1)	2794(1)	1148(1)	3120(1)	17(1)
N(2)	1548(1)	1600(1)	4189(1)	16(1)
O(1)	3017(1)	5583(1)	2086(1)	30(1)
C(1)	2675(2)	2120(1)	3826(1)	13(1)
C(2)	1590(2)	-2(1)	2889(1)	23(1)
C(3)	895(2)	189(1)	3756(1)	24(1)
C(4)	3772(2)	1569(1)	2507(1)	15(1)
C(5)	4826(2)	2808(1)	3103(1)	14(1)
C(6)	5883(2)	3399(1)	2522(1)	18(1)
C(7)	6561(2)	2385(2)	2128(1)	22(1)
C(8)	5520(2)	1118(1)	1540(1)	21(1)
C(9)	4902(2)	1436(2)	764(1)	25(1)
C(10)	4232(2)	2447(2)	1149(1)	23(1)
C(11)	3147(2)	1875(2)	1720(1)	20(1)
C(12)	4428(2)	543(1)	2111(1)	19(1)
C(13)	5246(2)	3710(2)	1749(1)	24(1)
C(14)	1248(2)	2212(1)	5064(1)	15(1)
C(15)	310(2)	2847(1)	5112(1)	20(1)
C(16)	40(2)	3456(2)	5967(1)	24(1)
C(17)	689(2)	3462(2)	6751(1)	24(1)
C(18)	1614(2)	2815(1)	6680(1)	21(1)
C(19)	1897(2)	2169(1)	5843(1)	17(1)
C(20)	-387(2)	2886(2)	4265(1)	29(1)
C(21)	402(2)	4148(2)	7672(1)	38(1)
C(22)	2878(2)	1451(2)	5795(1)	24(1)
C(23)	2980(2)	4429(1)	3494(1)	15(1)
C(24)	3234(2)	5857(1)	3652(1)	15(1)
C(25)	3423(2)	6669(1)	4532(1)	18(1)
C(26)	3624(2)	8006(2)	4714(1)	25(1)
C(27)	3647(2)	8546(2)	3999(1)	30(1)
C(28)	3466(2)	7773(2)	3116(1)	28(1)
C(29)	3246(2)	6427(1)	2938(1)	20(1)
C(30)	3220(3)	6129(2)	1317(1)	52(1)
C(31)	2522(4)	4987(3)	513(2)	92(1)
C(32)	4684(3)	6763(3)	1253(2)	79(1)
C(33)	9129(5)	2495(5)	-276(3)	72(2)
C(34)	9609(4)	2227(3)	540(3)	42(1)
C(35)	8788(4)	907(4)	632(2)	38(1)
C(36)	9125(5)	708(6)	1495(3)	59(2)
C(37)	8278(6)	-681(8)	1601(6)	65(2)
C(38)	9636(7)	-464(8)	284(5)	83(2)
C(39)	8858(8)	46(10)	975(5)	70(2)
C(40)	8010(20)	-910(20)	1476(16)	56(6)

Table B.18: Bond lengths [Å] and angles [°] for 4.29

Ru(1)-O(2)#1	2.1357(10)
Ru(1)-O(2)	2.0313(11)
Ru(1)-C(1)	1.9453(14)
Ru(1)-C(5)	2.0601(14)
Ru(1)-C(23)	1.8316(15)
O(2)-Ru(1)#1	2.1357(10)
O(2)-H(2)	0.644(18)
N(1)-C(1)	1.3667(17)
N(1)-C(2)	1.4593(19)
N(1)-C(4)	1.4589(18)
N(2)-C(1)	1.3514(18)
N(2)-C(3)	1.4722(18)
N(2)-C(14)	1.4349(18)
O(1)-C(29)	1.3711(19)
O(1)-C(30)	1.448(2)
C(2)-H(2A)	0.9900
C(2)-H(2B)	0.9900
C(2)-C(3)	1.533(2)
C(3)-H(3A)	0.9900
C(3)-H(3B)	0.9900
C(4)-C(5)	1.534(2)
C(4)-C(11)	1.535(2)
C(4)-C(12)	1.536(2)
C(5)-H(5)	1.0000
C(5)-C(6)	1.532(2)
C(6)-H(6)	1.0000
C(6)-C(7)	1.541(2)
C(6)-C(13)	1.528(2)
C(7)-H(7A)	0.9900
C(7)-H(7B)	0.9900
C(7)-C(8)	1.541(2)
C(8)-H(8)	1.0000
C(8)-C(9)	1.528(2)
C(8)-C(12)	1.538(2)
C(9)-H(9A)	0.9900
C(9)-H(9B)	0.9900
C(9)-C(10)	1.530(2)
C(10)-H(10)	1.0000
C(10)-C(11)	1.533(2)
C(10)-C(13)	1.533(2)
C(11)-H(11A)	0.9900
C(11)-H(11B)	0.9900
C(12)-H(12A)	0.9900
C(12)-H(12B)	0.9900
C(13)-H(13A)	0.9900
C(13)-H(13B)	0.9900
C(14)-C(15)	1.398(2)
C(14)-C(19)	1.395(2)
C(15)-C(16)	1.396(2)
C(15)-C(20)	1.508(2)
C(16)-H(16)	0.9500

C(16)-C(17)	1.379(3)
C(17)-C(18)	1.393(2)
C(17)-C(21)	1.515(2)
C(18)-H(18)	0.9500
C(18)-C(19)	1.395(2)
C(19)-C(22)	1.506(2)
C(20)-H(20A)	0.9800
C(20)-H(20B)	0.9800
C(20)-H(20C)	0.9800
C(21)-H(21A)	0.9800
C(21)-H(21B)	0.9800
C(21)-H(21C)	0.9800
C(22)-H(22A)	0.9800
C(22)-H(22B)	0.9800
C(22)-H(22C)	0.9800
C(23)-H(23)	0.9500
C(23)-C(24)	1.4862(18)
C(24)-C(25)	1.394(2)
C(24)-C(29)	1.399(2)
C(25)-H(25)	0.9500
C(25)-C(26)	1.394(2)
C(26)-H(26)	0.9500
C(26)-C(27)	1.376(3)
C(27)-H(27)	0.9500
C(27)-C(28)	1.384(3)
C(28)-H(28)	0.9500
C(28)-C(29)	1.400(2)
C(30)-H(30)	1.0000
C(30)-C(31)	1.508(4)
C(30)-C(32)	1.511(4)
C(31)-H(31A)	0.9800
C(31)-H(31B)	0.9800
C(31)-H(31C)	0.9800
C(32)-H(32A)	0.9800
C(32)-H(32B)	0.9800
C(32)-H(32C)	0.9800
C(33)-H(33A)	0.9800
C(33)-H(33B)	0.9800
C(33)-H(33C)	0.9800
C(33)-C(34)	1.481(6)
C(34)-H(34A)	0.9900
C(34)-H(34B)	0.9900
C(34)-C(35)	1.498(5)
C(35)-H(35A)	0.9900
C(35)-H(35B)	0.9900
C(35)-C(36)	1.457(6)
C(35)-H(39D)	0.7058
C(36)-H(36A)	0.9900
C(36)-H(36B)	0.9900
C(36)-C(37)	1.577(9)
C(36)-H(39C)	1.4843
C(36)-H(39D)	1.3584
C(36)-H(39E)	0.3768
C(37)-H(37A)	0.9800

C(37)-H(37B)	0.9800
C(37)-H(37C)	0.9800
C(37)-H(39C)	0.5829
C(38)-C(38)#2	1.547(14)
C(38)-H(38A)	0.9900
C(38)-H(38B)	0.9900
C(38)-C(39)	1.471(10)
C(39)-H(39A)	0.9900
C(39)-H(39B)	0.9900
C(39)-H(39C)	1.0161
C(39)-H(39D)	0.9408
C(39)-H(39E)	0.9877
C(39)-C(40)	1.54(2)
C(40)-H(39C)	0.5657
C(40)-H(40A)	0.9800
C(40)-H(40B)	0.9800
C(40)-H(40C)	0.9800

O(2)-Ru(1)-O(2)#1	73.26(4)
O(2)-Ru(1)-C(5)	137.26(5)
C(1)-Ru(1)-O(2)#1	169.14(5)
C(1)-Ru(1)-O(2)	103.67(5)
C(1)-Ru(1)-C(5)	78.72(6)
C(5)-Ru(1)-O(2)#1	96.38(5)
C(23)-Ru(1)-O(2)#1	100.30(5)
C(23)-Ru(1)-O(2)	119.11(5)
C(23)-Ru(1)-C(1)	90.30(6)
C(23)-Ru(1)-C(5)	103.42(6)
Ru(1)-O(2)-Ru(1)#1	106.73(4)
Ru(1)#1-O(2)-H(2)	128.9(17)
Ru(1)-O(2)-H(2)	123.4(17)
C(1)-N(1)-C(2)	112.22(12)
C(1)-N(1)-C(4)	115.95(11)
C(4)-N(1)-C(2)	126.35(12)
C(1)-N(2)-C(3)	112.57(12)
C(1)-N(2)-C(14)	123.25(11)
C(14)-N(2)-C(3)	121.33(11)
C(29)-O(1)-C(30)	118.45(14)
N(1)-C(1)-Ru(1)	119.26(10)
N(2)-C(1)-Ru(1)	133.55(10)
N(2)-C(1)-N(1)	107.19(11)
N(1)-C(2)-H(2A)	111.4
N(1)-C(2)-H(2B)	111.4
N(1)-C(2)-C(3)	101.81(12)
H(2A)-C(2)-H(2B)	109.3
C(3)-C(2)-H(2A)	111.4
C(3)-C(2)-H(2B)	111.4
N(2)-C(3)-C(2)	101.80(12)
N(2)-C(3)-H(3A)	111.4
N(2)-C(3)-H(3B)	111.4
C(2)-C(3)-H(3A)	111.4
C(2)-C(3)-H(3B)	111.4
H(3A)-C(3)-H(3B)	109.3
N(1)-C(4)-C(5)	104.31(11)

N(1)-C(4)-C(11)	111.39(13)
N(1)-C(4)-C(12)	112.56(11)
C(5)-C(4)-C(11)	110.91(11)
C(5)-C(4)-C(12)	109.12(13)
C(11)-C(4)-C(12)	108.51(12)
Ru(1)-C(5)-H(5)	101.7
C(4)-C(5)-Ru(1)	112.46(10)
C(4)-C(5)-H(5)	101.7
C(6)-C(5)-Ru(1)	125.66(9)
C(6)-C(5)-C(4)	109.60(11)
C(6)-C(5)-H(5)	101.7
C(5)-C(6)-H(6)	109.6
C(5)-C(6)-C(7)	107.91(12)
C(7)-C(6)-H(6)	109.6
C(13)-C(6)-C(5)	110.57(13)
C(13)-C(6)-H(6)	109.6
C(13)-C(6)-C(7)	109.50(12)
C(6)-C(7)-H(7A)	109.8
C(6)-C(7)-H(7B)	109.8
H(7A)-C(7)-H(7B)	108.2
C(8)-C(7)-C(6)	109.58(14)
C(8)-C(7)-H(7A)	109.8
C(8)-C(7)-H(7B)	109.8
C(7)-C(8)-H(8)	109.4
C(9)-C(8)-C(7)	108.87(13)
C(9)-C(8)-H(8)	109.4
C(9)-C(8)-C(12)	109.52(14)
C(12)-C(8)-C(7)	110.31(12)
C(12)-C(8)-H(8)	109.4
C(8)-C(9)-H(9A)	109.8
C(8)-C(9)-H(9B)	109.8
C(8)-C(9)-C(10)	109.51(12)
H(9A)-C(9)-H(9B)	108.2
C(10)-C(9)-H(9A)	109.8
C(10)-C(9)-H(9B)	109.8
C(9)-C(10)-H(10)	109.5
C(9)-C(10)-C(11)	108.92(13)
C(9)-C(10)-C(13)	110.52(15)
C(11)-C(10)-H(10)	109.5
C(13)-C(10)-H(10)	109.5
C(13)-C(10)-C(11)	109.00(12)
C(4)-C(11)-H(11A)	109.7
C(4)-C(11)-H(11B)	109.7
C(10)-C(11)-C(4)	109.69(14)
C(10)-C(11)-H(11A)	109.7
C(10)-C(11)-H(11B)	109.7
H(11A)-C(11)-H(11B)	108.2
C(4)-C(12)-C(8)	108.78(11)
C(4)-C(12)-H(12A)	109.9
C(4)-C(12)-H(12B)	109.9
C(8)-C(12)-H(12A)	109.9
C(8)-C(12)-H(12B)	109.9
H(12A)-C(12)-H(12B)	108.3
C(6)-C(13)-C(10)	109.54(12)

C(6)-C(13)-H(13A)	109.8
C(6)-C(13)-H(13B)	109.8
C(10)-C(13)-H(13A)	109.8
C(10)-C(13)-H(13B)	109.8
H(13A)-C(13)-H(13B)	108.2
C(15)-C(14)-N(2)	118.80(14)
C(19)-C(14)-N(2)	119.70(14)
C(19)-C(14)-C(15)	121.50(14)
C(14)-C(15)-C(20)	121.05(14)
C(16)-C(15)-C(14)	118.27(15)
C(16)-C(15)-C(20)	120.69(15)
C(15)-C(16)-H(16)	119.1
C(17)-C(16)-C(15)	121.76(16)
C(17)-C(16)-H(16)	119.1
C(16)-C(17)-C(18)	118.59(15)
C(16)-C(17)-C(21)	121.03(17)
C(18)-C(17)-C(21)	120.38(17)
C(17)-C(18)-H(18)	119.1
C(17)-C(18)-C(19)	121.85(16)
C(19)-C(18)-H(18)	119.1
C(14)-C(19)-C(22)	121.71(14)
C(18)-C(19)-C(14)	118.00(15)
C(18)-C(19)-C(22)	120.29(15)
C(15)-C(20)-H(20A)	109.5
C(15)-C(20)-H(20B)	109.5
C(15)-C(20)-H(20C)	109.5
H(20A)-C(20)-H(20B)	109.5
H(20A)-C(20)-H(20C)	109.5
H(20B)-C(20)-H(20C)	109.5
C(17)-C(21)-H(21A)	109.5
C(17)-C(21)-H(21B)	109.5
C(17)-C(21)-H(21C)	109.5
H(21A)-C(21)-H(21B)	109.5
H(21A)-C(21)-H(21C)	109.5
H(21B)-C(21)-H(21C)	109.5
C(19)-C(22)-H(22A)	109.5
C(19)-C(22)-H(22B)	109.5
C(19)-C(22)-H(22C)	109.5
H(22A)-C(22)-H(22B)	109.5
H(22A)-C(22)-H(22C)	109.5
H(22B)-C(22)-H(22C)	109.5
Ru(1)-C(23)-H(23)	119.8
C(24)-C(23)-Ru(1)	120.38(11)
C(24)-C(23)-H(23)	119.8
C(25)-C(24)-C(23)	120.29(13)
C(25)-C(24)-C(29)	117.66(13)
C(29)-C(24)-C(23)	122.02(13)
C(24)-C(25)-H(25)	118.8
C(26)-C(25)-C(24)	122.32(15)
C(26)-C(25)-H(25)	118.8
C(25)-C(26)-H(26)	120.6
C(27)-C(26)-C(25)	118.89(16)
C(27)-C(26)-H(26)	120.6
C(26)-C(27)-H(27)	119.7

C(26)-C(27)-C(28)	120.52(14)
C(28)-C(27)-H(27)	119.7
C(27)-C(28)-H(28)	119.8
C(27)-C(28)-C(29)	120.33(16)
C(29)-C(28)-H(28)	119.8
O(1)-C(29)-C(24)	115.52(12)
O(1)-C(29)-C(28)	124.20(15)
C(24)-C(29)-C(28)	120.27(15)
O(1)-C(30)-H(30)	109.1
O(1)-C(30)-C(31)	104.60(19)
O(1)-C(30)-C(32)	110.9(2)
C(31)-C(30)-H(30)	109.1
C(31)-C(30)-C(32)	114.0(2)
C(32)-C(30)-H(30)	109.1
C(30)-C(31)-H(31A)	109.5
C(30)-C(31)-H(31B)	109.5
C(30)-C(31)-H(31C)	109.5
H(31A)-C(31)-H(31B)	109.5
H(31A)-C(31)-H(31C)	109.5
H(31B)-C(31)-H(31C)	109.5
C(30)-C(32)-H(32A)	109.5
C(30)-C(32)-H(32B)	109.5
C(30)-C(32)-H(32C)	109.5
H(32A)-C(32)-H(32B)	109.5
H(32A)-C(32)-H(32C)	109.5
H(32B)-C(32)-H(32C)	109.5
C(33)-C(34)-H(34A)	109.3
C(33)-C(34)-H(34B)	109.3
C(33)-C(34)-C(35)	111.6(4)
H(34A)-C(34)-H(34B)	108.0
C(35)-C(34)-H(34A)	109.3
C(35)-C(34)-H(34B)	109.3
C(34)-C(35)-H(35A)	109.2
C(34)-C(35)-H(35B)	109.2
C(34)-C(35)-H(39D)	162.6
H(35A)-C(35)-H(35B)	107.9
H(35A)-C(35)-H(39D)	56.9
H(35B)-C(35)-H(39D)	86.4
C(36)-C(35)-C(34)	112.2(4)
C(36)-C(35)-H(35A)	109.2
C(36)-C(35)-H(35B)	109.2
C(36)-C(35)-H(39D)	67.9
C(35)-C(36)-H(36A)	109.0
C(35)-C(36)-H(36B)	109.0
C(35)-C(36)-C(37)	112.9(5)
C(35)-C(36)-H(39C)	93.4
C(35)-C(36)-H(39D)	28.8
C(35)-C(36)-H(39E)	106.9
H(36A)-C(36)-H(36B)	107.8
H(36A)-C(36)-H(39C)	126.8
H(36A)-C(36)-H(39D)	112.4
H(36A)-C(36)-H(39E)	116.2
H(36B)-C(36)-H(39C)	109.2
H(36B)-C(36)-H(39D)	129.5

H(36B)-C(36)-H(39E)	8.7
C(37)-C(36)-H(36A)	109.0
C(37)-C(36)-H(36B)	109.0
C(37)-C(36)-H(39C)	21.7
C(37)-C(36)-H(39D)	85.6
C(37)-C(36)-H(39E)	102.9
H(39C)-C(36)-H(39D)	68.4
H(39C)-C(36)-H(39E)	101.1
H(39D)-C(36)-H(39E)	124.1
C(36)-C(37)-H(39C)	70.2
H(37A)-C(37)-H(39C)	101.9
H(37B)-C(37)-H(39C)	146.1
H(37C)-C(37)-H(39C)	45.8
C(38)#2-C(38)-H(38A)	108.2
C(38)#2-C(38)-H(38B)	108.2
H(38A)-C(38)-H(38B)	107.3
C(39)-C(38)-C(38)#2	116.5(9)
C(39)-C(38)-H(38A)	108.2
C(39)-C(38)-H(38B)	108.2
C(38)-C(39)-H(39A)	108.0
C(38)-C(39)-H(39B)	108.0
C(38)-C(39)-H(39C)	107.6
C(38)-C(39)-H(39D)	112.2
C(38)-C(39)-H(39E)	108.9
C(38)-C(39)-C(40)	117.1(11)
H(39A)-C(39)-H(39B)	107.3
H(39A)-C(39)-H(39C)	110.5
H(39A)-C(39)-H(39D)	4.4
H(39A)-C(39)-H(39E)	115.5
H(39B)-C(39)-H(39C)	115.2
H(39B)-C(39)-H(39D)	104.2
H(39B)-C(39)-H(39E)	10.0
H(39C)-C(39)-H(39D)	109.7
H(39C)-C(39)-H(39E)	106.0
H(39D)-C(39)-H(39E)	112.1
C(40)-C(39)-H(39A)	108.0
C(40)-C(39)-H(39B)	108.0
C(40)-C(39)-H(39C)	9.9
C(40)-C(39)-H(39D)	106.4
C(40)-C(39)-H(39E)	99.4
C(39)-C(40)-H(39C)	17.9
C(39)-C(40)-H(40A)	109.5
C(39)-C(40)-H(40B)	109.5
C(39)-C(40)-H(40C)	109.5
H(39C)-C(40)-H(40A)	96.1
H(39C)-C(40)-H(40B)	126.5
H(39C)-C(40)-H(40C)	104.4
H(40A)-C(40)-H(40B)	109.5
H(40A)-C(40)-H(40C)	109.5
H(40B)-C(40)-H(40C)	109.5

Table B.19: Anisotropic displacement parameters ($Å^2 x\ 10^4$) for 4.29. The anisotropic displacement factor exponent takes the form: $-2\pi^2 [h^2 a^{*2} U^{11} + ... + 2 h k a^* b^* U^{12}]$

	U^{11}	U^{22}	U^{33}	U^{23}	U^{13}	U^{12}
Ru(1)	138(1)	60(1)	113(1)	28(1)	46(1)	5(1)
O(2)	160(6)	114(4)	136(5)	45(4)	57(4)	-28(4)
N(1)	202(7)	72(5)	166(6)	9(4)	69(5)	-13(4)
N(2)	169(6)	78(5)	190(6)	28(4)	71(5)	-10(4)
O(1)	545(9)	290(6)	200(6)	143(5)	151(6)	245(6)
C(1)	164(7)	97(5)	128(6)	39(5)	38(5)	35(5)
C(2)	224(9)	104(6)	253(8)	-11(6)	75(7)	-33(6)
C(3)	252(9)	104(6)	284(9)	16(6)	106(7)	-41(6)
C(4)	190(8)	96(5)	134(6)	22(5)	58(5)	24(5)
C(5)	160(7)	99(5)	140(6)	36(5)	41(5)	27(5)
C(6)	207(8)	131(6)	181(7)	29(5)	91(6)	21(6)
C(7)	220(9)	217(7)	215(8)	50(6)	87(6)	61(6)
C(8)	286(9)	167(7)	189(7)	34(6)	100(7)	97(6)
C(9)	344(10)	241(8)	156(7)	40(6)	93(7)	111(7)
C(10)	345(10)	260(8)	139(7)	80(6)	76(7)	145(7)
C(11)	244(9)	185(7)	143(7)	13(5)	25(6)	72(6)
C(12)	269(9)	115(6)	185(7)	26(5)	62(6)	57(6)
C(13)	357(10)	181(7)	216(8)	108(6)	159(7)	103(7)
C(14)	144(7)	96(5)	192(7)	47(5)	79(6)	-6(5)
C(15)	162(8)	171(7)	244(8)	76(6)	65(6)	26(6)
C(16)	196(8)	186(7)	324(9)	54(6)	114(7)	71(6)
C(17)	219(9)	171(7)	243(8)	7(6)	110(7)	-19(6)
C(18)	193(8)	185(7)	187(7)	68(6)	39(6)	-29(6)
C(19)	143(7)	115(6)	229(8)	76(5)	59(6)	-8(5)
C(20)	261(10)	342(9)	323(10)	140(8)	61(8)	130(8)
C(21)	397(12)	332(10)	295(10)	-36(8)	156(9)	47(9)
C(22)	222(9)	214(7)	317(9)	140(7)	64(7)	68(6)
C(23)	172(7)	110(6)	147(7)	36(5)	51(5)	28(5)
C(24)	141(7)	115(6)	207(7)	61(5)	56(6)	47(5)
C(25)	166(8)	153(6)	237(8)	37(6)	26(6)	65(6)
C(26)	198(9)	154(7)	353(10)	-18(6)	0(7)	74(6)
C(27)	239(9)	122(6)	544(12)	86(7)	74(8)	76(6)
C(28)	314(10)	210(8)	424(11)	206(7)	139(8)	128(7)
C(29)	237(9)	178(7)	253(8)	112(6)	104(7)	97(6)
C(30)	1010(20)	584(14)	327(11)	320(11)	297(12)	576(15)
C(31)	2080(40)	860(20)	217(12)	147(13)	93(17)	1020(30)
C(32)	1180(30)	960(20)	890(20)	803(18)	820(20)	780(20)
C(33)	530(30)	720(30)	850(40)	200(30)	-270(30)	170(30)
C(34)	390(20)	307(17)	570(30)	150(17)	199(19)	78(16)
C(35)	230(18)	510(20)	390(20)	83(17)	21(15)	147(16)
C(36)	270(20)	1180(50)	440(30)	340(30)	10(20)	290(30)
C(37)	240(30)	720(40)	1010(50)	600(40)	-140(30)	-60(30)
C(38)	490(50)	1170(70)	730(50)	260(40)	-110(40)	180(40)
C(39)	680(50)	1170(70)	530(40)	530(50)	190(40)	440(50)

Table B.20: Hydrogen coordinates (x 10^3) and isotropic displacement parameters ($Å^2$x 10^3) for 4.29

	x	y	z	U_{iso}
H(2)	380(2)	419(2)	573(1)	18
H(2A)	180	-82	276	27
H(2B)	104	-1	236	27
H(3A)	-7	-3	362	29
H(3B)	105	-35	414	29
H(5)	532	243	345	16
H(6)	656	422	291	22
H(7A)	726	275	176	27
H(7B)	698	219	263	27
H(8)	596	46	129	25
H(9A)	424	63	38	30
H(9B)	560	179	39	30
H(10)	382	265	64	28
H(11A)	248	106	134	24
H(11B)	269	251	196	24
H(12A)	376	-26	173	23
H(12B)	482	31	261	23
H(13A)	594	410	138	28
H(13B)	480	435	200	28
H(16)	-61	388	601	28
H(18)	206	282	722	25
H(20A)	27	332	390	44
H(20B)	-100	338	443	44
H(20C)	-89	199	391	44
H(21A)	-4	477	760	57
H(21B)	124	462	806	57
H(21C)	-18	350	794	57
H(22A)	241	51	556	36
H(22B)	332	163	640	36
H(22C)	355	175	539	36
H(23)	227	381	307	18
H(25)	341	630	503	22
H(26)	374	854	532	30
H(27)	379	946	411	36
H(28)	349	816	263	34
H(30)	278	680	139	63
H(31A)	293	430	46	138
H(31B)	261	528	-4	138
H(31C)	158	463	60	138
H(32A)	510	740	183	119
H(32B)	480	721	77	119
H(32C)	511	609	112	119
H(33A)	920	184	-82	108
H(33B)	967	338	-30	108
H(33C)	820	244	-24	108
H(34A)	958	291	108	51
H(34B)	1054	227	50	51

H(35A)	784	82	58	46
H(35B)	892	22	13	46
H(36A)	898	140	199	71
H(36B)	1008	81	155	71
H(37A)	735	-73	166	97
H(37B)	864	-82	214	97
H(37C)	832	-136	107	97
H(38A)	903	-128	-14	99
H(38B)	1031	-70	59	99
H(39A)	826	38	68	84
H(39B)	948	81	143	84
H(39C)	832	-71	122	105
H(39D)	828	40	74	105
H(39E)	947	70	149	105
H(40A)	737	-166	104	84
H(40B)	753	-46	191	84
H(40C)	859	-122	180	84

Table B.21: Crystal Data and Structure Analysis Details for 4.33

Empirical formula	C32 H42 I2 N2 O Ru
Formula weight	825.55
Crystallization solvent	
Crystal shape	triangular block
Crystal color	dark green, almost black
Crystal size	0.23 x 0.26 x 0.35 mm

Data Collection

Preliminary photograph(s)	rotation	
Type of diffractometer	Bruker SMART 1000 CCD	
Wavelength	0.71073 Å MoK	
Data collection temperature	100 K	
Theta range for 9189 reflections used in lattice determination	2.19 to 44.15°	
Unit cell dimensions	a = 18.4395(6) Å b = 11.5328(4) Å c = 29.7072(9) Å	α= 90° β= 90° γ = 90°
Volume	6317.5(4) $Å^3$	
Z	8	
Crystal system	orthorhombic	
Space group	P b c a (# 61)	
Density (calculated)	1.736 g/cm^3	
F(000)	3248	
Theta range for data collection	1.4 to 45.9°	
Completeness to theta = 25.00°	100.0%	
Index ranges	$-37 \le h \le 37$, $-23 \le k \le 23$, $-59 \le l \le 59$	
Data collection scan type	and scans	
Reflections collected	252143	
Independent reflections	27049 [R_{int}= 0.0620]	
Reflections > 2σ(I)	19651	
Average σ(I)/(net I)	0.0409	
Absorption coefficient	2.48 mm^{-1}	
Absorption correction	Semi-empirical from equivalents	
Max. and min. transmission	1.0000 and 0.8707	

Table B.21 (cont.):

Structure Solution and Refinement

Primary solution method	direct
Secondary solution method	difmap
Hydrogen placement	geom
Refinement method	Full-matrix least-squares on F^2
Data / restraints / parameters	27049 / 0 / 348
Treatment of hydrogen atoms	constr
Goodness-of-fit on F^2	2.09
Final R indices [I>2σ(I), 19651 reflections]	R1 = 0.0536, wR2 = 0.0684
R indices (all data)	R1 = 0.0823, wR2 = 0.0710
Type of weighting scheme used	calc
Weighting scheme used	calc w=1/[^2^(Fo^2^)]
Max shift/error	0.002
Average shift/error	0.000
Largest diff. peak and hole	6.47 and -5.07 e·$Å^{-3}$

Programs Used

Cell refinement	SAINT V8.18C (Bruker-AXS, 2007)
Data collection	APEX2 2012.2-0 (Bruker-AXS, 2007)
Data reduction	SAINT V8.18C (Bruker-AXS, 2007)
Structure solution	SHELXS-97 (Sheldrick, 1990)
Structure refinement	SHELXL-97 (Sheldrick, 1997)
Graphics	DIAMOND 3 (Crystal Impact, 1999)

Table B.22: Atomic coordinates (x 10^4) and equivalent isotropic displacement parameters ($Å^2$x 10^3) for 4.33. U(eq) is defined as one third of the trace of the orthogonalized U^{ij} tensor

	x	y	z	U_{eq}
Ru(1)	-134(1)	6848(1)	1404(1)	9(1)
I(1)	-1122(1)	5395(1)	1049(1)	16(1)
I(2)	978(1)	7807(1)	1854(1)	15(1)
O(1)	-528(1)	6166(1)	2094(1)	14(1)
N(1)	649(1)	6835(1)	533(1)	14(1)
N(2)	-26(1)	8395(1)	574(1)	15(1)
C(1)	183(1)	7430(1)	805(1)	11(1)
C(2)	787(1)	7431(2)	101(1)	21(1)
C(3)	290(1)	8472(2)	123(1)	24(1)
C(4)	1152(1)	5884(1)	660(1)	12(1)
C(5)	832(1)	5137(2)	1037(1)	15(1)
C(6)	1364(1)	4163(2)	1169(1)	19(1)
C(7)	1495(1)	3392(2)	760(1)	25(1)
C(8)	1837(1)	4128(2)	381(1)	23(1)
C(9)	2549(1)	4654(2)	548(1)	23(1)
C(10)	2409(1)	5419(2)	959(1)	19(1)
C(11)	1886(1)	6398(2)	818(1)	16(1)
C(12)	1300(1)	5097(2)	254(1)	20(1)
C(13)	2070(1)	4693(2)	1334(1)	22(1)
C(14)	-491(1)	9325(2)	714(1)	13(1)
C(15)	-185(1)	10295(2)	929(1)	14(1)
C(16)	-641(1)	11189(2)	1062(1)	17(1)
C(17)	-1390(1)	11152(2)	983(1)	19(1)
C(18)	-1668(1)	10208(2)	748(1)	18(1)
C(19)	-1231(1)	9292(2)	607(1)	14(1)
C(20)	620(1)	10383(2)	1013(1)	21(1)
C(21)	-1877(1)	12115(2)	1149(1)	33(1)
C(22)	-1551(1)	8277(2)	359(1)	20(1)
C(23)	-816(1)	7941(2)	1567(1)	13(1)
C(24)	-1249(1)	7782(2)	1966(1)	13(1)
C(25)	-1814(1)	8534(2)	2088(1)	20(1)
C(26)	-2222(1)	8328(2)	2472(1)	28(1)
C(27)	-2066(1)	7369(2)	2738(1)	29(1)
C(28)	-1508(1)	6606(2)	2631(1)	22(1)
C(29)	-1100(1)	6822(2)	2244(1)	14(1)
C(30)	-283(1)	5201(2)	2385(1)	18(1)
C(31)	133(1)	5684(2)	2786(1)	25(1)
C(32)	181(1)	4409(2)	2101(1)	25(1)

Table B.23: Bond lengths [Å] and angles [°] for 4.33

Ru(1)-I(1)	2.69151(18)
Ru(1)-I(2)	2.68589(18)
Ru(1)-O(1)	2.3116(12)
Ru(1)-C(1)	1.9916(17)
Ru(1)-C(23)	1.8448(17)
O(1)-C(29)	1.372(2)
O(1)-C(30)	1.479(2)
N(1)-C(1)	1.365(2)
N(1)-C(2)	1.477(2)
N(1)-C(4)	1.486(2)
N(2)-C(1)	1.362(2)
N(2)-C(3)	1.462(2)
N(2)-C(14)	1.435(2)
C(2)-H(2A)	0.9900
C(2)-H(2B)	0.9900
C(2)-C(3)	1.512(3)
C(3)-H(3A)	0.9900
C(3)-H(3B)	0.9900
C(4)-C(5)	1.531(2)
C(4)-C(11)	1.549(2)
C(4)-C(12)	1.534(2)
C(5)-H(5)	0.9900
C(5)-H(1)	0.9900
C(5)-C(6)	1.542(3)
C(6)-H(6)	1.0000
C(6)-C(7)	1.525(3)
C(6)-C(13)	1.520(3)
C(7)-H(7A)	0.9900
C(7)-H(7B)	0.9900
C(7)-C(8)	1.544(3)
C(8)-H(8)	1.0000
C(8)-C(9)	1.530(3)
C(8)-C(12)	1.540(3)
C(9)-H(9A)	0.9900
C(9)-H(9B)	0.9900
C(9)-C(10)	1.527(3)
C(10)-H(10)	1.0000
C(10)-C(11)	1.544(2)
C(10)-C(13)	1.529(3)
C(11)-H(11A)	0.9900
C(11)-H(11B)	0.9900
C(12)-H(12A)	0.9900
C(12)-H(12B)	0.9900
C(13)-H(13A)	0.9900
C(13)-H(13B)	0.9900
C(14)-C(15)	1.406(2)
C(14)-C(19)	1.403(2)
C(15)-C(16)	1.388(3)
C(15)-C(20)	1.509(2)
C(16)-H(16)	0.9500
C(16)-C(17)	1.402(3)

C(17)-C(18)	1.391(3)
C(17)-C(21)	1.510(3)
C(18)-H(18)	0.9500
C(18)-C(19)	1.393(3)
C(19)-C(22)	1.504(3)
C(20)-H(20A)	0.9800
C(20)-H(20B)	0.9800
C(20)-H(20C)	0.9800
C(21)-H(21A)	0.9800
C(21)-H(21B)	0.9800
C(21)-H(21C)	0.9800
C(22)-H(22A)	0.9800
C(22)-H(22B)	0.9800
C(22)-H(22C)	0.9800
C(23)-H(23)	0.9500
C(23)-C(24)	1.441(2)
C(24)-C(25)	1.403(2)
C(24)-C(29)	1.409(2)
C(25)-H(25)	0.9500
C(25)-C(26)	1.389(3)
C(26)-H(26)	0.9500
C(26)-C(27)	1.388(3)
C(27)-H(27)	0.9500
C(27)-C(28)	1.391(3)
C(28)-H(28)	0.9500
C(28)-C(29)	1.396(2)
C(30)-H(30)	1.0000
C(30)-C(31)	1.523(3)
C(30)-C(32)	1.509(3)
C(31)-H(31A)	0.9800
C(31)-H(31B)	0.9800
C(31)-H(31C)	0.9800
C(32)-H(32A)	0.9800
C(32)-H(32B)	0.9800
C(32)-H(32C)	0.9800

I(2)-Ru(1)-I(1)	165.559(7)
O(1)-Ru(1)-I(1)	85.51(3)
O(1)-Ru(1)-I(2)	86.55(3)
C(1)-Ru(1)-I(1)	93.30(5)
C(1)-Ru(1)-I(2)	94.76(5)
C(1)-Ru(1)-O(1)	178.62(6)
C(23)-Ru(1)-I(1)	93.77(5)
C(23)-Ru(1)-I(2)	96.29(5)
C(23)-Ru(1)-O(1)	77.66(6)
C(23)-Ru(1)-C(1)	101.73(7)
C(29)-O(1)-Ru(1)	110.00(10)
C(29)-O(1)-C(30)	117.38(14)
C(30)-O(1)-Ru(1)	132.62(10)
C(1)-N(1)-C(2)	112.78(14)
C(1)-N(1)-C(4)	127.95(14)
C(2)-N(1)-C(4)	117.21(14)
C(1)-N(2)-C(3)	113.47(15)
C(1)-N(2)-C(14)	129.30(15)

C(14)-N(2)-C(3)	117.22(14)
N(1)-C(1)-Ru(1)	122.95(12)
N(2)-C(1)-Ru(1)	130.02(13)
N(2)-C(1)-N(1)	106.94(14)
N(1)-C(2)-H(2A)	111.1
N(1)-C(2)-H(2B)	111.1
N(1)-C(2)-C(3)	103.16(14)
H(2A)-C(2)-H(2B)	109.1
C(3)-C(2)-H(2A)	111.1
C(3)-C(2)-H(2B)	111.1
N(2)-C(3)-C(2)	103.44(15)
N(2)-C(3)-H(3A)	111.1
N(2)-C(3)-H(3B)	111.1
C(2)-C(3)-H(3A)	111.1
C(2)-C(3)-H(3B)	111.1
H(3A)-C(3)-H(3B)	109.0
N(1)-C(4)-C(5)	111.12(14)
N(1)-C(4)-C(11)	109.80(14)
N(1)-C(4)-C(12)	110.35(15)
C(5)-C(4)-C(11)	109.34(15)
C(5)-C(4)-C(12)	108.11(14)
C(12)-C(4)-C(11)	108.06(15)
C(4)-C(5)-H(5)	109.6
C(4)-C(5)-H(1)	109.6
C(4)-C(5)-C(6)	110.47(14)
H(5)-C(5)-H(1)	108.1
C(6)-C(5)-H(5)	109.6
C(6)-C(5)-H(1)	109.6
C(5)-C(6)-H(6)	109.2
C(7)-C(6)-C(5)	108.84(17)
C(7)-C(6)-H(6)	109.2
C(13)-C(6)-C(5)	109.56(16)
C(13)-C(6)-H(6)	109.2
C(13)-C(6)-C(7)	110.85(17)
C(6)-C(7)-H(7A)	109.9
C(6)-C(7)-H(7B)	109.9
C(6)-C(7)-C(8)	108.95(16)
H(7A)-C(7)-H(7B)	108.3
C(8)-C(7)-H(7A)	109.9
C(8)-C(7)-H(7B)	109.9
C(7)-C(8)-H(8)	109.7
C(9)-C(8)-C(7)	109.43(18)
C(9)-C(8)-H(8)	109.7
C(9)-C(8)-C(12)	110.09(16)
C(12)-C(8)-C(7)	108.34(17)
C(12)-C(8)-H(8)	109.7
C(8)-C(9)-H(9A)	109.7
C(8)-C(9)-H(9B)	109.7
H(9A)-C(9)-H(9B)	108.2
C(10)-C(9)-C(8)	110.03(16)
C(10)-C(9)-H(9A)	109.7
C(10)-C(9)-H(9B)	109.7
C(9)-C(10)-H(10)	109.6
C(9)-C(10)-C(11)	108.22(16)

C(9)-C(10)-C(13)	109.61(16)
C(11)-C(10)-H(10)	109.6
C(13)-C(10)-H(10)	109.6
C(13)-C(10)-C(11)	110.06(15)
C(4)-C(11)-H(11A)	109.6
C(4)-C(11)-H(11B)	109.6
C(10)-C(11)-C(4)	110.30(14)
C(10)-C(11)-H(11A)	109.6
C(10)-C(11)-H(11B)	109.6
H(11A)-C(11)-H(11B)	108.1
C(4)-C(12)-C(8)	110.56(16)
C(4)-C(12)-H(12A)	109.5
C(4)-C(12)-H(12B)	109.5
C(8)-C(12)-H(12A)	109.5
C(8)-C(12)-H(12B)	109.5
H(12A)-C(12)-H(12B)	108.1
C(6)-C(13)-C(10)	109.55(17)
C(6)-C(13)-H(13A)	109.8
C(6)-C(13)-H(13B)	109.8
C(10)-C(13)-H(13A)	109.8
C(10)-C(13)-H(13B)	109.8
H(13A)-C(13)-H(13B)	108.2
C(15)-C(14)-N(2)	119.16(16)
C(19)-C(14)-N(2)	119.74(16)
C(19)-C(14)-C(15)	120.95(17)
C(14)-C(15)-C(20)	121.50(17)
C(16)-C(15)-C(14)	118.56(17)
C(16)-C(15)-C(20)	119.93(17)
C(15)-C(16)-H(16)	119.1
C(15)-C(16)-C(17)	121.73(17)
C(17)-C(16)-H(16)	119.1
C(16)-C(17)-C(21)	120.55(18)
C(18)-C(17)-C(16)	118.12(18)
C(18)-C(17)-C(21)	121.33(19)
C(17)-C(18)-H(18)	119.0
C(17)-C(18)-C(19)	122.10(18)
C(19)-C(18)-H(18)	119.0
C(14)-C(19)-C(22)	120.88(17)
C(18)-C(19)-C(14)	118.34(17)
C(18)-C(19)-C(22)	120.76(17)
C(15)-C(20)-H(20A)	109.5
C(15)-C(20)-H(20B)	109.5
C(15)-C(20)-H(20C)	109.5
H(20A)-C(20)-H(20B)	109.5
H(20A)-C(20)-H(20C)	109.5
H(20B)-C(20)-H(20C)	109.5
C(17)-C(21)-H(21A)	109.5
C(17)-C(21)-H(21B)	109.5
C(17)-C(21)-H(21C)	109.5
H(21A)-C(21)-H(21B)	109.5
H(21A)-C(21)-H(21C)	109.5
H(21B)-C(21)-H(21C)	109.5
C(19)-C(22)-H(22A)	109.5
C(19)-C(22)-H(22B)	109.5

C(19)-C(22)-H(22C)	109.5
H(22A)-C(22)-H(22B)	109.5
H(22A)-C(22)-H(22C)	109.5
H(22B)-C(22)-H(22C)	109.5
Ru(1)-C(23)-H(23)	119.8
C(24)-C(23)-Ru(1)	120.39(13)
C(24)-C(23)-H(23)	119.8
C(25)-C(24)-C(23)	123.02(17)
C(25)-C(24)-C(29)	118.66(16)
C(29)-C(24)-C(23)	118.32(15)
C(24)-C(25)-H(25)	119.7
C(26)-C(25)-C(24)	120.55(19)
C(26)-C(25)-H(25)	119.7
C(25)-C(26)-H(26)	120.2
C(27)-C(26)-C(25)	119.5(2)
C(27)-C(26)-H(26)	120.2
C(26)-C(27)-H(27)	119.1
C(26)-C(27)-C(28)	121.78(19)
C(28)-C(27)-H(27)	119.1
C(27)-C(28)-H(28)	120.8
C(27)-C(28)-C(29)	118.30(19)
C(29)-C(28)-H(28)	120.8
O(1)-C(29)-C(24)	113.13(15)
O(1)-C(29)-C(28)	125.65(17)
C(28)-C(29)-C(24)	121.21(17)
O(1)-C(30)-H(30)	109.2
O(1)-C(30)-C(31)	109.64(16)
O(1)-C(30)-C(32)	107.58(14)
C(31)-C(30)-H(30)	109.2
C(32)-C(30)-H(30)	109.2
C(32)-C(30)-C(31)	111.89(18)
C(30)-C(31)-H(31A)	109.5
C(30)-C(31)-H(31B)	109.5
C(30)-C(31)-H(31C)	109.5
H(31A)-C(31)-H(31B)	109.5
H(31A)-C(31)-H(31C)	109.5
H(31B)-C(31)-H(31C)	109.5
C(30)-C(32)-H(32A)	109.5
C(30)-C(32)-H(32B)	109.5
C(30)-C(32)-H(32C)	109.5
H(32A)-C(32)-H(32B)	109.5
H(32A)-C(32)-H(32C)	109.5
H(32B)-C(32)-H(32C)	109.5

Table B.24: Anisotropic displacement parameters ($Å^2 x 10^4$) for 4.33. The anisotropic displacement factor exponent takes the form: $-2\pi^2 [h^2 a^{*2} U^{11} + ... + 2 h k a^* b^* U^{12}]$

	U^{11}	U^{22}	U^{33}	U^{23}	U^{13}	U^{12}
Ru(1)	92(1)	96(1)	83(1)	8(1)	-1(1)	9(1)
I(1)	152(1)	144(1)	186(1)	-4(1)	-25(1)	-36(1)
I(2)	123(1)	190(1)	144(1)	-52(1)	-19(1)	0(1)
O(1)	166(6)	153(6)	113(5)	42(4)	33(4)	37(5)
N(1)	148(7)	165(7)	100(6)	25(5)	21(5)	40(5)
N(2)	173(7)	151(7)	119(6)	49(5)	24(5)	43(5)
C(1)	99(7)	120(7)	120(6)	6(5)	-11(5)	-2(5)
C(2)	268(10)	243(10)	115(7)	49(7)	69(7)	74(8)
C(3)	257(10)	296(11)	156(8)	112(8)	76(7)	91(8)
C(4)	140(7)	87(6)	140(7)	-14(5)	30(6)	-1(5)
C(5)	139(7)	152(7)	165(7)	18(6)	47(6)	22(6)
C(6)	185(9)	136(8)	243(9)	39(7)	76(7)	50(7)
C(7)	256(10)	115(8)	369(12)	-15(8)	114(9)	-8(7)
C(8)	260(10)	125(8)	294(10)	-38(7)	90(8)	-2(7)
C(9)	220(9)	145(8)	322(11)	2(8)	128(8)	3(7)
C(10)	131(8)	159(8)	270(9)	9(7)	29(6)	18(6)
C(11)	149(8)	109(7)	207(8)	-8(6)	17(6)	-10(6)
C(12)	253(10)	167(8)	180(8)	-52(7)	50(7)	-20(7)
C(13)	190(9)	193(9)	280(10)	63(8)	19(7)	57(7)
C(14)	130(7)	140(7)	123(7)	45(6)	3(5)	2(6)
C(15)	114(7)	158(8)	164(7)	65(6)	-9(6)	-21(6)
C(16)	168(8)	138(8)	209(8)	17(7)	-11(7)	-22(6)
C(17)	175(9)	147(8)	249(9)	7(7)	7(7)	8(7)
C(18)	124(8)	157(8)	250(9)	42(7)	-18(6)	2(6)
C(19)	143(8)	127(7)	161(7)	50(6)	-19(6)	-14(6)
C(20)	123(8)	229(9)	274(10)	54(8)	-25(7)	-22(7)
C(21)	228(11)	222(10)	532(16)	-99(10)	14(10)	61(9)
C(22)	212(9)	167(8)	234(9)	21(7)	-64(7)	-27(7)
C(23)	128(7)	126(7)	127(7)	12(5)	10(5)	19(6)
C(24)	105(7)	124(7)	167(7)	6(6)	22(5)	5(6)
C(25)	171(9)	208(9)	230(9)	12(7)	60(7)	43(7)
C(26)	221(10)	304(12)	306(11)	23(9)	132(8)	70(9)
C(27)	237(10)	345(12)	275(11)	22(9)	156(8)	25(9)
C(28)	218(9)	230(10)	196(9)	46(7)	77(7)	3(7)
C(29)	134(7)	152(7)	128(7)	2(6)	26(5)	-4(6)
C(30)	238(9)	169(8)	139(7)	58(6)	23(7)	45(7)
C(31)	292(11)	309(11)	138(8)	50(8)	-19(8)	56(9)
C(32)	347(12)	212(10)	197(9)	68(7)	49(8)	111(9)

Table B.25: Hydrogen coordinates (x 10^3) and isotropic displacement parameters ($Å^2$x 10^3) for 4.33

	x	y	z	U_{iso}
H(2A)	66	693	-16	25
H(2B)	130	767	8	25
H(3A)	56	920	8	28
H(3B)	-9	843	-11	28
H(5)	37	479	94	18
H(1)	73	563	130	18
H(6)	115	369	142	23
H(7A)	103	306	66	30
H(7B)	182	275	84	30
H(8)	193	363	11	27
H(9A)	289	403	63	27
H(9B)	277	512	30	27
H(10)	288	576	107	22
H(11A)	210	686	57	19
H(11B)	180	692	108	19
H(12A)	150	556	0	24
H(12B)	84	475	15	24
H(13A)	241	407	142	27
H(13B)	198	519	160	27
H(16)	-44	1184	121	21
H(18)	-217	1019	68	21
H(20A)	72	1105	121	31
H(20B)	87	1048	72	31
H(20C)	79	967	116	31
H(21A)	-184	1278	94	49
H(21B)	-173	1235	145	49
H(21C)	-238	1184	116	49
H(22A)	-208	836	34	31
H(22B)	-143	756	52	31
H(22C)	-135	825	5	31
H(23)	-88	861	139	15
H(25)	-192	919	191	24
H(26)	-260	884	255	33
H(27)	-235	723	300	34
H(28)	-141	595	282	26
H(30)	-72	476	250	22
H(31A)	58	604	268	37
H(31B)	25	505	300	37
H(31C)	-16	626	294	37
H(32A)	-8	419	183	38
H(32B)	30	371	227	38
H(32C)	63	481	202	38